NASA/TM–2018-219027/ Vol. 5

PACE Technical Report Series, Volume 5

Ivona Cetinić, Charles R. McClain, and P. Jeremy Werdell, Editors

Mission Formulation Studies

Paula Bontempi, Brian Cairns, Susanne E. Craig, André Dress, Bryan Franz, Robert Lossing, Antonio Mannino, Lachlan I. W. McKinna, Nima Pahlevan, Frederick S. Patt, Robert Schweiss, and Jeremy Werdell

National Aeronautics and
Space Administration

Goddard Space Flight Center
Greenbelt, Maryland 20771

December 2018

NASA STI Program ... in Profile

Since its founding, NASA has been dedicated to the advancement of aeronautics and space science. The NASA scientific and technical information (STI) program plays a key part in helping NASA maintain this important role.

The NASA STI program operates under the auspices of the Agency Chief Information Officer. It collects, organizes, provides for archiving, and disseminates NASA's STI. The NASA STI program provides access to the NASA Aeronautics and Space Database and its public interface, the NASA Technical Report Server, thus providing one of the largest collections of aeronautical and space science STI in the world. Results are published in both non-NASA channels and by NASA in the NASA STI Report Series, which includes the following report types:

- TECHNICAL PUBLICATION. Reports of completed research or a major significant phase of research that present the results of NASA Programs and include extensive data or theoretical analysis. Includes compilations of significant scientific and technical data and information deemed to be of continuing reference value. NASA counterpart of peer-reviewed formal professional papers but has less stringent limitations on manuscript length and extent of graphic presentations.
- TECHNICAL MEMORANDUM. Scientific and technical findings that are preliminary or of specialized interest, e.g., quick release reports, working papers, and bibliographies that contain minimal annotation. Does not contain extensive analysis.
- CONTRACTOR REPORT. Scientific and technical findings by NASA-sponsored contractors and grantees.
- CONFERENCE PUBLICATION. Collected papers from scientific and technical conferences, symposia, seminars, or other meetings sponsored or co-sponsored by NASA.
- SPECIAL PUBLICATION. Scientific, technical, or historical information from NASA programs, projects, and missions, often concerned with subjects having substantial public interest.
- TECHNICAL TRANSLATION. English-language translations of foreign scientific and technical material pertinent to NASA's mission.

Specialized services also include organizing and publishing research results, distributing specialized research announcements and feeds, providing help desk and personal search support, and enabling data exchange services. For more information about the NASA STI program, see the following:

- Access the NASA STI program home page at http://www.sti.nasa.gov
- E-mail your question via the Internet to help@sti.nasa.gov
- Phone the NASA STI Information Desk at 757-864-9658
- Write to:
  NASA STI Information Desk
  Mail Stop 148
  NASA's Langley Research Center
  Hampton, VA 23681-2199

NASA/TM–2018-219027/ Vol. 5

PACE Technical Report Series, Volume 5

Editors:

Ivona Cetinić
GESTAR/Universities Space Research Association, Columbia, Maryland
Charles R. McClain
Science Applications International Corporation, Reston, Virginia
P. Jeremy Werdell
NASA Goddard Space Flight Center, Greenbelt, Maryland

Mission Formulation Studies

Paula Bontempi
NASA Headquarters, Washington, DC
Brian Cairns
NASA Goddard Institute for Space Studies, New York, NY
Susanne E. Craig
GESTAR/Universities Space Research Association, Columbia, MD
André Dress
NASA Goddard Space Flight Center, Greenbelt, MD
Bryan Franz
NASA Goddard Space Flight Center, Greenbelt, MD
Robert Lossing
Science Applications International Corporation, Reston, VA
Antonio Mannino
NASA Goddard Space Flight Center, Greenbelt, MD
Lachlan I. W. McKinna
Go2Q Pty Ltd, Buderim, Australia
Nima Pahlevan
Science Systems and Applications Inc, Lanham, MD
Frederick S. Patt
Science Applications International Corporation, Reston, VA
Robert Schweiss
NASA Goddard Space Flight Center, Greenbelt, MD
Jeremy Werdell
NASA Goddard Space Flight Center, Greenbelt, MD

National Aeronautics and
Space Administration

Goddard Space Flight Center
Greenbelt, Maryland 20771

December 2018

Level of Review: This material has been technically reviewed by technical management.

Available from

NASA STI Program
Mail Stop 148
NASA's Langley Research Center
Hampton, VA 23681-2199

National Technical Information Service
5285 Port Royal Road
Springfield, VA 22161
703-605-6000

Available in electronic form at http://

INTRODUCTION

Introduction to Volume 5: Mission Formulation Studies

The Plankton, Aerosol, Cloud, ocean Ecosystem (PACE; https://pace.gsfc.nasa.gov) mission represents NASA's next great investment in satellite ocean color and the combined study of Earth's ocean-atmosphere system. At its core, PACE builds upon NASA's multi-decadal legacies of the Coastal Zone Color Scanner (1978-1986), Sea-viewing Wide Field-of-view Sensor (SeaWiFS; 1997-2010), Moderate Resolution Imaging Spectroradiometers (MODIS) onboard Terra (1999-present) and Aqua (2002-present), and Visible Infrared Imaging Spectroradiometer (VIIRS) onboard Suomi NPP (2012-present) and JPSS-1 (2017-present; to be renamed NOAA-20). The ongoing, combined climate data record from these instruments changed the way we view our planet and – to this day – offers an unparalleled opportunity to expand our senses into space, compress time, and measure life itself.

This volume presents PACE Project scientific studies related to the general formulation of the mission and PACE observatory – that is, those studies that influenced preliminary mission design during its Pre-phase A (2014-2016; pre-formulation: define a viable and affordable concept) and Phase A (2016-2017; concept and technology development). The volume begins with a history of the direction of the mission to NASA Goddard Space Flight Center, then proceeds with topical summaries of various aspects of the ocean color instrument (OCI) concept design and general observatory behavior (e.g., the need to tilt OCI to mitigate contamination by Sun glint and the altitude at which it should be flown). Many of these studies were integral in shaping an amorphous observatory concept into something viable and scientifically meaningful. Subsequent volumes will capture more specific details related to fine-tuning of the mission and the design of OCI.

I would like to congratulate the full PACE Project for maintaining the required bandwidth and enthusiasm to whittle broad mission ideas and expectations into a viable mission concept, particularly under the relentless reminders of being cost-capped. I would also like to thank the Project Science team for their pursuit of these studies – and their subsequent documentation in this Technical Report series – that share our experiences and lessons learned. We hope the user community enjoys and benefits from our sharing of this journey.

P. J. Werdell
PACE Project Scientist
March 2018

Contents

Chapter 1

PACE Mission Formulation and Architecture

Jeremy Werdell, NASA Goddard Space Flight Center, Greenbelt, Maryland[1]

Paula Bontempi, NASA Headquarters, Washington, DC

Andre' Dress, NASA Goddard Space Flight Center, Greenbelt, Maryland

Bryan Franz, NASA Goddard Space Flight Center, Greenbelt, Maryland

Robert Schweiss, NASA Goddard Space Flight Center, Greenbelt, Maryland

Executive Summary

This chapter summarizes the mission architecture for the Plankton, Aerosol, Cloud, ocean Ecosystem (PACE) mission, ranging from its scientific rationale to the history of its realized conception to its present-day organization and management. This volume in the PACE Technical Report series focuses on trade studies that informed the formulation of the mission in its pre-Phase A (2014-2016; pre-formulation: define a viable and affordable concept) and Phase A (2016-2017; concept and technology development). With that in mind, this chapter serves to introduce the mission by providing: (1) a brief summary of the science drivers for the mission; (2) a history of the direction of the mission to NASA's Goddard Space Flight Center (GSFC); (3) a synopsis of the mission's and instruments' management and development structures; and (4) a brief description of the primary components and elements that form the foundation of the mission, encompassing the major mission segments (space, ground, and science data processing) and their roles in integration, testing, and operations.

1.1. Scientific Background

Global ocean color measurements are essential for understanding ocean ecology and the global carbon cycle and how it affects and is affected by climate change. A key step toward helping scientists understand how the Earth has responded to its changing climate over time – and how it may respond in the future – is through the establishment of high-quality, long-term, global time series of various geophysical parameters. Given the nature of the phenomena and the timescales needed to distinguish trends, such measurements will require combining data from several missions. These climate-quality time series are called climate data records (CDRs), and are being generated for a variety of geophysical parameters, including ocean color. Additionally, the mission seeks to move beyond heritage sensor capabilities and data products to allow measurements of new biogeochemical properties, such as phytoplankton community contribution (that is, the discrimination of different classes of phytoplankton and their global distributions).

Dissolved and suspended organic and inorganic material within the upper layer of ocean water provide the basis for ocean color science. Many particulate and dissolved constituents of the near-surface water column absorb and scatter light differently in the ultraviolet (UV) and visible (VIS) regions of the electromagnetic spectrum (these are the colors that humans see). At its most fundamental level, ocean

[1] Cite as: Werdell, P. J., P. Bontempi, A. Dress, B. Franz, and R. Schweiss (2018), PACE Mission Formulation and Architecture, in PACE Technical Report Series, Volume 5: Mission Formulation Studies (NASA/TM-2018 – 2018-219027/ Vol. 5), edited by I. Cetinić, C. R. McClain and P. J. Werdell, NASA Goddard Space Flight Space Center Greenbelt, MD.

color science is about relating the spectral variations in the UV-VIS marine light field (that is, differences in the ocean's color) to the concentrations of the various constituents residing in the sunlit, near-surface water column.

The requirements for PACE's primary instrument, the Ocean Color Instrument (OCI), predominantly focus on improving our ability to observe phytoplankton. These microscopic algae form the base of the marine food chain and produce some of the oxygen we breathe. They also play an important role in converting inorganic carbon in carbon dioxide (CO_2) to organic compounds, fueling global ocean ecosystems and driving oceanic biogeochemical cycles through grazing (i.e., they provide a food source for zooplankton) and their degradation products via the microbial loop (where bacteria reintroduce dissolved organic carbon and nutrients to the water, effectively recycling both back into the food web). Phytoplankton are therefore a critical part of the ocean's biological carbon pump, whereby atmospheric CO_2 gets sequestered to the deep ocean, and are responsible for roughly half of Earth's net primary production. Phytoplankton growth, however, is highly sensitive to variations in ocean and atmospheric physical properties, such as upper-ocean stratification, nutrient concentrations (e.g., nitrate and iron) and light availability within this mixed layer. They also vary greatly in their size, function, response to ecosystem changes or stresses, and nutritional value for species higher in the food web. Hence, measurements of phytoplankton community composition and their distributions remain essential for understanding global carbon cycles and how living marine resources are responding to Earth's changing climate.

While PACE is predominantly an ocean color mission, it will also have secondary objectives and two secondary instruments, both multi-angle polarimeters. An additional overarching goal for the mission is to help determine the roles of the ocean and atmosphere in global biogeochemical cycling and how perturbations to Earth's energy balance both affect and are affected by rising atmospheric CO_2 levels and Earth's changing climate. The PACE mission will contribute to the continuation of atmospheric CDRs as well as those for ocean color. The OCI will allow continuation of heritage aerosol measurements made using MODIS onboard Terra and Aqua and the Ozone Monitoring Instrument (OMI) onboard Aura. It will also provide additional characterization of aerosol particles because its spectral range will include shortwave infrared wavelengths. This will enable continuation of MODIS-like and OMI-like characterization of aerosol properties, MODIS-like measurements of water vapor, and MODIS-like retrievals of some cloud optical properties. These are the key atmospheric components affecting our ability to predict climate change as they contribute the largest uncertainties in our understanding of climate forcings and cloud feedbacks in an increasingly warmer planet. The interactions between these species are key to such understanding, as aerosols, water vapor, and clouds remain intertwined within the hydrologic cycle because most cloud droplets are seeded by small aerosol particles called cloud condensation nuclei. Changes in the amount, type, and distribution of aerosols, therefore, can alter the micro- and macro-physical characteristics of clouds. Furthermore, natural and anthropogenic changes to the aerosol system may affect clouds and precipitation, which can alter where, when, and how much precipitation may fall.

A summary of PACE science objectives are as follows:

- Extending key systematic ocean biological, ecological, and biogeochemical data records and cloud and aerosol data records;
- Making global measurements of ocean color data products that are essential for understanding the global carbon cycle and ocean ecosystem responses to a changing climate, as well as managing marine fisheries and water quality;

- Collecting global observations of aerosol and cloud properties, focusing on reducing the largest uncertainties in climate and radiative forcing models of the Earth system; and,
- Improving our understanding of how aerosols influence ocean ecosystems and biogeochemical cycles and how ocean biological and photochemical processes affect the atmosphere, as well as understanding air quality.

Volumes 1 and 2 of this Technical Memorandum series (ACE Ocean Working Group recommendations and instrument requirements for an advanced ocean ecology mission [2018] and The PACE Science Definition Team Report [2018]) expand on the rationale for PACE.

1.2. Realizing the PACE Mission

The PACE mission is a strategic climate continuity mission that was formally first defined in the 2010 document *Responding to the Challenge of Climate and Environmental Change: NASA's Plan for Climate-Centric Architecture for Earth Observations and Applications from Space* (http://science.nasa.gov/media/medialibrary/2010/07/01/Climate_Architecture_Final.pdf). This Climate Initiative complements NASA's implementation of the National Research Council's 2007 Decadal Survey of Earth Science at NASA, the National Oceanic and Atmospheric Administration (NOAA), and the United States Geological Survey (USGS), entitled *Earth Science and Applications from Space: National Imperatives for the Next Decade and Beyond*. From 2011-2012, NASA HQ convened a PACE Science Definition Team, whose report provides overall scientific guidance for the mission during its formulation and execution (see [PACE Science Definition *Team*, 2018]).

NASA HQ directed the PACE mission to GSFC in January 2014. The scope of this direction included overall mission management (e.g., budget and schedule), safety and mission assurance, acquisition of the spacecraft and launch vehicle, integration and testing of all mission elements, mission operations and ground systems, development of the ocean color instrument (OCI), day-to-day scientific guidance related to mission formulation and execution, and science data processing. NASA HQ specifically assigned science data processing to the GSFC Ocean Biology Processing Group (OBPG; https://oceancolor.gsfc.nasa.gov). NASA HQ allocated a not-to-be-exceeded $805M to the mission – $705M to be managed by GSFC and $100M to be managed independently by HQ's Earth Science Division (ESD). The GSFC $705M encompasses all elements listed above with the exception of science data processing. The ESD $100M encompasses science data processing, calibration and validation systems (including a vicarious calibration instrument system), and all competed community science teams. NASA HQ also directed GSFC to explore acquisition of a polarimeter as an optional secondary instrument within their $705M allocation, to be obtained from the NASA Jet Propulsion Laboratory (JPL), procured commercially, or contributed by entity external to GSFC.

In addition, NASA HQ directed mission development to be guided by a Design-to-Cost (DTC) process. Within DTC, all elements of the mission other than the cost are in a tradeable space guided by mission studies that are performed across all mission elements. In practice, mission studies result in definition of approaches within and across elements that maximize science capabilities at a high cost confidence. Volumes 3 (this volume) through 5 of this Technical Report series document scientific mission studies that guided mission formulation.

1.3. Mission Organization and Management

Project implementation authority is delegated from the NASA Associate Administrator for the Science Mission Directorate to ESD, with mission execution directed to GSFC (Figure 1.1). The GSFC directed work falls under the Earth Systematic Missions Program, which is administratively located within the Flight Projects Directorate at GSFC. The PACE Project (Figure 1.1; lower right pink box; $705M) and HQ Program Science (Figure 1.1; lower left green box; $100M) work collaboratively through the life of the mission to ensure its scientific value and ultimate mission success. Briefly, Project responsibilities at GSFC include design, development, manufacturing, integration and test, verification, documentation, and mission operations. Key roles not described elsewhere in this chapter include:

- A Project Manager that is responsible and accountable for technical, cost, schedule management, and performance;
- A Project Scientist that is responsible for the ongoing scientific output through all phases of the mission (data and, by extension, sensor characteristics and performance, as well as ongoing instrument calibration and science product validation);
- A Mission System Engineer that provides ultimate engineering technical authority for all mission systems and elements; and,
- A Chief Safety and Mission Assurance Officer that provides independent technical authority for all flight assurance and safety disciplines of the Project.

Briefly, HQ Program Science responsibilities include establishment of competed science teams, provision of the vicarious calibration and validation system(s), and supporting the science data segment (SDS) located within the OBPG. Key roles within PACE include:

- A Program Scientist that is responsible for ensuring maximization of science output of the mission, in particular verifying that important areas of science are not neglected; and,
- A Program Executive that is responsible for ensuring the Project successfully passes all HQ gate reviews, obtaining HQ concurrence on Project plans, and development of Project budget guidelines.

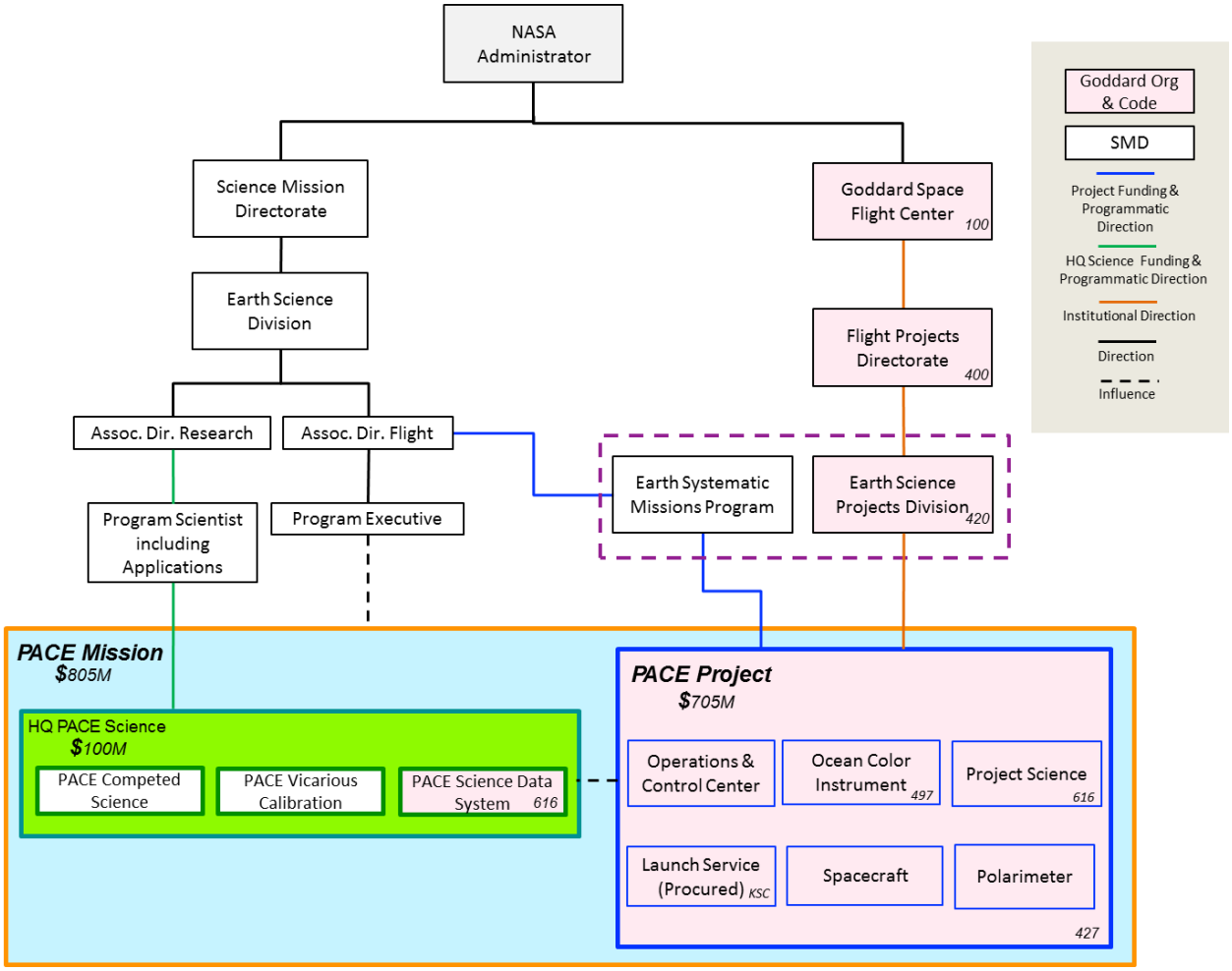

Figure 1.1. Programmatic and institutional authority.

1.4. Mission Infrastructure

NASA HQ designated PACE as a Category 2, Class C mission, defined as medium national priority, risk, complexity, and cost with targeted redundancies and limited flight spare parts (see NASA Procedural Requirements documents 7120.5E and 8705.4 for additional details on risk classifications for NASA payloads). PACE carries a baseline observatory design life of three years after 60-day in-orbit checkout. GSFC hosts three major mission segments: the space segment (SG), ground segment (GS), and science data segment (SDS) (Figure 1.2).

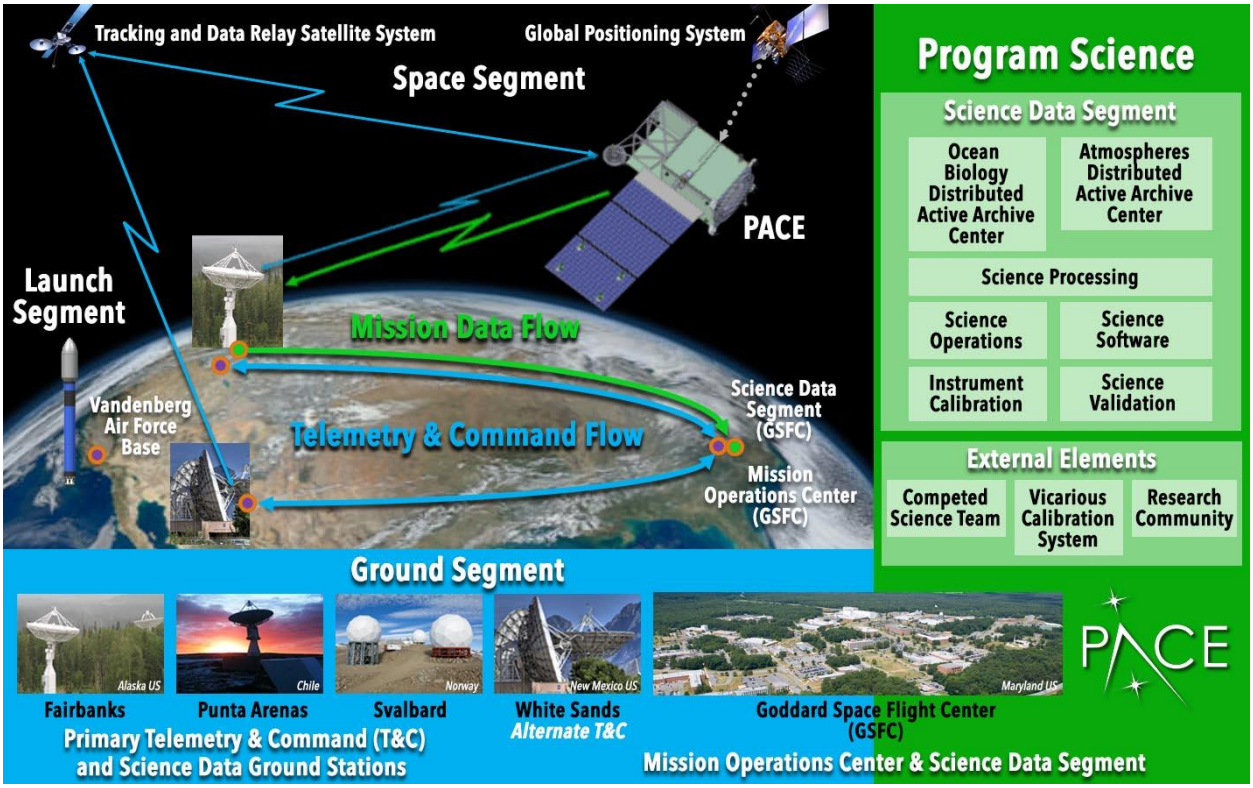

Figure 1.2. Mission segment architecture.

The space segment (SS) is funded and managed by the PACE Project and consists of the observatory (the spacecraft, the OCI, and two cubesat-sized polarimeters), as well as pre-launch ground support equipment (GSE). GSFC will build the PACE spacecraft per a NASA Headquarters Acquisition Strategy Meeting held in August 2016 (Figure 1.3). Science data (as well as housekeeping telemetry data from the spacecraft and the instruments) are stored on solid-state recorders. Data are downlinked to the Near-Earth Network (NEN) ground stations via a Ka-band communications link, as scheduled by the ground segment. The observatory will also receive ground commands and transmit real-time housekeeping telemetry via an S-band up link via the NEN during nominal operations and via the Space Network (SN)/Tracking and Data Relay Satellite System (TDRSS) during launch and early orbit, and contingency operations.

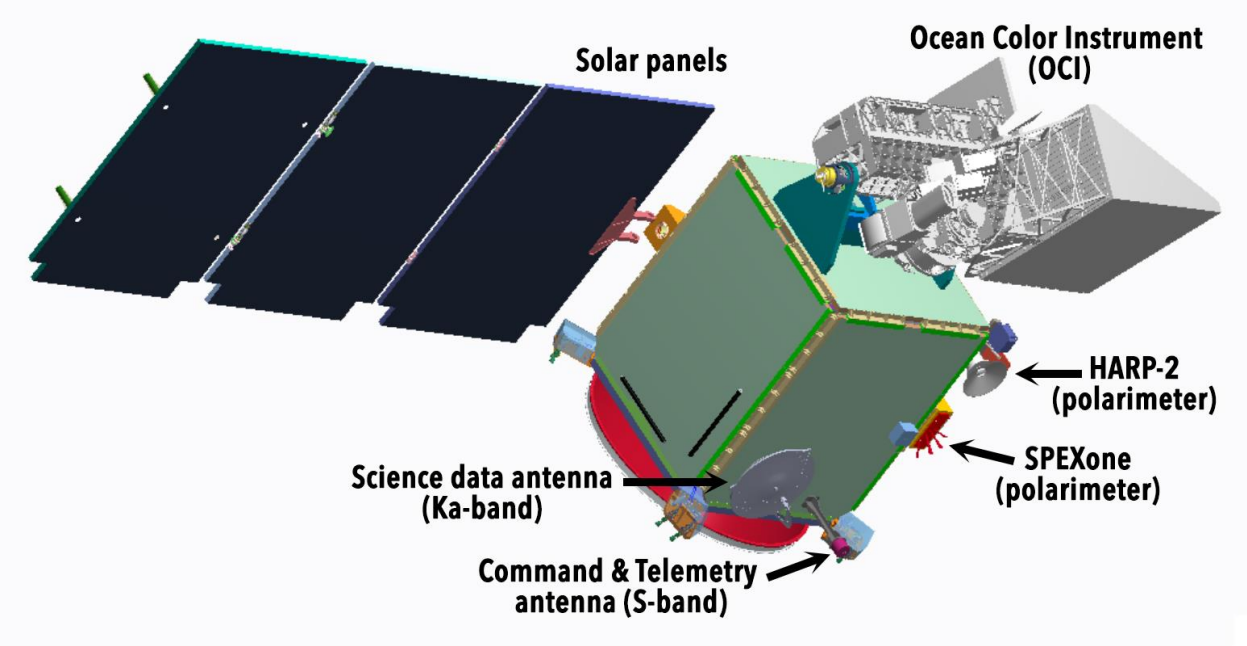

Figure 1.3. Potential PACE spacecraft concept design (as of February 2018).

The ground segment (GS) is funded and managed by the PACE Project and provides for the command and control, monitoring, and health and safety of the observatory on-orbit, as well as ensuring the science data are accounted for and delivered to the SDS (Figure 1.4). The GS provides mission planning and scheduling, coordination with the ground stations for the Ka-band downlink of the data, generation of the observatory command loads necessary to execute the mission plan, spacecraft and instrument trending, and all day to day operations required to sustain of the PACE observatory. The Mission Operations Center (MOC) will be developed, integrated, and operated at GSFC. The MOC houses the flight operations team (FOT) and is being operated and managed by the PACE Project through observatory commissioning. After commissioning, the PACE Mission and FOT will be managed by the GSFC Earth Science Mission Operations (ESMO) project.

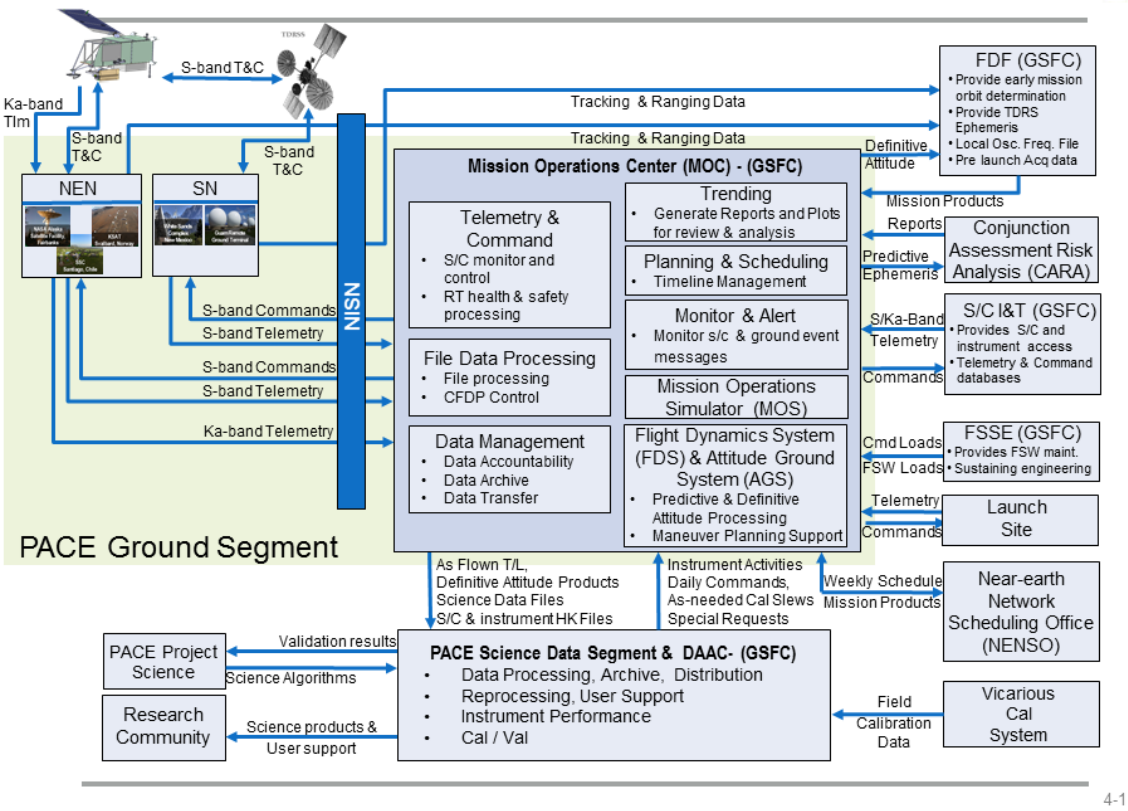

Figure 1.4. PACE ground and operations architecture.

The science data segment (SDS), co-located within the OBPG, is funded by HQ Program Science, and works directly with the PACE Project to define interfaces, develop mission operations concepts, support mission reviews, and participate in routine schedule and budget activities. The SDS provides the ingest, processing, and quality control of the science data, science software development and algorithm integration, science data interface to the competed science team, and delivery of all science data products to the ESD-assigned Ocean Biology Distributed Active Archive Center (OB.DAAC) (Figure 1.5). The OB.DAAC will acquire science mission data from the SDS, but is not a part of the PACE GS and is funded separately by ESDIS. In support of the mission operations after launch, the SDS also works with the Project Science team and the flight operations team to generate de-conflicted instrument schedules for routine, special, and contingency operations.

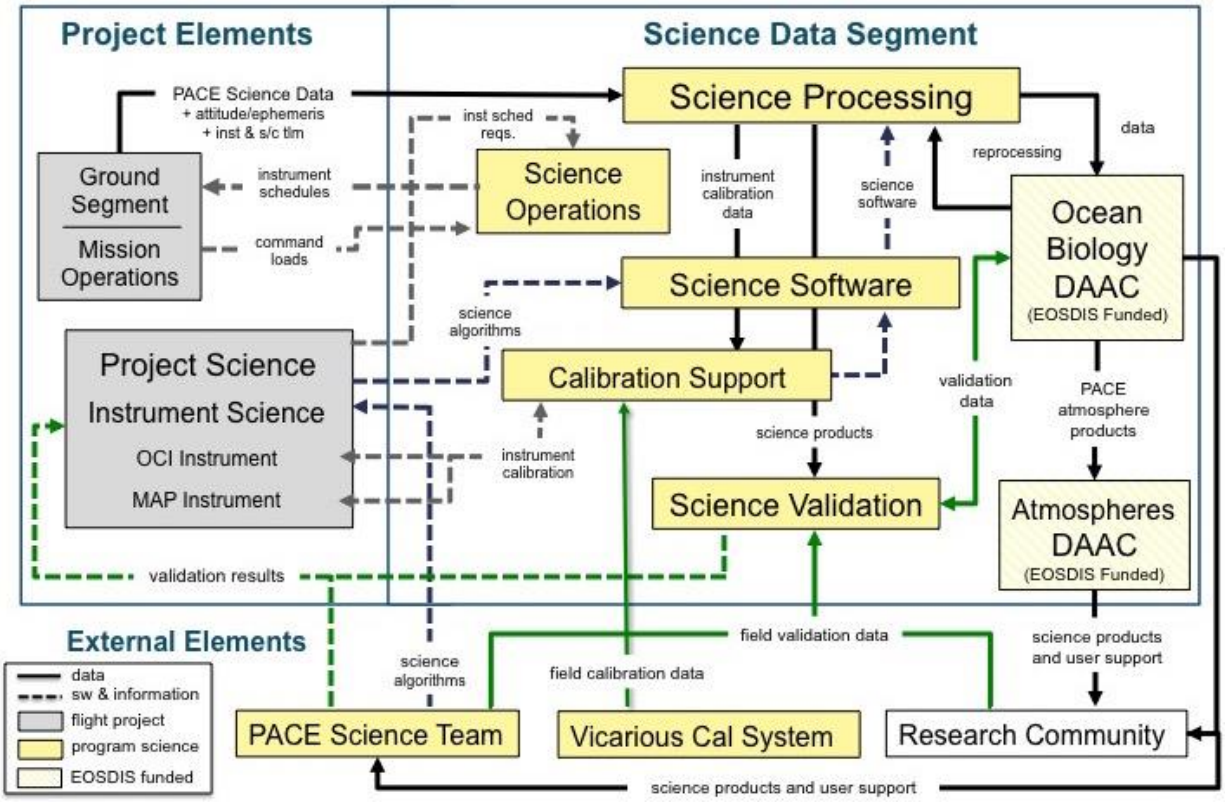

Figure 1.5. Science data segment interfaces.

1.5. Instrument Management and Organization

At the time of the publication of this volume, the PACE observatory is planned to be comprised of three instruments, the OCI and two cubesat multi-angle polarimeters, the Hyper-Angular Rainbow Polarimeter instrument (HARP2) and the Spectro-Polarimeter for Planetary Exploration One (SPEXOne). The OCI is the primary instrument on the observatory and is being developed at GSFC. It is a hyper-spectral scanning radiometer designed to measure spectral radiances from the ultraviolet to shortwave infrared to enable advanced ocean color and heritage cloud and aerosol particle science. Mission-level and OCI-specific requirements are provided in Volume 6 of this Technical Report series. Mission trade studies related specifically to OCI are provided in Volume 7 of this Technical Report series.

The OCI is being developed in-house by GSFC Flight Projects Directorate (FPD) Instrument Projects Division (IPD). The IPD has primary institutional management responsibility and assigns an Instrument Project Manager (IPM) that manages the design, development, integration and testing, and delivery of instrument hardware, software, and GSE needed to perform the scientific experiments, calibration, science data analysis, and data gathering defined for PACE. An Instrument Scientist (IS) reports to the Project Scientist and IPM and maintains responsibility for instrument performance assessment, calibration assessment, and other analyses necessary to ensure that science requirements are being met by the instrument.

Both the HARP2 and SPEXOne are acquired outside of GSFC and will be described in detail in a subsequent volume in this series. The HARP2 is a contribution to PACE by the University of Maryland Baltimore County (UMBC) and the SPEXOne is a contribution to PACE from the Netherlands Institute for Space Research (SRON). These instruments will be developed and qualified at the developer's home institution. Following a successful Pre-ship Review, where requirements will be verified by the Project, each instrument will be formally delivered to the PACE Project. The instruments will be integrated on to the spacecraft at the GSFC. Project Science will work with the instrument providers through the life of the mission.

1.6. Integration and Testing and Mission Operations

The Integration and Testing (I&T) effort will be managed by the PACE Project and executed by the I&T team, spacecraft subsystem teams, instrument teams, and ground system teams at GSFC. This effort will demonstrate that the flight hardware and ground system hardware comply with the mission requirements. All components will be fully qualified, including environmental testing, prior to delivery to I&T. The OCI Team is responsible for the integration, performance testing, and environmental testing of the OCI at GSFC. The Polarimeter providers are responsible for the integration, performance testing, and environmental testing of the polarimeter instruments at the provider facilities. Upon completion, the instruments will be delivered to the spacecraft at GSFC for spacecraft integration and testing. Prior to the instrument integration onto the spacecraft, interface simulators will be used to verify the interfaces and software.

Once the PACE observatory is fully integrated and configured, observatory testing will be performed including comprehensive performance tests. Observatory tests will include environmental tests that are appropriate at the observatory level including thermal vacuum, vibration, acoustics, electromagnetic interference/compatibility, and magnetics. Observatory testing will also include mission simulations and end-to-end testing with the ground system to ensure command and telemetry capability with the mission and science control centers. These mission simulation exercises will also validate nominal and contingency mission operations procedures and provide operator training. Recorded and real-time satellite data will be relayed through the operational ground system to verify data compatibility with the ground system and data processing facility. At the completion of the observatory performance, environmental, and mission test program, the Project will ship the observatory to the launch site. The observatory will be processed at the payload processing facility and integrated onto the launch vehicle.

All PACE operations will be located at GSFC. The observatory flight operations will be conducted from the GSFC MOC. The MOC will perform all real-time operations and off-line operations functions, including planning and scheduling, orbit and attitude analysis, housekeeping telemetry data processing, monitoring/managing the spacecraft and instruments, first line health/safety for the instruments, and housekeeping archiving and analysis. In support of the mission operations, the SDS works with the Project Science team and the flight operations team to generate de-conflicted instrument activity schedules for routine, special, and contingency operations. This instrument activity schedule is provided to the mission operations team, located at the MOC, for mission planning and integration with observatory activities and ground contact schedules.

1.7. Concluding Remarks

The PACE mission represents NASA's next great investment in satellite ocean color and the combined study of Earth's ocean-atmosphere system. This chapter serves as an introduction to this volume by summarizing the mission architecture, ranging from its scientific rationale to the history of its realized conception to its present-day organization and management. The remainder of this volume provides topical summaries of various aspects of the OCI concept design and general observatory behavior. Many of these studies were integral in shaping an amorphous observatory concept into something viable and scientifically meaningful.

Chapter 2

Analysis of PACE OCI Coverage Loss from Glint and Tilt Change

Frederick S. Patt, Science Applications International Corporation, Reston, Virginia[2]

Executive Summary

The Phytoplankton, Aerosol, Cloud, ocean Ecosystem (PACE) Ocean Color Instrument (OCI) is required to mitigate Sun glint from the ocean surface. This mitigation is performed by tilting the instrument field-of-regard along-track, aft prior to the spacecraft subsolar point in the orbit and forward after this point. A capability has been developed to model the combined effects of the glint and tilt change on global coverage. This paper describes the methods and presents sample results. The results have been used to arrive at a mission requirement to perform the tilt change in 60 seconds to limit the combined global coverage loss from high glint and the tilt change.

2.1. Introduction

The Plankton, Aerosol, Cloud, ocean Ecosystem (PACE) mission is a polar-orbiting, Earth remote sensing mission that is planned to launch in 2022. The primary instrument on the PACE observatory is the Ocean Color Instrument (OCI). The OCI is a hyper-spectral scanning (HSS) radiometer designed to measure radiances continuously in the ultraviolet to near-infrared spectral region over the range 350 to 800 nm, and in the near-infrared to short wave infrared (SWIR) spectral region. The OCI threshold spatial resolution is approximately 1 km-squared at nadir with 2-day global coverage. The OCI design has a scanning telescope with a field of regard of +/- 56.5 degrees across track. PACE will be launched into a Sun-synchronous orbit at an altitude of 676.5 nm and an ascending node crossing local time of 13:00.

A significant contaminant of ocean remote-sensing data is sunlight reflected from the ocean surface, known as Sun glint. The magnitude and extent of Sun glint is a function of viewing geometry, solar illumination and wind speed [*Cox and Munk*, 1954]. The effects of glint can be modelled and corrected up to a point, but severe ("high") glint, which occurs close to the specular reflection geometry, degrades the science data quality and therefore reduces effective coverage, i.e, it is "masked" and not used to derive data products.

The most effective glint mitigation strategy is to rotate, or tilt, the sensor view along-track, thereby shifting the sensor view away from specular reflection angles and reducing the glint magnitude. Tilting can be performed by either the sensor or the spacecraft; in the latter case, the tilt is performed by a pitch maneuver. Past sensors designed specifically for ocean color remote sensing, including the Coastal Zone Color Scanner (CZCS), Ocean Color and Temperature Scanner (OCTS) and Sea-viewing Wide Field-of-view Sensor (SeaWiFS), had a tilt capability included in the sensor design.

[2] Cite as: Patt, F. S. (2018), Analysis of PACE OCI Coverage Loss from Glint and Tilt Change, in *PACE Technical Report Series, Volume 5: Mission Formulation Studies (NASA/TM-2018 – 2018-219027/ Vol. 5)*, edited by I. Cetinić, C. R. McClain and P. J. Werdell, NASA Goddard Space Flight Space Center Greenbelt, MD.

The most commonly used tilt angle is 20 degrees. CZCS had a commandable range for the tilt angle of the scanning mirror (not the entire instrument), and while in the beginning of the mission tilt angles less than 20 degrees were used, soon after was decided to always command the tilt to 20 degrees. Both OCTS (scan mirror) and SeaWiFS (spacecraft pitch) had commandable tilt angles of +/- 20 degrees and 0 (i.e., nadir).

In order to effectively reduce Sun glint, the sensor must be tilted away from the orbit subsolar point (the point in the orbit where the subsatellite track is closest to the Earth subsolar location). This requires that the tilt angle be changed from aft to forward at or near the subsolar point. The tilt change results in a gap in sensor coverage, resulting from the combination of the change in viewing geometry and the time required for the change. Although the sensor does not stop collecting data during the tilt change, the pointing knowledge is less accurate, so the data are flagged. At the PACE altitude, the change in the tilt angle results in a gap of about 4.5 degrees latitude, plus 0.061 seconds for each second of tilt change time plus settling.

Although tilting the sensor is effective at reducing the glint, some amount of data will be lost to high glint even at a tilt angle of 20 degrees. This, plus the tilt change coverage loss, results in a net loss of coverage that depends on the tilt angle and change time. The method used to analyze the loss in coverage and the results for a range of tilt angles and change times are presented in the following sections.

2.2. Analysis Methods

The PACE Level 1 requirement (when this chapter was written) is to achieve two-day coverage for OCI within the solar zenith angle limit of 75 degrees. This analysis was structured to determine the impact of high glint and the tilt change as they relate to data losses within this two-day coverage. The analysis consisted of the following stages:

A. Simulate PACE geolocation for the mission orbit and OCI viewing geometry.

B. Develop a tilt change strategy to maximize two-day coverage for a given tilt angle and change time.

C. Simulate the Sun glint based on the sensor geolocation.

D. Determine the loss in global coverage over a two-day period.

Each of these steps is described in the following sections.

2.2.1. PACE Geolocation Simulation

The simulation of PACE geolocation involves the following steps:

1. Simulate the PACE orbit
2. Construct the OCI view vectors
3. Compute the OCI geolocation for each desired time sample

To reduce the time required for the analysis runs, it was decided to subsample the PACE geolocation for the simulation. Specifically, the scan period was set to 2 seconds and the scan angle interval to 0.5 degree, compared to 1/6 second and 0.085 degree for OCI. These settings correspond to a maximum GSD of 18 km. As will be explained below, the coverage analysis used a spatial resolution coarser than this GSD, so the subsampling had no effect on the results.

The PACE orbit was simulated for March 24 and 25, 2020. The simulation was performed using a set of two-line elements (TLEs) and the SGP4 orbit model software. The TLEs were based on a set provided by the Flight Dynamics Facility (FDF), representing the PACE orbit described in the Introduction, and modified for an epoch of 00:00 UTC on March 24, 2020. The SGP4 model was run with a 1-minute sample interval, and the output was then interpolated to 2-second intervals using the method of *Patt* [2002]. Only the ascending orbit samples were used, corresponding to the daylit part of the orbit.

The OCI view vectors were based on a simple, planar scan model, representing the ideal sensor scan geometry; in the sensor reference frame, the vectors lie in the Y-Z plane, where +Z is the scan center. The vectors were constructed, as stated above, at 0.5-degree intervals over the scan angle range of +/-56.5 degrees, or 227 samples per scan.

The geolocation calculations were performed using the method of *Patt and Gregg* [1994]. The tilt angle was set as the pitch angle for the sensor attitude (the roll and yaw were set to zero). The tilt change strategy is described in the following section. The output of the geolocation includes the viewed location (geodetic longitude and latitude) for each sample, sensor zenith and azimuth and solar zenith and azimuth; the zenith and azimuth angles are used for the glint calculation and also for data selection during the coverage analysis.

2.2.2. Tilt Change Strategy

The tilt change results in a gap in the science data; the size of the gap depends on the tilt angle and change time. The size of the gap vs. tilt angle and change time is illustrated in Figure 2.1. If the tilt change is always performed at the subsolar point each orbit, a persistent gap in global coverage around this latitude range will result. Although the subsolar point moves north and south during the year, on shorter time scales this gap would be present in global data.

For SeaWiFS, a strategy was developed to stagger the tilt change point in the orbit in order to fill in the coverage gap [*Gregg and Patt*, 1994]. The strategy was to shift the tilt change latitude north of the subsolar point for two consecutive days, and then south for the next two days. Thus, over a four-day period the high glint and tilt change gaps were largely filled in.

For the OCI tilt analysis, a two-day tilt stagger strategy was developed. This was based on two factors: 1) the period used for the analysis was two days, based on the Level 1 requirement; 2) the difference between the PACE and SeaWiFS orbits results in a shift in the glint pattern off-center for OCI and a difference in the day-to-day shift in the orbit tracks for PACE compared to SeaWiFS. It was confirmed using the simulations that the two-day strategy resulted in better two-day coverage for the PACE orbit.

As stated above, the subsolar point in the orbit is the point where the orbit track is closest to the subsolar point on the Earth. For the PACE orbit (13:00 local time ascending node) this point will be slightly north of the subsolar latitude. During actual OCI scheduling the subsolar point will be computed each orbit using the actual orbit track and Sun vector; however, given the limited duration of this simulation, the subsolar point was estimated to be 0.035 above the solar latitude (all angles in radians). The nominal (non-staggered) tilt change start point was determined using the orbit rate (0.001064/sec) and the tilt change time; the start point was shifted south by half of the tilt change time.

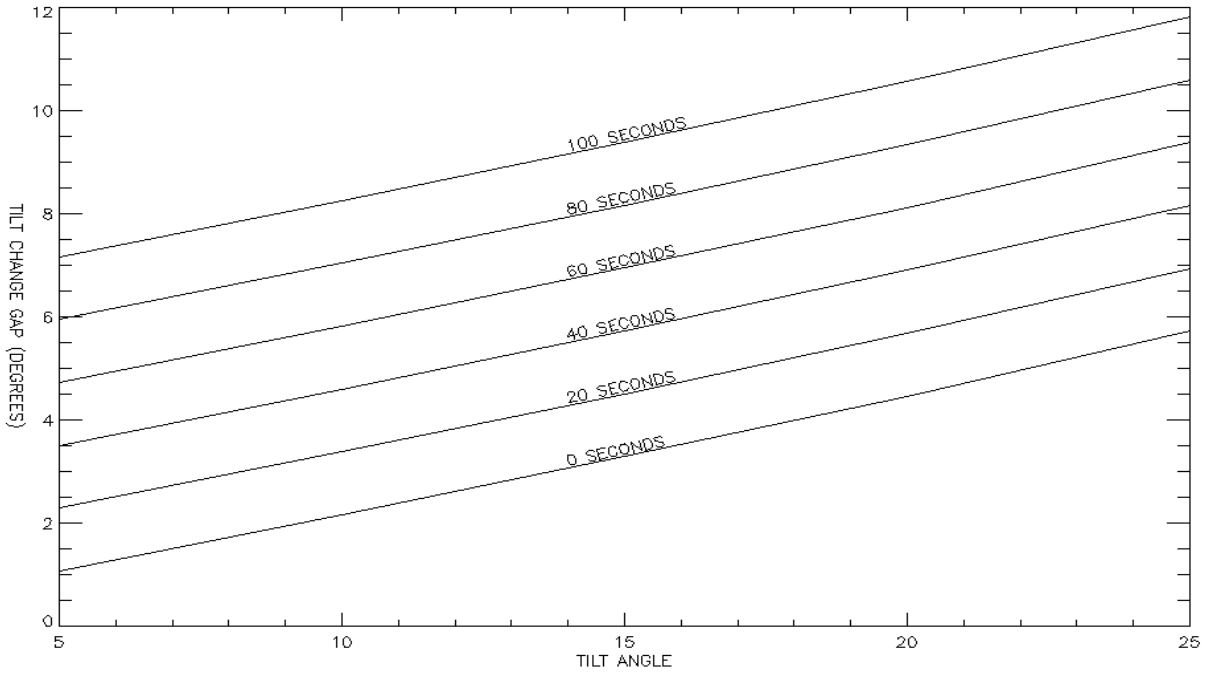

Figure 2.1. Tilt change gap, in degrees along the subsatellite track, for various tilt angles and tilt change times.

The implementation of the staggered tilt strategy requires the calculation of an offset to the tilt change start point; the start point is then offset either north or south by this amount. In order to effectively fill in the tilt change gap, the offset is computed using both the tilt angle and change time:

$$Poff = Ttilt*0.001064/2 + 0.106*\tan(tilt) + 0.015 \qquad \text{(Eq. 2.1)}$$

where Poff is the offset (in radians) to the tilt change start point in the orbit, and Ttilt is the tilt change time. As stated previously, the orbit rate is 0.001064/sec, and the factor of 0.106 is the ratio of the tilt coverage gap to the tangent of the tilt angle. Finally, the constant of 0.015 was determined empirically to improve the two-day coverage. The results of this tilt change strategy will be shown in combination with the glint results below.

2.2.3. Sun Glint Simulation

The Sun glint was simulated using a method based on *Wang and Bailey* [2001]. These are the same equations implemented in the ocean color processing software. The glint was simulated using a wind speed of 7 m/sec, approximately the global average at the ocean surface [*Archer and Jacobson*, 2005]. As stated above, the glint calculation also uses the sensor and solar zenith and azimuth angles computed as part of geolocation. The output of the glint calculation is the glint coefficient, which has units of sr^{-1}, for each geolocated OCI sample. The threshold for high glint is a coefficient of 0.005 sr^{-1}, also from *Wang and Bailey* [2001].

2.2.4. Global Coverage Analysis

The global coverage analysis was based on the Level 1 requirement for two-day coverage within the solar zenith limit of 75 degrees and based on a sensor zenith limit of 60 degrees. The first step in the coverage analysis was to select the geolocated OCI samples using these limits. Samples were also excluded that exceeded the glint coefficient threshold of 0.005 sr^{-1}. The results of this data selection for a single day

near an Equinox are shown in Figure 2.2; this example used a tilt angle of 20 degrees and a tilt change time of 30 seconds. The figure shows the inter-orbit gaps resulting from the sensor zenith limit, the tilt change gaps at mid-orbit, and the small residual high glint before and after the tilt change.

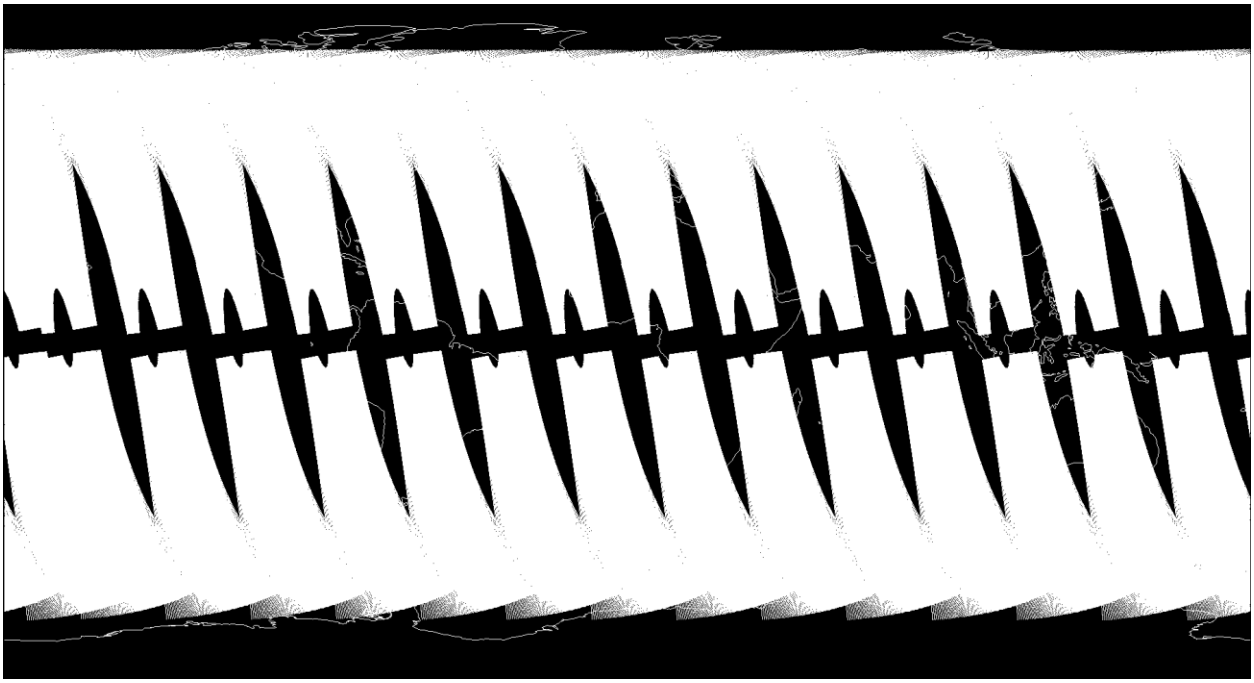

Figure 2.2. One-day OCI coverage showing the solar and sensor zenith limits, the tilt change gaps and the high glint exclusion.

To analyze the global coverage, the data were binned at ⅛-degree resolution in latitude and longitude. This resolution provides coverage analysis accuracy of better than 0.001%. The binning avoids the double-counting of locations at higher latitudes where the orbits overlap. The coverage was computed within the 75-degree solar zenith limit. To convert the equal-angle bin results to equal-area, the number of bins in each row was scaled by the cosine of the latitude. The total number of filled bins was then divided by the maximum number within the solar zenith range to determine the global coverage.

2.3. Results

The geolocation/glint simulation and coverage analysis were initially run for a tilt angle of 20 degrees, and tilt change times ranging from 30 to 120 seconds, including settling time. The results for a two-day run with a tilt change time of 30 seconds are shown in Figure 2.3. As shown in the figure, the inter-orbit gaps have filled in except where they coincide with high glint or tilt change gaps from the other day. Unlike the one-day results, there is no latitude zone of missing coverage. The staggered tilt appears to be doing a reasonable job of optimizing the global coverage.

Figure 2.3. Two-day OCI coverage showing the residual tilt change gaps and high glint for 20 degrees tilt and 30 seconds tilt change time.

The results for a 60-second tilt change time are shown in Figure 2.4. This figure shows the larger tilt change gaps resulting from the longer change time.

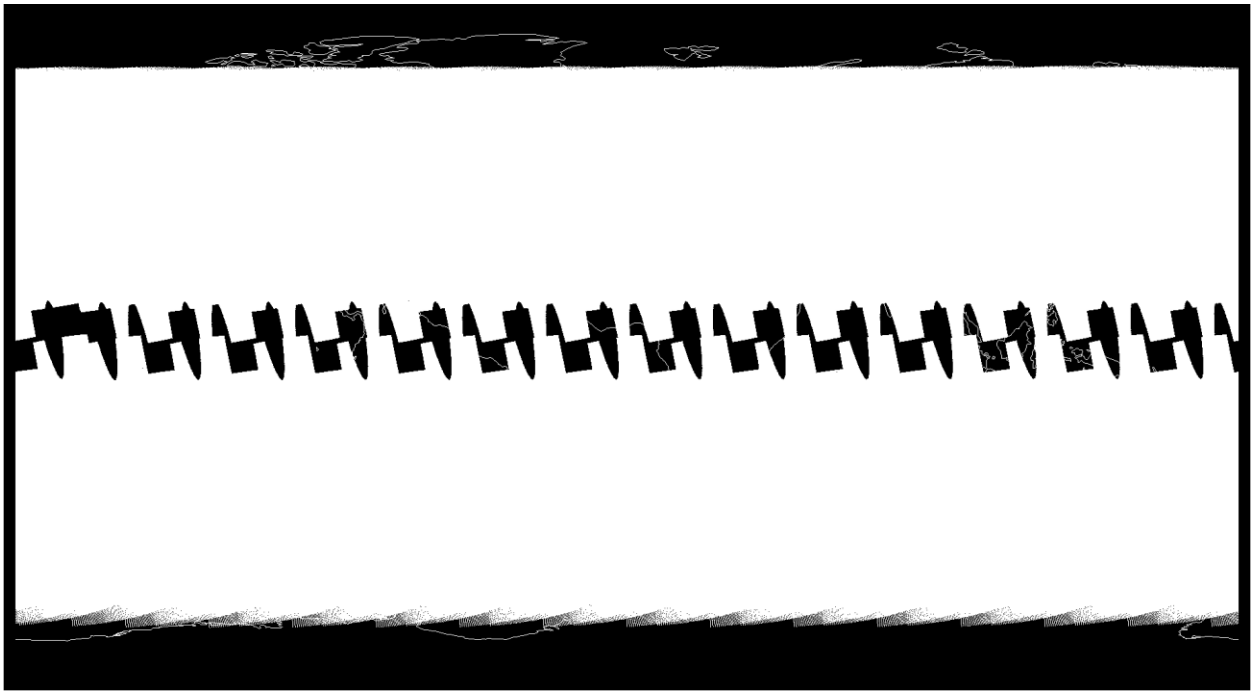

Figure 2.4. Two-day OCI coverage for a tilt change time of 60 seconds.

The simulation and analysis were repeated for dates near the Summer and Winter solstices as well as the Equinox, and also for the no-tilt case for comparison. The coverage loss results for all cases are shown in Table 2.1.

Table 2.1. Global and Tropical Coverage Loss vs. Tilt Change Time for a 20-degree Tilt

Tilt Change Time (seconds)	Global Coverage Loss (%)		
	Summer Solstice	**Equinox**	**Winter Solstice**
30	5.689	6.828	6.305
60	6.538	7.879	7.073
80	7.115	8.603	7.612
100	7.665	9.315	8.184
120	8.151	9.996	8.742
No tilt	9.261	12.641	10.589

Based on the results of this analysis, the mission requirement for the tilt change time was set to 60 seconds, including settling time.

Following the initial analysis, a more extensive analysis was performed to consider a range of tilt angles as well as tilt change times. The range of tilt angles included was 0 to 25 degrees at 5-degree increments, and the range of tilt change times was 0 to 100 seconds (including settling) at 20-second increments (except for 0 degrees tilt, which does not require a tilt change). Although a tilt change time of 0 seconds is not possible for a non-zero tilt, this was included to illustrate the geometric effect of the tilt change.

The geolocation simulation and coverage analysis were performed for each combination of tilt angle and change time, following the same steps as described in Section II. The results are shown in Figure 2.5; coverage loss of 7%, approximately the annual average for a 60-second tilt change time, is shown as the horizontal line on the plot.

The figure shows that the time allowed for the tilt change decreases rapidly as the tilt angle decreases, in order to maintain a given coverage loss. This is due to the rapid increase in the area affected by high glint at lower tilt angles, even though the tilt change gap is also reduced. The figure also shows an additional reduction in coverage loss for a tilt angle of 25 degrees, although the improvement is less than that seen between 15 and 20 degrees.

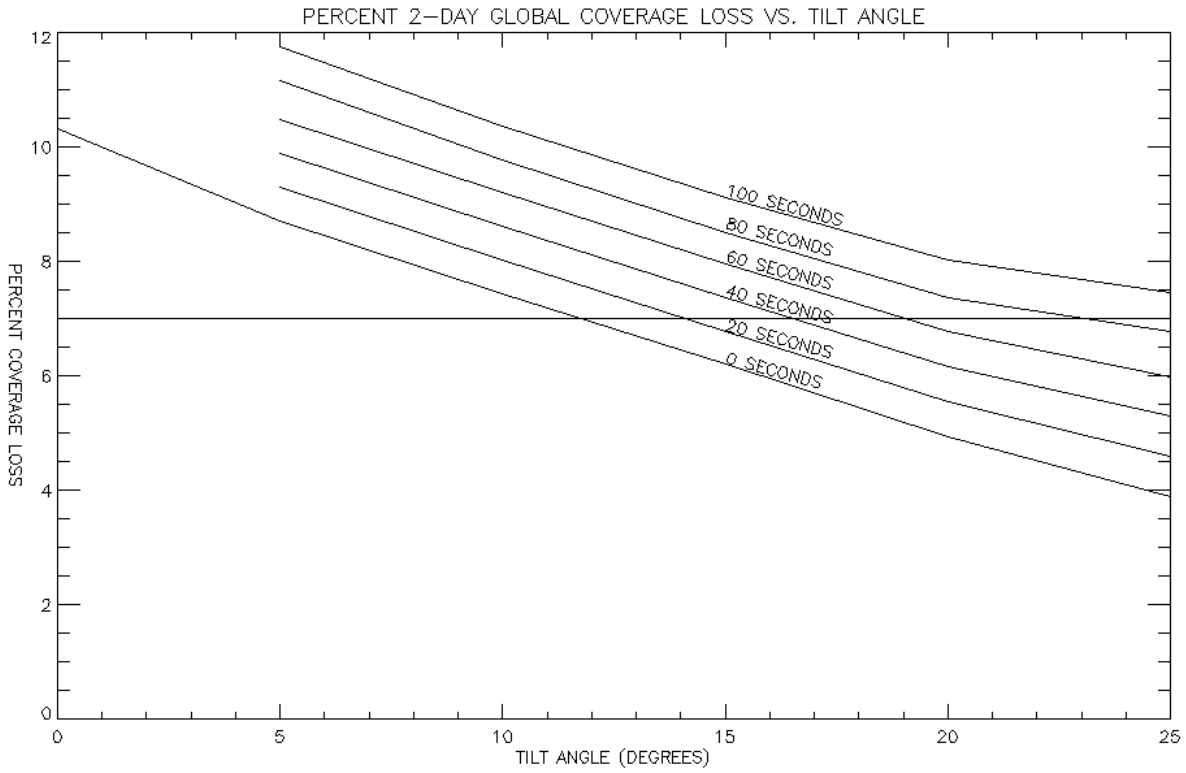

Figure 2.5. Coverage Loss vs. Tilt Angle and Tilt Change Time

2.4. Conclusion

An analysis was performed of the PACE OCI global coverage loss due to high glint and tilt change. This consisted of simulating the OCI geolocation, modeling the glint at the viewed locations, and determining the global coverage within mission parameters. As part of the simulation, a tilt change stagger strategy was developed to optimize the two-day coverage.

The analysis was performed over a range of tilt angles and change times that span the values currently being considered for the mission. The results of this analysis were used to arrive at the mission requirement to perform the tilt change in 60 seconds or less, to minimize the global coverage loss over two days due to the combined effects of high glint and tilt change. These results will also inform decisions regarding the design and configuration of the tilt capability and the development of the operational tilt strategy.

Chapter 3

Case Study on the Science Data Completeness Requirement for PACE

Jeremy Werdell, NASA Goddard Space Flight Center, Greenbelt, Maryland[3]

Executive Summary

This case study defines the science data completeness requirement for the Plankton, Aerosol, Cloud, ocean Ecosystem (PACE) Ocean Color Instrument (OCI). The mission adopted a >93.33% data completeness requirement, with data completeness defined as normal operations of the OCI (e.g., versus time spent in safe hold) and held separately from the Level-1 requirement for two-day global coverage. The 99.33% corresponds to allowing <2-days of data loss per month on average, which is sufficient to meet PACE Level-1 requirements related to data product generation and their associated uncertainties.

3.1. Introduction

Resolving critical ocean basin- and climate-scale science questions requires complete global maps on weekly and monthly time scales, respectively. Note that other regional science questions (e.g., upwelling zones, at frontal boundaries, and in tidal estuaries) require much finer temporal resolution, but do not drive the prime science of this mission and do not appear as considerations in this study (see, e.g., the PACE Science Definition Team report [2018]) An instrument that avoids contamination by Sun glint (normally accomplished by tilting) with two-day global coverage and a ground sample distance (GSD) of no more than 1000 m at nadir provides the best-known polar-orbiter configuration for achieving the temporal and spatial scales required to address basin- and climate-scale science questions. OCI will likely achieve this configuration, however, the question remains as to how often it can fail to collect data and still meet the science requirements for the mission.

3.2. Analysis

3.2.1. A Review of Global Ocean Color Retrievals

The case study presented here defines the science data completeness requirement for OCI in terms of allowable days lost each month. In this study, two heritage satellite instruments are considered: (1) SeaWiFS, which tilted to avoid Sun glint and provided 9-km global maps; and (2) MODISA, which does not tilt and provides 4-km global maps.

[3] Cite as: Werdell, P. J. (2018), Case study on the science data completeness requirement for PACE, in *PACE Technical Report Series, Volume 5: Mission Formulation Studies (NASA/TM-2018 – 2018-219027/ Vol. 5)*, edited by I. Cetinić, C. R. McClain and P. J. Werdell, NASA Goddard Space Flight Space Center Greenbelt, MD.

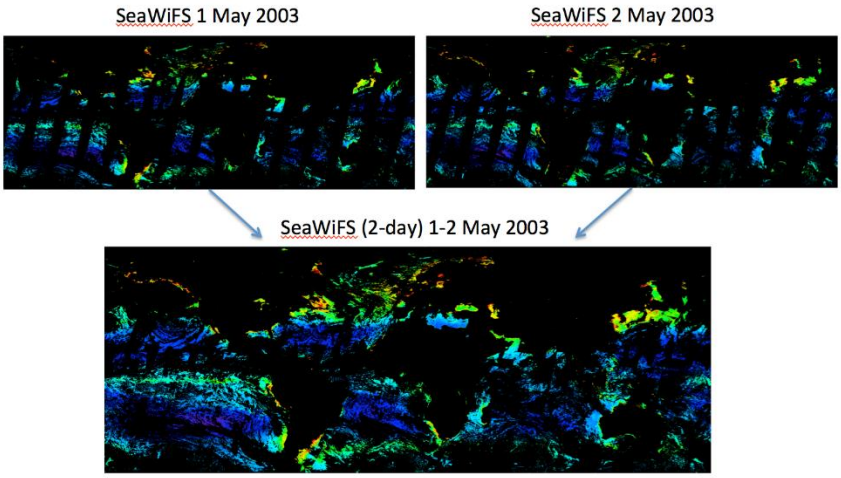

Figure 3.1: Two days of SeaWiFS data and their two-day composite (9-km). Black pixels indicate either land or missing data due to clouds, atmospheric aerosols, and Sun glint.

Despite the truncation of SeaWiFS Global Area Coverage (GAC) data at ±45° (unlike MODISA and OCI, which will provide data to ~58°), SeaWiFS provides the best example to illustrate the anticipated OCI coverage because it tilted to avoid Sun glint (Figure 3.1). While SeaWiFS had two-day coverage (all Earth pixels were viewed at least once every two days) and minimized the loss of pixels due to Sun glint, ocean retrievals were still missed. Ocean color retrievals are limited by the presence of clouds, substantial atmospheric aerosols, and Sun glint. PACE is a multi-discipline mission encompassing clouds, aerosols, and ocean color, however, cloud or aerosol retrievals have fewer limiting factors. As such, ocean retrievals are considered to be the driving requirement for data completeness within this study.

3.2.2. Analysis of Data Completeness

MODISA is used in the remainder of this analysis, as it provides a GSD similar to OCI and, therefore, best illustrates the 4-km spatial compositing expected to be applied to PACE. Figure 3.2 shows chlorophyll-a (a standard ocean color product) from MODISA composited to 7, 14, 21, and 31 days. Figure 3.3 shows the number of daily scenes (N) included in each 4-km ground bin.

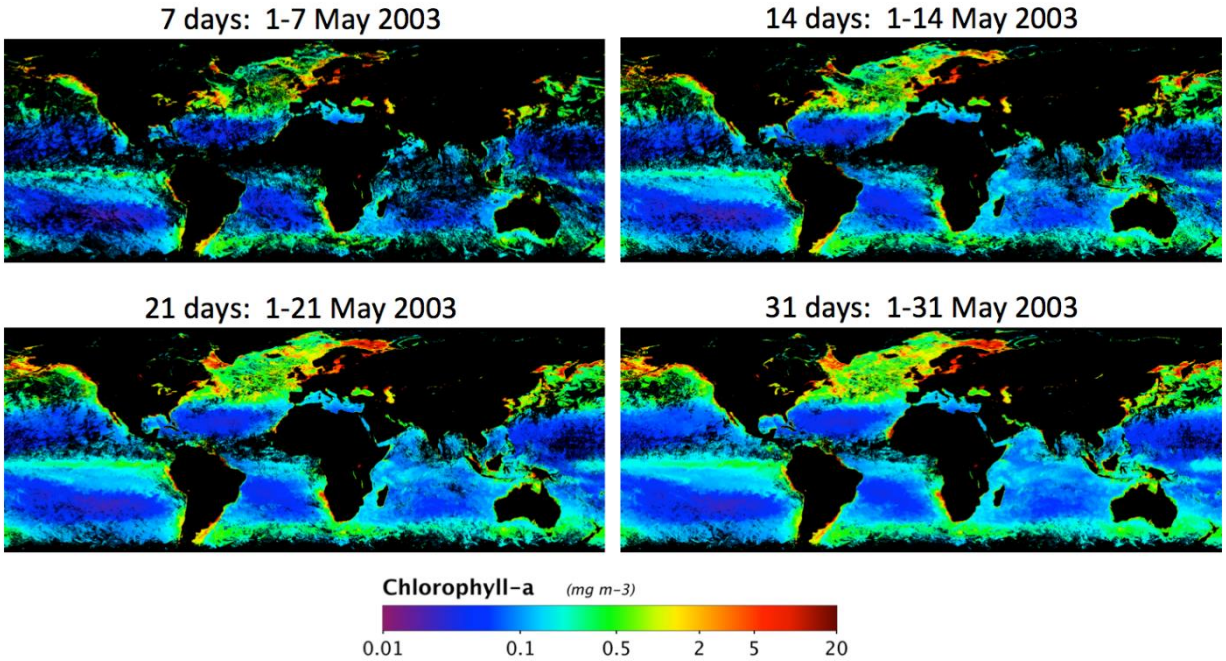

Figure 3.2. MODISA 4-km chlorophyll-a composites. Black pixels defined as in Figure 3.1.

Spatially, the monthly composites are not completely filled and many monthly bins include data from only one or two days. Many of the losses near the Equator are due to Sun glint. OCI is expected to recover those pixels by tilting and the number of observations shown in Figure 3.3 near the Equator will mimic those at higher latitudes. That is, in most cases N=1 will become N>1 and the maps will fill similarly to what is shown for SeaWiFS in Figure 3.1. While not the primary purpose of this study, the use of MODISA in this analysis also illustrates the data completeness impacts of not tilting to avoid Sun glint.

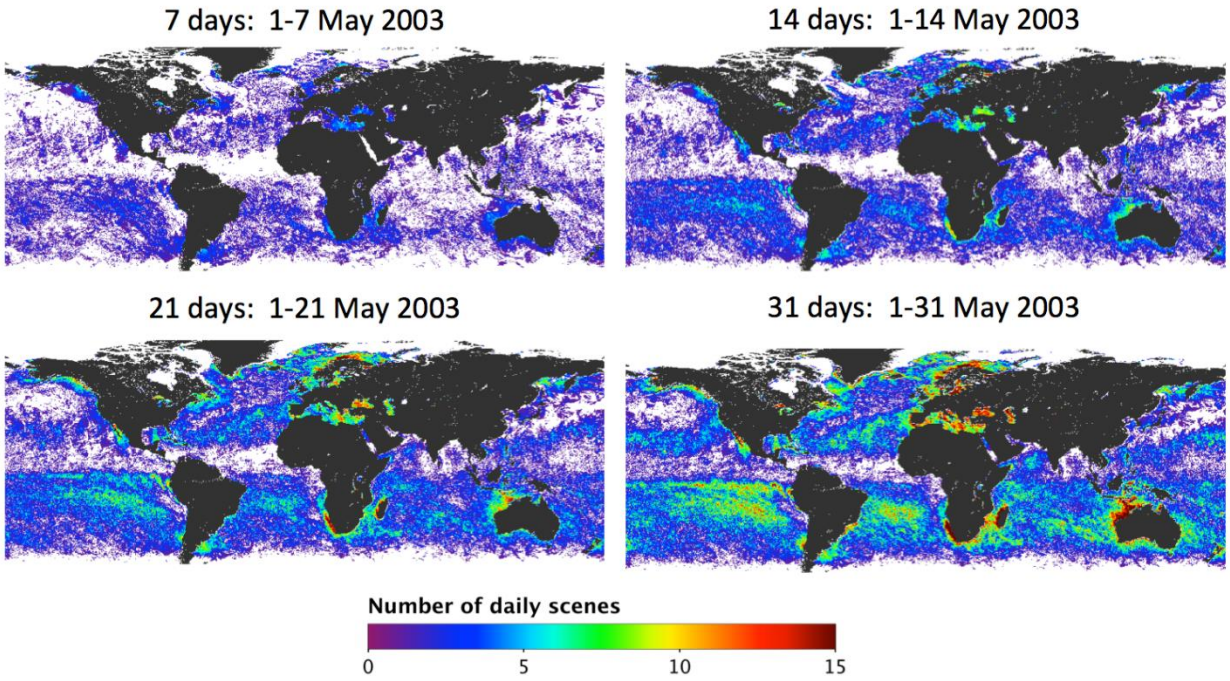

Figure 3.3. MODISA number of daily scenes per 4-km ground bin for the data presented in Figure 3.2.

Histograms of the number of daily scenes per 4-km ground bin reveal that ~60% of weekly scenes include data from only one day and ~37% of monthly bins include data from only one or two days (Figure 3.4 and Appendix A).

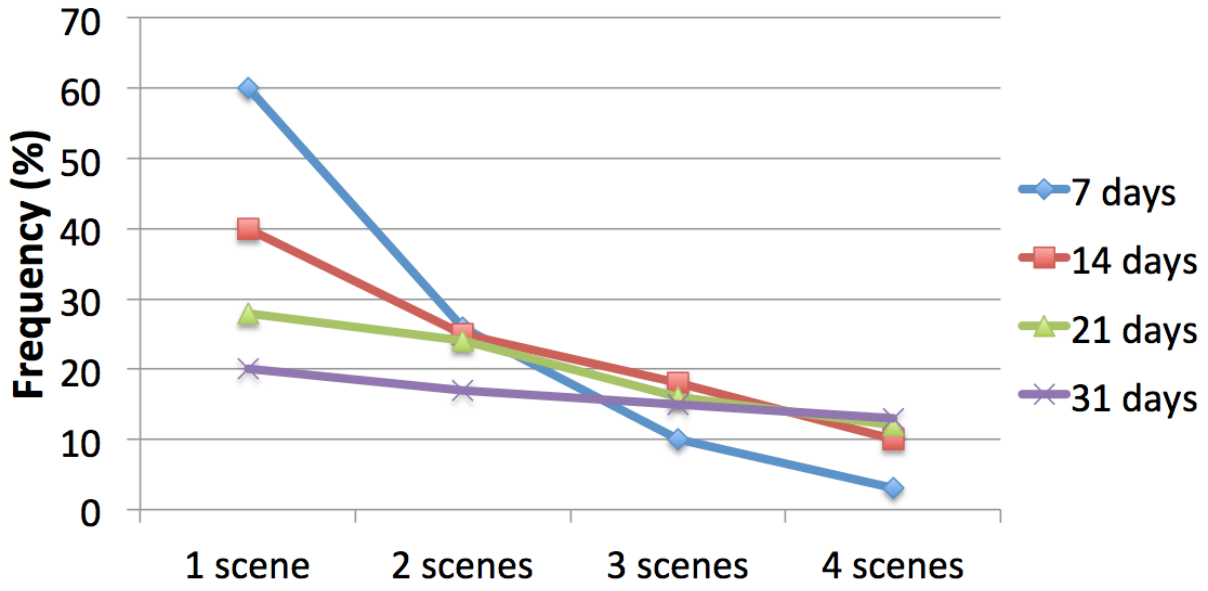

Figure 3.4. Frequency of number of daily scenes (limited to N=1…4) included in the 4-km ground bins for each of the four MODISA temporal composites. The frequency values were generated using data presented in Appendix A.

3.3. Discussion and Conclusion

Given these results, it remains tempting to infer that ocean color science cannot tolerate the loss of any data. This case study suggests that parts of the ocean may not be seen by PACE over the course of the month given cloud cover. Note, that cloud cover varies with season and this analysis only reports results from one month in one season. Ultimately, cloud presence will vary per science pixel over the course of time in an unpredictable manner (unlike Sun glint). Furthermore, the temporal scales of many oceanographic features vary on daily time-scales such that every missed pixel may result in a lost opportunity to see something that may disappear by the time of the next overpass. But, all of that said, these results demonstrate a worst-case scenario because MODISA does not tilt. As stated previously, OCI will recover many more science pixels, particularly between 30°S and 30°N, by tilting to avoid Sun glint (reference TM chapter on Sun glint).

Ultimately, the PACE mission needed to make a choice on allowable data completeness, and other factors come into play under the PACE design-to-cost paradigm:

(1) PACE is primarily a research mission and does not have operational requirements (such as satellites run as part of the National Weather Service);

(2) Safe-holds will inevitably occur during the life of the mission;

(3) Requiring near perfect data completeness adds to mission costs; and,

(4) The Project Science team did not wish to impose harm on the instrument by imposing requirements that, for example, pull the instrument out of safe-hold prematurely.

Furthermore, OCI pushes well beyond the current state of the art in ocean color – adopting all of the benefits of SeaWiFS, which remains the current state of the art with regards to data coverage, while

increasing its composited spatial resolution from 9-km to 4-km. OCI is expected to ultimately provide the best ever global data coverage for the ocean color community.

Given the above and with conscientious consideration of mission costs, the PACE mission adopted the data completeness requirement of >93.33%, which translates to an allowable data loss of <2-days per month. While this recommendation does not strictly follow the results presented in this case study, increasing this requirement to 95% would have added substantial financial burden that could not be tolerated under design-to-cost.

The recommended data completeness requirement does not substantially impact the PACE mission's ability to meet any Level-1 science requirement. The most relevant Level-1 requirement to this study remains the uncertainties assigned to science data products. Achievement of these uncertainties will be verified using coincident satellite-to-*in situ* match-ups using satellite data processed only to Level-2 (daily science data products from Level-1B; neither spatially or temporally composited). Following, data completeness only comes in to play by potentially extending the time period over which one accumulates a statistically relevant number of satellite-to-*in situ* match-ups. Given that many *in situ* data sources collect data autonomously on daily scales, extending this time period is not expected to substantially deter accumulating match-ups over the 18-month threshold mission life. As a thought exercise, consider that MODISA achieved ~240 match-ups in 2007, or roughly 20 match-ups per month. If only 90% of these match-ups were possible because of 10% loss of MODISA data, we would be left with an average of 18 match-ups per month, or 216 total, a sufficiently robust sample size for evaluation of instrument performance.

Finally, this recommended data completeness requirement is not intended to compete with or violate the Level-1 requirement for 2-day global coverage, the intent for which is to offer an opportunity to retrieve a valid ocean color, aerosol, or cloud data product globally every 2-days under normal operating conditions.

3.4. Appendix A.

This appendix provides frequency and cumulative distributions of the number of daily scenes per 4-km ground bin for four MODISA temporal composites, used to generate Figure 3.4.

7 days: 1-7 May 2003

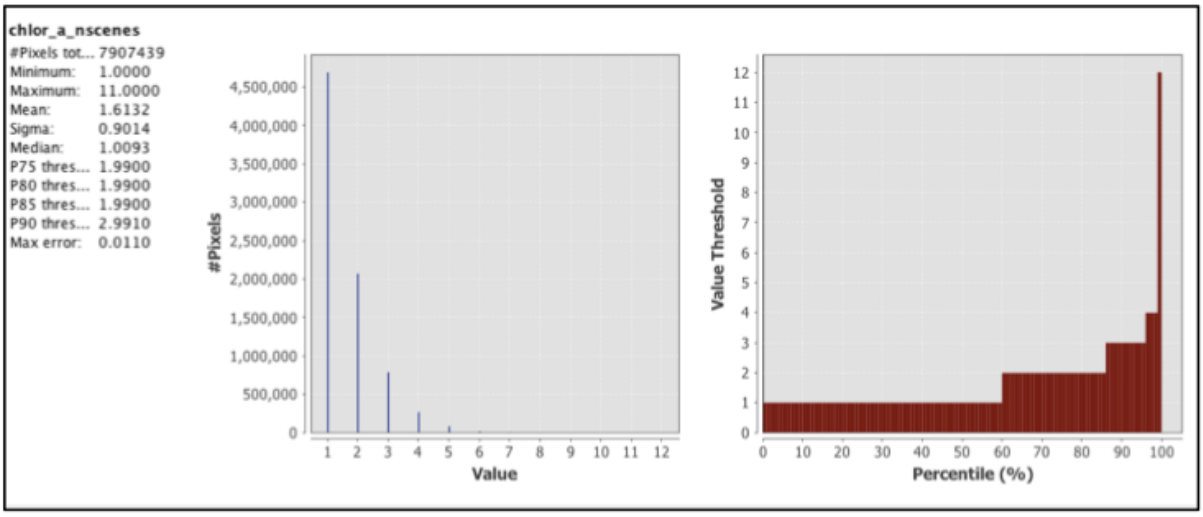

14 days: 1-14 May 2003

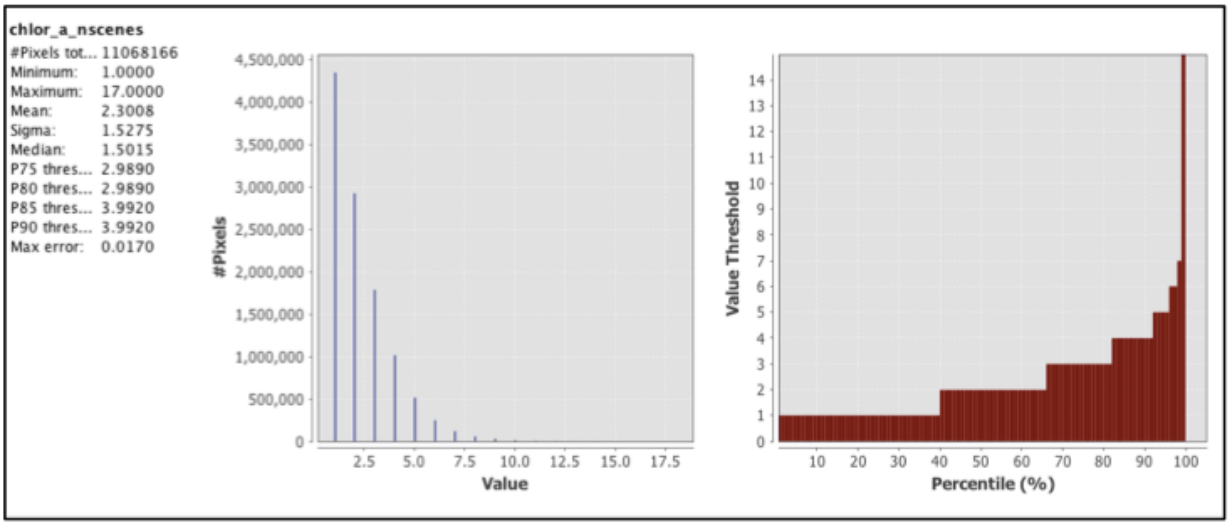

21 days: 1-21 May 2003

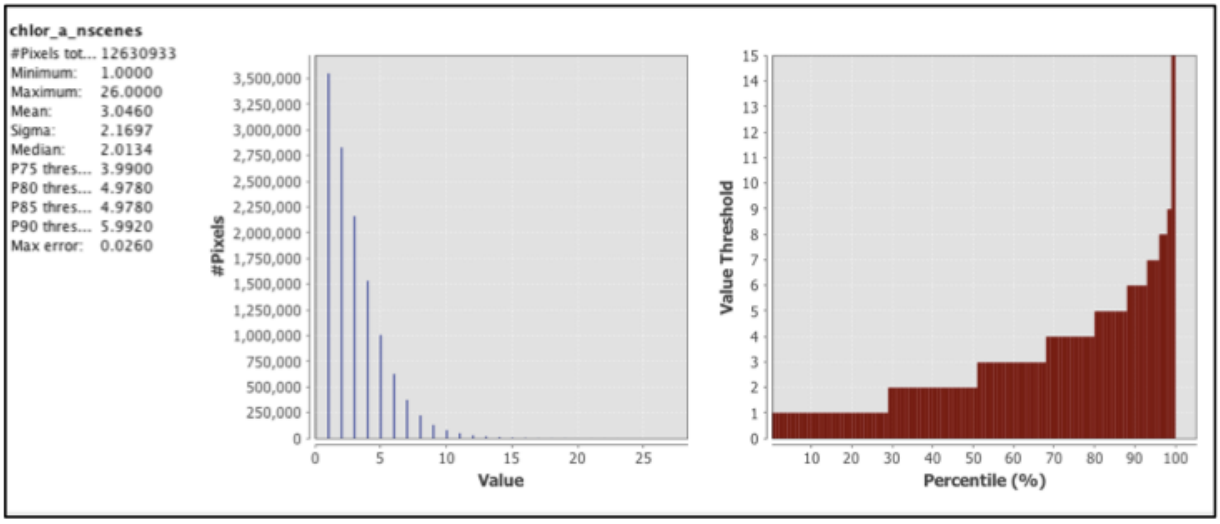

31 days: 1-31 May 2003

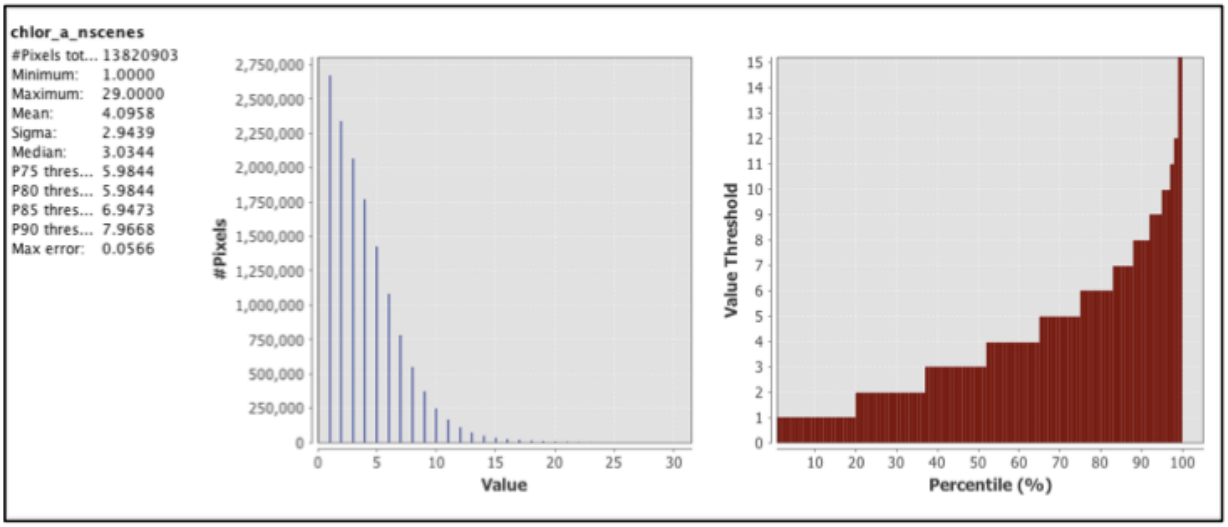

Chapter 4

Assessment of Hyperspectral Pushbroom Image Striping Artifacts in Ocean Color Products

Lachlan I. W. McKinna, Go2Q Pty Ltd, Buderim, Australia [4]

Robert Lossing, Science Applications International Corporation, Reston, VA

Jeremy Werdell, NASA Goddard Space Flight Center, Greenbelt, Maryland

Executive Summary

For pushbroom imaging spectroradiometers, detector-to-detector miscalibration error can cause along-track image striping artifacts. During the pre-Phase A period of the Plankton, Aerosol, Cloud, ocean Ecosystem (PACE) mission, a pushbroom imager design concept was considered for the Ocean Color Instrument (OCI). In this chapter, striping artifacts in the MERIS pushbroom ocean color data were examined, the affects striping artifacts have on science data products were assessed, and the feasibility of 'destriping' pushbroom imagery was considered. Collectively these analyses indicate that a pushbroom instrument would propagate striping artifacts through to ocean color data products causing unwanted uncertainty that may not be easily corrected out using destriping algorithms.

4.1. Introduction

The pushbroom sensor design is common in passive optical remote sensing. The sensor comprises a linear array of photodetectors that simultaneously image *m* cross-track pixels as the spacecraft progresses forward [*McClain et al.*, 2014]. For hyperspectral observations, an optical dispersion element (e.g. a grating) is typically used to split the observed optical beam into *n* spectral bands that are then projected onto the focal plane. Thus, a pushbroom sensor with *m* spatial pixels and *n* spectral bands requires a focal plane with *n* x *m* individual detectors.

Each individual pushbroom detector requires characterization and its own calibration coefficients. For a given spectral band, miscalibration of one or more detector elements can lead to those detectors recording cross-track radiances at intensities different to adjacent cross track pixels. This effect causes distinct along-track lines in imagery commonly referred to as "image striping" as shown in Figure 4.1. Similar to noise, striping artifacts are propagated through data processing algorithms, including atmospheric correction, into derived data products such as water-leaving reflectances (ρ_w) and inherent optical properties (IOPs).

Amongst early design guidelines for the OCI during the PACE Mission's pre-Phase A period was the following criteria for top-of-atmosphere radiometry:

[4] Cite as: McKinna, L. I. W., R. Lossing, and J. Werdell (2018), Assessment of hyperspectral pushbroom image striping artifacts in ocean color products, in *PACE Technical Report Series, Volume 5: Mission Formulation Studies (NASA/TM-2018 – 2018-219027/ Vol. 5)*, edited by I. Cetinić, C. R. McClain and P. J. Werdell, NASA Goddard Space Flight Space Center Greenbelt, MD.

Image striping artifacts, which result from uncharacterized differences in detector responsivity, that are <0.5% and correctable to noise levels

Accordingly, a study was scoped to assist in determining the likely impact pushbroom striping artifacts would have upon derived science data products. This chapter is a collection of four case studies: (i) investigating the magnitude of striping artifacts in heritage MERIS pushbroom sensor data, (ii) assessing the impact of striping artifacts on derived science data products, (iii) assessing the impact of striping artifacts on a novel derivative spectroscopy method, and (iv) considering the effectiveness of destriping methods at correcting striping to sensor noise levels. The latter three analyses relied on a simplified model for a hyperspectral pushbroom sensor in which detector miscalibration error could be defined.

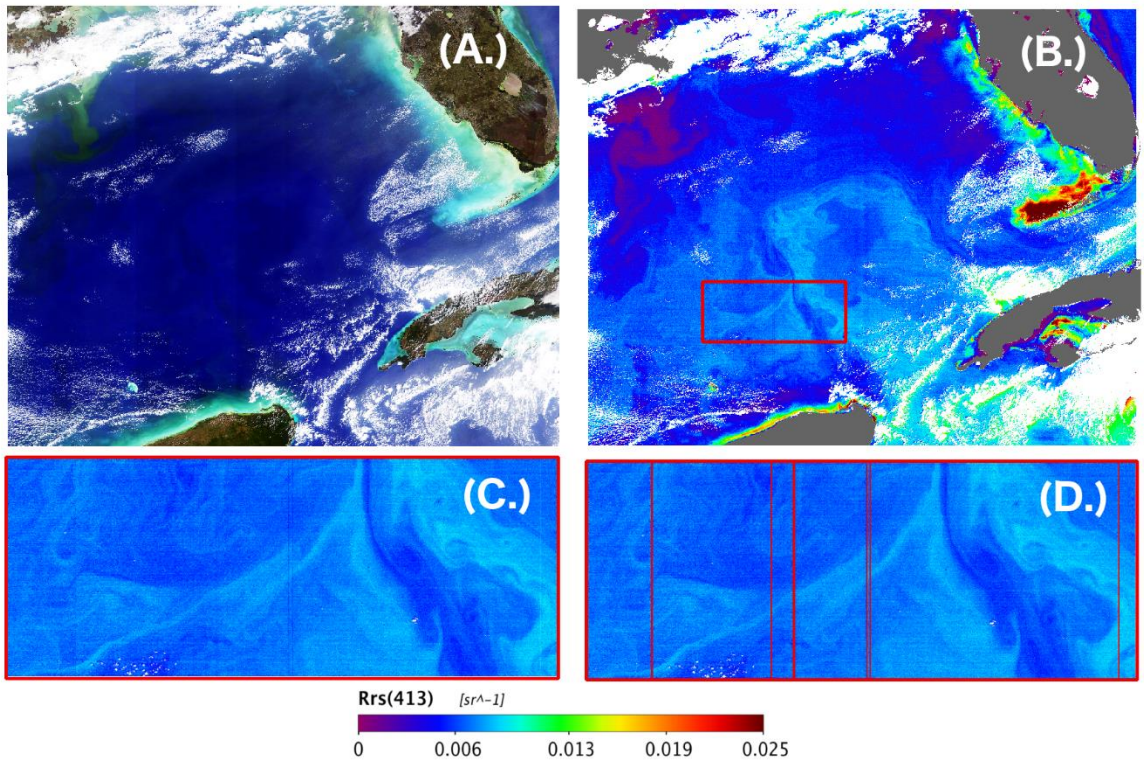

Figure 4.1: MERIS imagery of the Gulf of Mexico region captured on 13 December 2004. (A.) A quasi-true color image in which distinct vertical contrast boundaries are visible associated with where the sensor's five individual cameras overlap. (B.) An image of derived remote sensing reflectances at 413 nm, $R_{rs}(413)$, with a red zoom box. (C.) The zoomed-in region shows vertical along-track image striping in $R_{rs}(413)$ which are delineated more clearly in (D.) using vertical red lines.

4.2. Heritage Instrument Data

The MERIS instrument, flown aboard ESA's ENVISAT (2002-2012), comprised five separate pushbroom cameras, each with a backlit silicon frame transfer charge coupled device (CCD) focal plane having 740 spatial pixels and 520 spectral pixels [*Bézy et al.*, 2000]. Thus, the number of total detectors elements on the MERIS pushbroom system was 1.924×10^6 (5 x 520 x 740). The MERIS sensor exhibited three distinct along-track striping artifacts:

Detector-to-detector miscalibration

Miscalibrations cause pixel-to-pixel contrast variations and appear as along-track stripe artifacts as the scene is built up due to the push broom motion.

Between-camera discontinuities

The radiometric contrast between the sensor's five separate cameras varies. This causes distinct vertical boundaries where each sub-image overlaps.

Dead detector interpolation

Non-functional, or "dead", detectors on the CCD focal plane can occur due to aging and/or manufacturer fault. Once identified, dead pixels are replaced by interpolating between adjacent detectors. These appear as along-track stripes similar to those caused by detector-to-detector miscalibration.

A cursory evaluation of along-track striping artifacts in MERIS imagery was performed using an image of the South Atlantic Gyre captured on 12 March 2009. Near-surface waters within a sub-tropical gyre are oligotrophic and can be treated quasi-homogenous at local horizontal scales. Such a region was thus useful for evaluating along-track striping artifacts in spectral top-of-atmosphere radiances, $L_{toa}(\lambda)$, as the magnitude of an identified stripe can be compared with adjacent pixels to ascertain its deviation from the neighborhood value.

$L_{toa}(\lambda)$ stripes occurring at cross-track pixel number 229 and 645 were evaluated. For each stripe, a 60 pixel-long along-track region-of-interest was considered. Immediately either side of the stripe two boxes 20 pixels wide and 60 pixels long (see Figure 4.2) were averaged and then compared with the average of the 60 pixel-long image stripe. The metric used for comparison was the relative percent difference. Similarly, the difference between cameras 3 and 4 and cameras 4 and 5 were computed. Specifically, two boxes 40 pixels wide and 60 pixels (see Figure 4.2) were averaged either side of each camera seam and then the relative percent difference (RPD) was calculated.

Figure 4.2A shows a striping artifact in top-of-atmosphere radiances at 443 nm, $L_{toa}(443)$, for cross-track pixel number 229. The RPD between this stripe and neighboring pixels was 0.50%. The spectral results detailed in Table 4.1 and shown in Figure 4.2 indicate that image striping artifacts in L_{toa} differed from neighborhood values by ±0.5% or more on five occasions. Figure 4.2B shows the difference between cameras 4 and 5 in top-of-atmosphere radiances at 443 nm, $L_{toa}(443)$. The relative percent difference between cameras was 0.18% with full spectral results presented in Table 4.2 and shown in Figure 4.4 indicating.

The results shown in Figures 4.2 and 4.3 and summarized in Tables 4.1 and 4.2 indicate that striping artifacts exceeded the ±0.5% error threshold on four occasions. Whereas, cameras seam edges exceeded the ±0.5% threshold on twelve occasions. We note that these results comes after much post-processing to remove detector-to-detector artifacts by *Bouvet and Ramino* [2009].

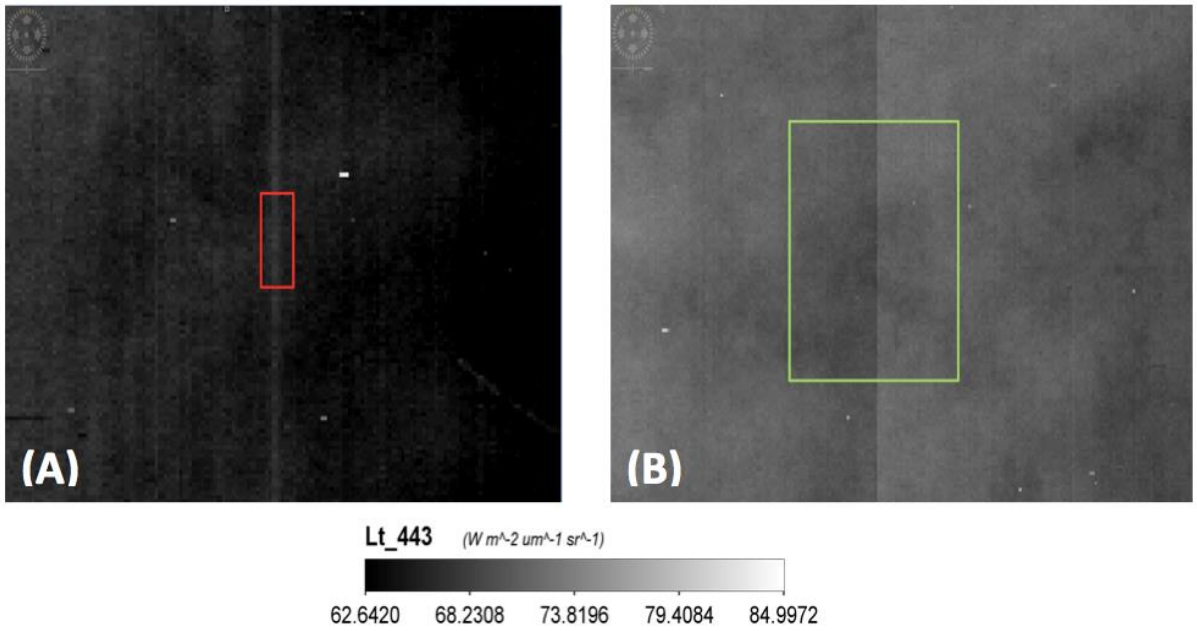

Figure 4.2: Subplots from a MERIS image captured over the South Atlantic Gyre on 12 March 2009. (A) An example of a miscalibration stripe in $L_{toa}(443)$ occurring at cross track pixel number 229. The magnitude of the stripe was compared with adjacent pixels for a box 20 pixels wide and 60 pixels long. (B) Comparison of MERIS cameras 4 and 5 at $L_{toa}(443)$. The magnitude of the difference between adjacent cameras was calculated by comparing the average pixel values either side of the seam for a test region 40 pixels wide and 60 pixels long.

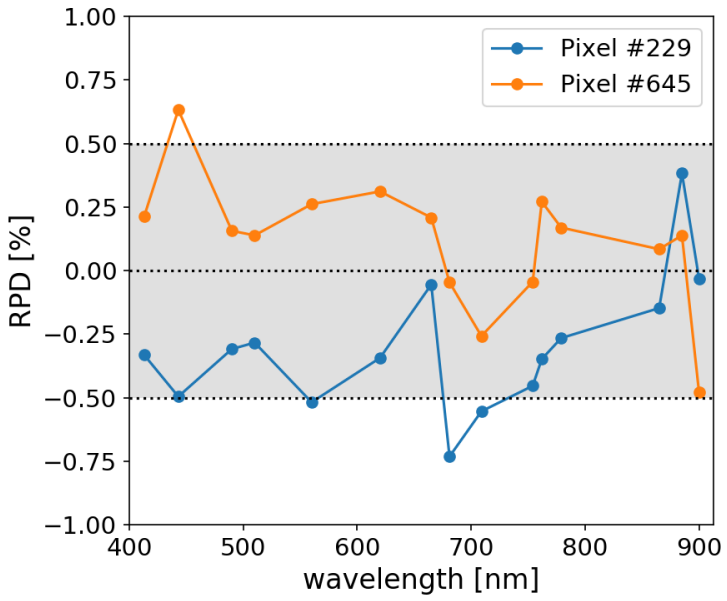

Figure 4.3: For miscalibration stripes occurring at cross-track pixels 229 and 645, the relative percent difference (RPD) between the stripe and the neighboring region was calculated for each spectral band. The shaded grey box represents ±0.5% difference.

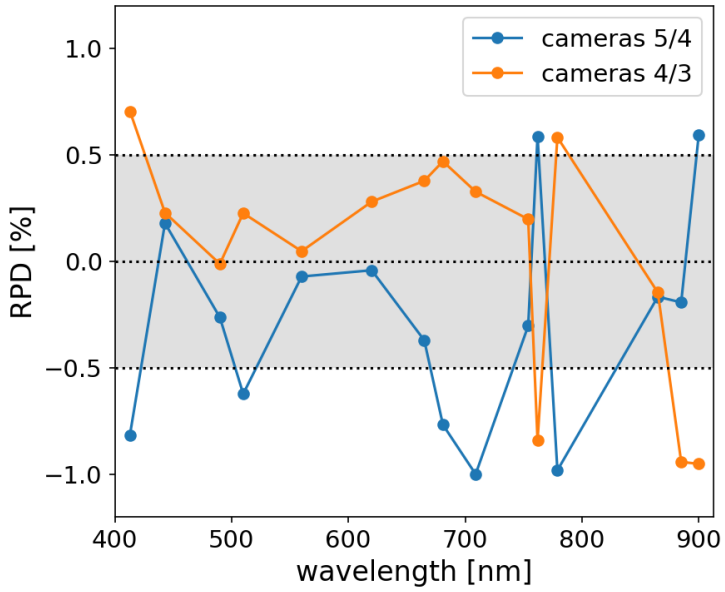

Figure 4.4: The relative percent difference (RPD) was computed at the seams of cameras 3 and 4 and cameras 4 and 5. RPD were calculated for each spectral band. The shaded grey box represents ±0.5% difference.

4.3. Pushbroom Conceptual Model

A basic model was developed to conceptualize image striping in a contiguous multispectral pushbroom ocean color sensor analogous to MERIS with 14-bit digitization resolution. The theoretical CCD focal plane had n=740 spatial pixels and m=83 spectral bands (340 - 750 nm, 5 nm resolution). Within the scope of this study, the theoretical sensor was assumed to be ideal (i.e. no other artifacts) with at-launch noise levels as determined from prescribed signal-to-noise ratios (SNRs) in the PACE Science Definition Team (SDT) Report and random calibration uncertainties that were adjustable.

The model first calculates hypothetical top-of-atmosphere sensor-observed digital counts for the i^{th} spatial and j^{th} spectral detector, $DN_{i,j}$, as follows:

1. A simple bio-optical model was used to generate spectral remote sensing reflectance for each spatial pixel, $Rrs_{i,j}$, as a function of chlorophyll-a, Chl_i, concentration.

2. Theoretical $Rrs_{i,j}$ was converted to water leaving radiances, $Lw_{i,j}$, by multiplying by an idealized down-welling spectral irradiance constant, Ed_j.

3. An idealized atmospheric spectral radiance constant, $Latm_j$, was added to $Lw_{i,j}$ to generate top-of-atmosphere radiances, $Ltoa_{i,j}$. Based on Sea-Viewing Wide-Field-of-View Sensor (SeaWiFS) data captured over the North Pacific Ocean near Hawaii, the following power law relationship was used to approximate $Latm_j$

$$Latm_j = Latm_{555}\left(\frac{555}{\lambda_j}\right)^4. \qquad \text{(Eq. 4.1)}$$

where, λ_j, is j^{th} sensor spectral band center wavelength and the atmospheric radiance at 555, $Latm_{555}$, was set to 2.5 mW cm^{-2} um^{-1} sr^{-1}.

4. $Ltoa_{i,j}$ were converted to digital counts, $DN_{i,j}$, using idealized calibration coefficients, c_j, and idealized dark current, DC_j, offsets.

Next, miscalibrated top-of-atmosphere radiances were computed as follows:

5. Randomly generated sensor noise, $\Delta DN_{i,j} \sim N(0, \sigma_{i,j})$, was added to $DN_{i,j}$.

6. To induce 0.1% miscalibration error, calibration coefficients were multiplied by randomly generated gain coefficients, $\Delta e_{i,j} \in (0.999, 1.001)$.

7. Note that randomly generated gain coefficients could also be used to induce 0.25%, and 0.5% and 0.25% miscalibration error.

8. Perturbed top-of-atmosphere radiances, $L'toa_{i,j}$, where then generated as

$$L'toa_{i,j} = \left(\Delta c_{i,j} c_j\right)\left(DN_{i,j} - DC_{i,j} + \Delta DN_j\right). \qquad \text{(Eq. 4.2)}$$

Finally, $L'toa_{i,j}$ values were converted to perturbed remote-sensing reflectances, $R'rs_{i,j}$, and perturbed water-leaving reflectances, $\rho'w_{i,j}$, as follows:

9. $Latm_j$ was subtracted from $L'toa_{i,j}$ to give perturbed water-leaving radiances $L'w_{i,j}$

10. $R'rs_{i,j}$ was derived by dividing $L'w_{i,j}$ by Ed_j.

11. $\rho'w_{i,j}$ was derived by multiplying $R'rs_{i,j}$ by π.

For this study, we arbitrary set DC_j values as spectrally flat constants with values of 1% of the digital dynamic range (2^{14}). Theoretical spectral calibration coefficients were then calculated as

$$c_j = \frac{L\max_j}{2^{14} - DC_j} \qquad \text{(Eq. 4.3)}$$

where $Lmax_j$ are maximum observable spectral radiances before sensor saturation occurs (see Table 4.5).

Sensor noise, $\Delta DN_{i,j}$, for each detector element was randomly drawn from a normal distribution where $\Delta DN_{i,j} \sim N(0, \sigma_{i,j})$. The standard deviation of sensor noise for each detector, $\sigma_{i,j}$, was calculate as

$$\sigma_{i,j} = DN_{i,j} / SNR_j' \qquad \text{(Eq. 4.4)}$$

where SNR_j' is the scaled signal-to-noise ratio of the j^{th} spectral band as follows:

$$SNR_j' = SNR_j \left(\frac{Ltoa_j}{Ltyp_j}\right)^{0.5} \qquad \text{(Eq. 4.5)}$$

where SNR_j is the signal-to-noise ratio at typical radiances, $Ltyp_j$, as prescribed in the PACE SDT report [2018].

The quasi-single scattering approximation of Gordon et al. [1988] was used to simulate $Rrs_{i,j}$. For the i^{th} spatial pixel, the spectral sub-surface remote sensing reflectance was modeled as

$$rrs_j = 0.089u_j + 0.125u_j^2 \,. \qquad \text{(Eq. 4.6)}$$

Subsurface to above-water values were converted following *Lee et al.* [2002] as

$$Rrs_j = \frac{0.52rrs_j}{(1 - 1.7rrs_j)} \,. \qquad \text{(Eq. 4.7)}$$

The spectral parameter u_j is a function of the total spectral absorption coefficient, a_j, and the total spectral backscattering coefficient, $b_{b,j}$, expressed as

$$u_j = \frac{a_j}{a_j + b_{b,j}} \,. \qquad \text{(Eq. 4.8)}$$

Values of a_j and $b_{b,j}$ were modeled as functions of *Chl* following *IOCCG* [2006]. However, unlike *IOCCG* [2006], the spectral absorption coefficient of phytoplankton, $a_{\phi,j}$, was parameterized according to *Bricaud et al.* [1998].

4.4. Example of Synthesized Pushbroom Striping

Simulated $\rho_w(440)$ images that are 740 pixels (cross-track) wide and 500 pixels (along-track) long are shown in Figures 4.5A and 4.5B. The two images represent a uniform ocean with *Chl* value of 0.1 mg m^{-3} "imaged" by the conceptual pushbroom model. Figure 4.5A is modeled with 0.1% miscalibration error whilst Figure 4.5B is modeled with 0.1% miscalibration error and sensor noise. Along-track striping artifacts are clearly visible in both subplots. The addition of noise to the model introduces a speckle characteristic that qualitatively appears similar to MERIS imagery.

Figures 4.5C and 4.5D show cross-track transects of $\rho_w(440)$ corresponding to scanline 100 (denoted as red lines in Figure 5A and 5B). Relative percent difference (RPD) values in Figure 4.5C indicate that 0.1% miscalibration error causes values of $\rho_w(440)$ to vary ±0.8% from the mean value. Whereas, Figure 4.5D shows that miscalibration error and sensor noise cause values of $\rho_w(440)$ to vary ±3% from the mean value.

Figures 4.5E and 4.5F show the actual spectral value of $\rho_w(\lambda)$ for the simulated scene. The gray shaded area surrounding $\rho_w(\lambda)$ represents $\pm 1\sigma(\lambda)$ computed from all $\rho_w(\lambda)$ in the simulated image. The blue line represents the spectral mean absolute percent difference (MAPD) deviation from true $\rho_w(\lambda)$ and the horizontal dashed lines represents a 0.5% MAPD. Here, MAPD was calculated as:

$$MAPD = \left\langle \left| \left(\frac{r'_w - r_w}{r'_w} \right) \right| \right\rangle \times 100\% \qquad \text{(Eq. 4.9)}$$

where, ρ_w' is the miscalibrated water leaving reflectance value (wavelength has been omitted for brevity).

We note that in this study, atmospheric correction was treated as an exact subtraction of modeled $L_{atm}(\lambda)$ from $L_{toa}(\lambda)$. In practice, however, atmospheric correction uses near-infrared channels to estimate atmospheric parameters. Accordingly, this study did not capture how striping artifacts from near-infrared channels might propagate through to shorter wavelengths during the atmospheric correction procedure.

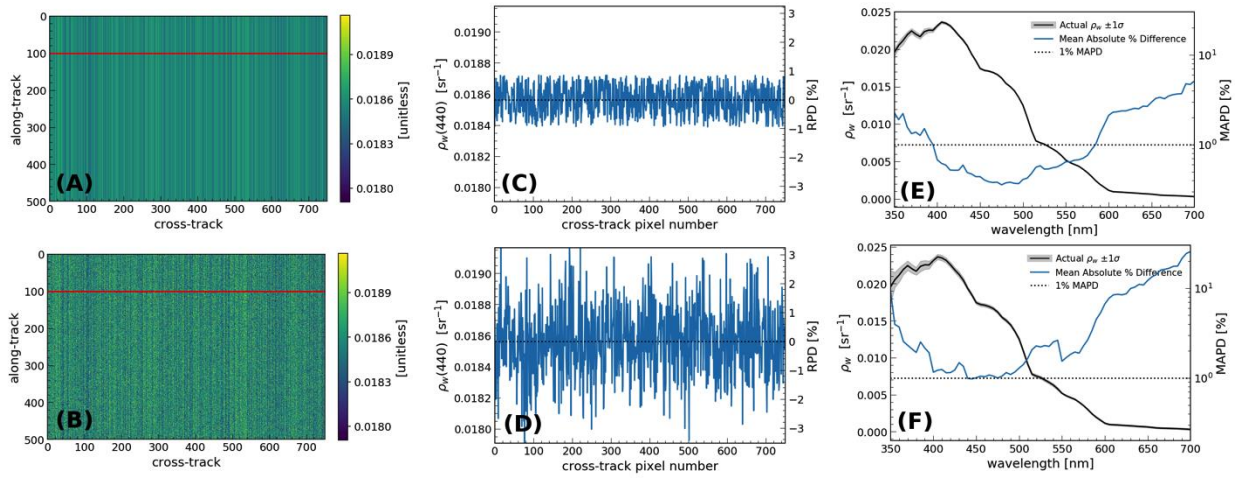

Figure 4.5: Subplots (A) and (B) show simulated pushbroom images of $\rho_w(440)$ for a uniform ocean: (A) is modeled with 0.1% miscalibration error, and (B) is modeled with 0.1% miscalibration error in the presence of noise. Subplots (C) and (D) show variability in $\rho_w(440)$ along a cross-track transect for scan number 100 (denoted as redlines in subplots (A) and (B)). Subplots (E) and (F) show the true $\rho_w(\lambda)$ and the transect-averaged spectral mean absolute percent differences (MAPD).

4.5. Impact of Striping on Derived Products

The impact of miscalibration error upon derived ocean color data products was explored using a synthesized ocean scene of a bio-optical gradient. Four hyperspectral pushbroom images were simulated: (i) for a well-calibrated sensor, (ii) for a sensor with 0.1% miscalibration error, (iii) for a sensor with 0.25%, and (iv) for a sensor with 0.5% miscalibration. Further, identical sensor noise characteristics were used for all three scenarios. The relative error, δDP, between the value of the data product derived from the perfectly calibrated sensor, DP, and the data product derived from the miscalibrated sensor, DP', was calculated as follows:

$$\delta Dp = \left[\frac{DP' - DP}{DP} \right] \times 100\% \ . \qquad \text{(Eq. 4.10)}$$

Chl values were derived using the OC4 band ratio-type algorithm [*O'Reilly et al.*, 1998] and inherent optical properties (IOPs) at 440 nm were derived using the default configuration of the Generalized Inherent Optical Properties algorithm framework (GIOP) [*Werdell et al.*, 2013]. In this study, the IOPs derived at 440 nm were the absorption coefficient of phytoplankton, $a_\phi(440)$, the absorption coefficient of colored dissolved and detrital matter, $a_{dg}(440)$, and the particulate backscattering coefficient, $b_{bp}(440)$.

Figure 4.6A and 4.6B shows $a_\phi(440)$ derived for a perfectly calibrated sensor and a sensor with 0.1% miscalibration error, respectively. In Figure 4.6B, along-track (vertical) miscalibration striping can be seen in derived $a_\phi(440)$. Figure 4.6C is a histogram of $\delta a_\phi(440)$ and shows that 0.1% miscalibration imparts approximately ±1% 1σ uncertainty in derived $a_\phi(440)$. Figure 4.6D is an image of the relative difference in which along-track (vertical) striping artifacts can be seen.

Table 4.6 summarizes the first standard deviation (1σ) values of δChl, $\delta\, a_\phi(440)$, $\delta\, a_{dg}(440)$, and $\delta b_{bp}(440)$ for the 0.1%, 0.25% and 0.5% miscalibration error scenarios. The results indicate that 1σ

uncertainty in derived data products scales nearly linearly with sensor miscalibration (striping) error. Notably, at the 0.5% miscalibration level the 1σ uncertainty in *Chl* approaches 10%.

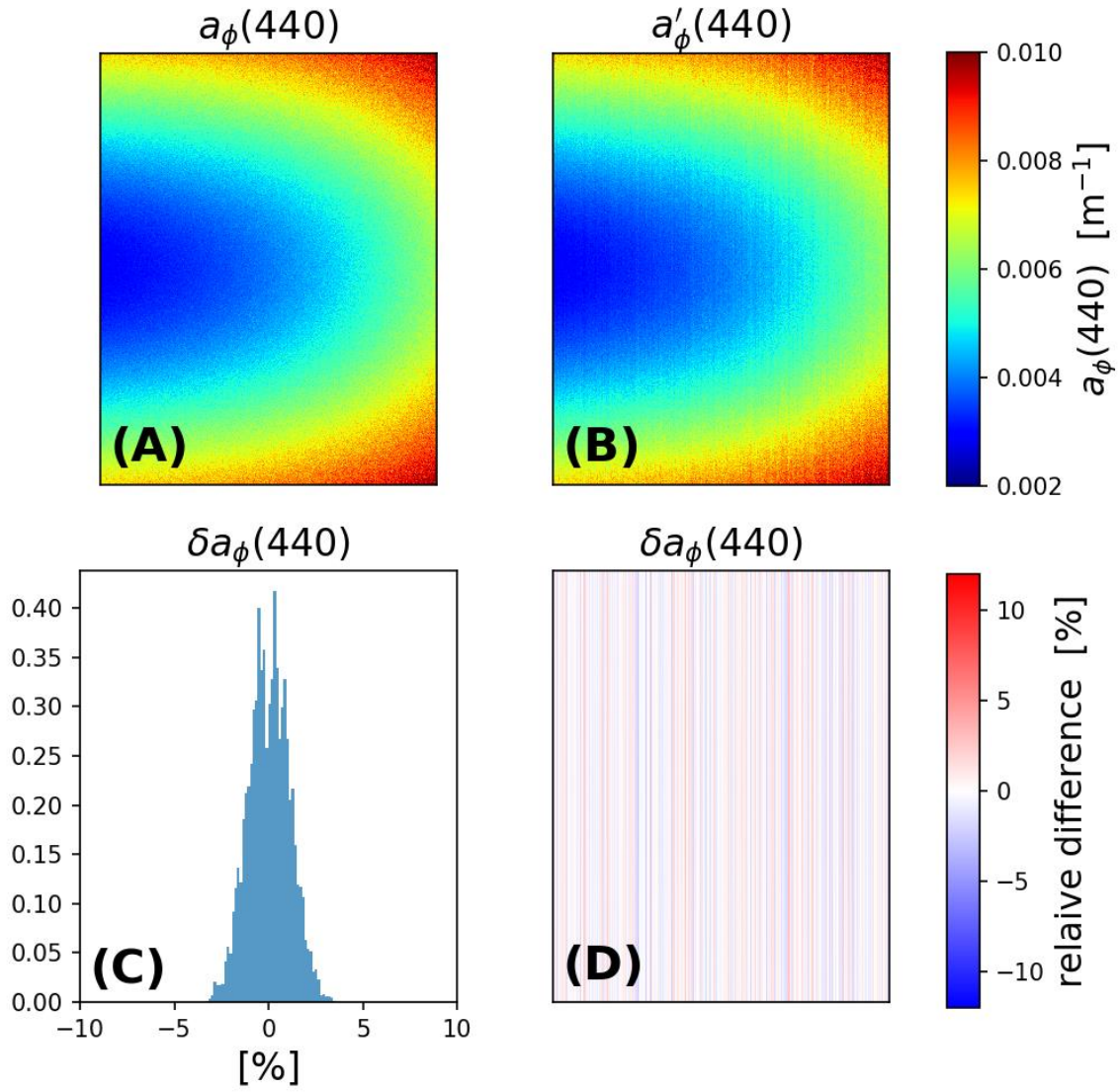

Figure 4.6: Derived $a_\phi(440)$ from a simulated hyperspectral pushbroom image of a synthesized non-uniform ocean. (A) $a_\phi(440)$ derived from a well-calibrated sensor, while (B) shows perturbed $a'_\phi(440)$ derived from sensor with 0.1% miscalibration errors and noise. (C) A histogram shows the distribution of the relative difference between (A) and (B). (D) Shows and image of the relative difference between (A) and (B).

4.6. Impact of Striping on Deriviative Spectroscopy

One novel aspect of a hyperspectral OCI is applying analytical spectroscopy methods common to chemometrics to ocean color data. In particular, derivative spectroscopy methods may lend themselves to hyperspectral ocean color radiometry for discerning subtle phytoplankton accessory pigment absorption peaks e.g. [*Craig et al.*, 2006; *Lubac et al.*, 2008; *Xi et al.*, 2015]. Here we briefly considered how miscalibration error in a pushbroom sensor might impact derivative spectroscopy of hyperspectral $\rho_w(\lambda)$.

Using the pushbroom conceptual model, a hyperspectral $\rho_w(\lambda)$ image was simulated for uniform ocean with *Chl* of 1 mg m^{-1}. An image 740 pixels (cross-track) wide and 500 pixels (along-track) long was simulated for a noiseless sensor with 0.1% miscalibration error. For comparison purposes, $\rho_w(\lambda)$ was modeled again for a noiseless perfectly calibrated sensor.

Figure 4.7A shows an image of the second derivative of $\rho_w(\lambda)$ at 513 nm, $d^2\rho_w(513)/d\lambda^2$. The mean value of $d^2\rho_w(513)/d\lambda^2$ is 5.6E-4 nm^{-2} and ranges from -4.9E-5 to 1.1E-3 nm^{-2} with a standard deviation of 2.0E-4 nm^{-2}. Figure 4.7B shows the relative comparison of $d^2\rho_w(513)/d\lambda^2$ values in Figure 4.7A with $d^2\rho_w(513)/d\lambda^2$ modeled for a perfect sensor. The results demonstrate that between-pixel variability due to image striping can be as much as ±120%.

A cross-track sample of spectral $d^2\rho_w/d\lambda^2$ is shown in Figure 4.7C as well as the true value for $\rho_w(\lambda)$. Second derivative features correspond as expected to spectral curvature features in $\rho_w(\lambda)$. It is clear that absolute uncertainty in $\rho_w(\lambda)$ associated with miscalibration error increases as wavelength decreases.

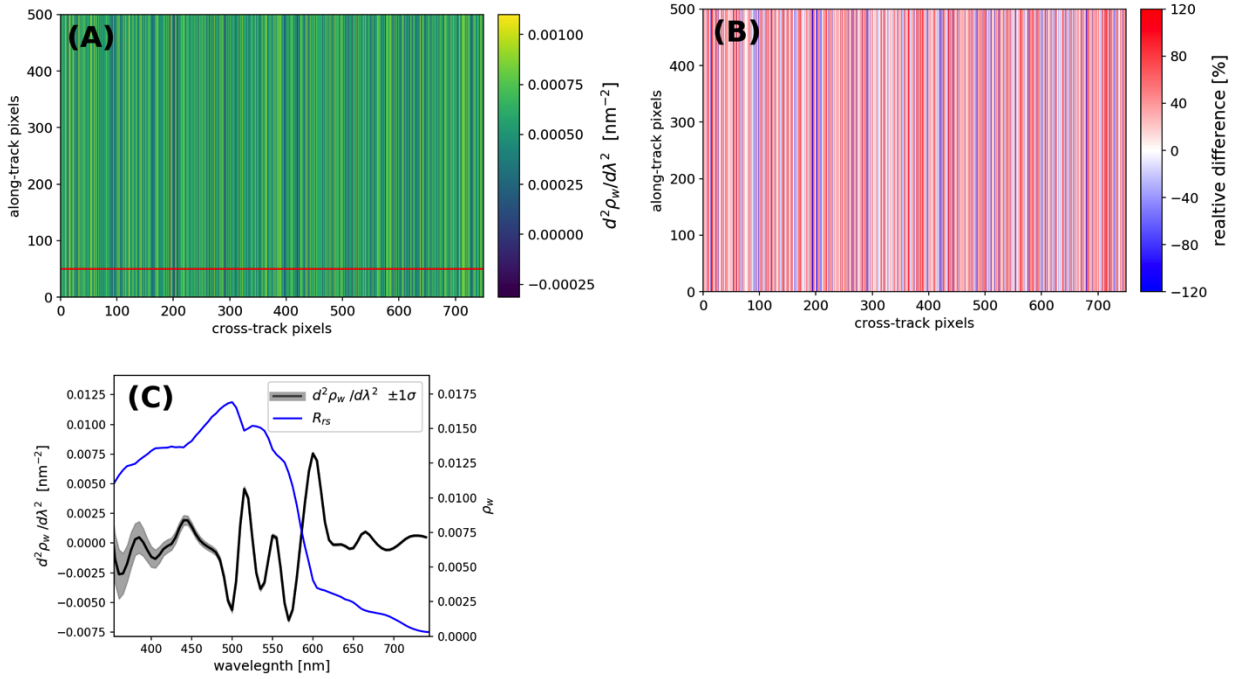

Figure 4.7: (A) An image of $d^2\rho_w(515)/d\lambda^2$ for a hypothetical uniform ocean. $d^2\rho_w(515)/d\lambda^2$ was calculated from a synthesized hyperspectral $\rho_w(\lambda)$ image modeled for a noiseless pushbroom sensor with 0.1% miscalibration error. The horizontal red line denote a cross-track transect at scanline number 50. (B) An image of the relative percent difference between ideal $d^2\rho_w(515)/d\lambda^2$ and $d^2\rho_w(515)/d\lambda^2$ shown in (A). (C) A cross-track sample of $d^2\rho_w(515)/d\lambda^2$ is plotted showing 1σ variability. The ideal $\rho_w(\lambda)$ spectrum for the uniform is also plotted.

4.7. Case Study of Destriping Method

A number of destriping algorithms have been developed to suppress along-track striping artifacts in pushboroom sensors (see examples in Table 4.5). Destriping methodologies vary in complexity and apart from efforts to suppress detector-to-detector striping artifacts in MERIS Level-1B data by Bouvet and Ramino [2009] none, to the best of our knowledge, have been implemented in routine global ocean color processing. We evaluated the wavelet-based method of Pande-Chhetri and Abd-Elrahman [2011] to ascertain how a computationally efficient destriping algorithm might suppress striping artifacts in modeled pushbroom $\rho_w(\lambda)$.

Figure 4.8A shows a modeled scene of $\rho_w(440)$ 740 pixels (cross-track) wide and 960 pixels (along-track) long of a non-uniform ocean imaged by a conceptual pushbroom sensor that is perfectly calibrated and noise free. Figure 4.8B shows the same scene imaged by a conceptual pushbroom sensor with 0.1% miscalibration error and noise. Along-track striping artifacts are visible in Figure 4.8B. Using the wavelet-based destriping algorithm, image stripes and noise appear suppressed in Figure 4.8C. However, the relative difference between the Figures4. 8A and 4.8C (Figure 4.8D) reveals that the destriping method has imparted residual vertical artifacts with 1σ values of ±0.6%.

For a multi-camera pushbroom system such as MERIS, each detector focal plane will have slightly different miscalibration characteristics. Accordingly, it is useful to know if residual artifacts imparted by a destriping method are repeatable or if they vary. To test this, three images of $\rho_w(440)$ were simulated for the same non-uniform ocean in Figure 4.8. The three images were generated with three separate, randomly generated 0.1% miscalibration error profiles. All three $\rho_w(440)$ images were then destriped using the same wavelet-based method. Figure 4.9 shows that spatial patterns in the three relative difference sub-plots are not identical. This result indicates that the destriping method does not perform consistently and imparts different residual artifacts for each miscalibration scenario.

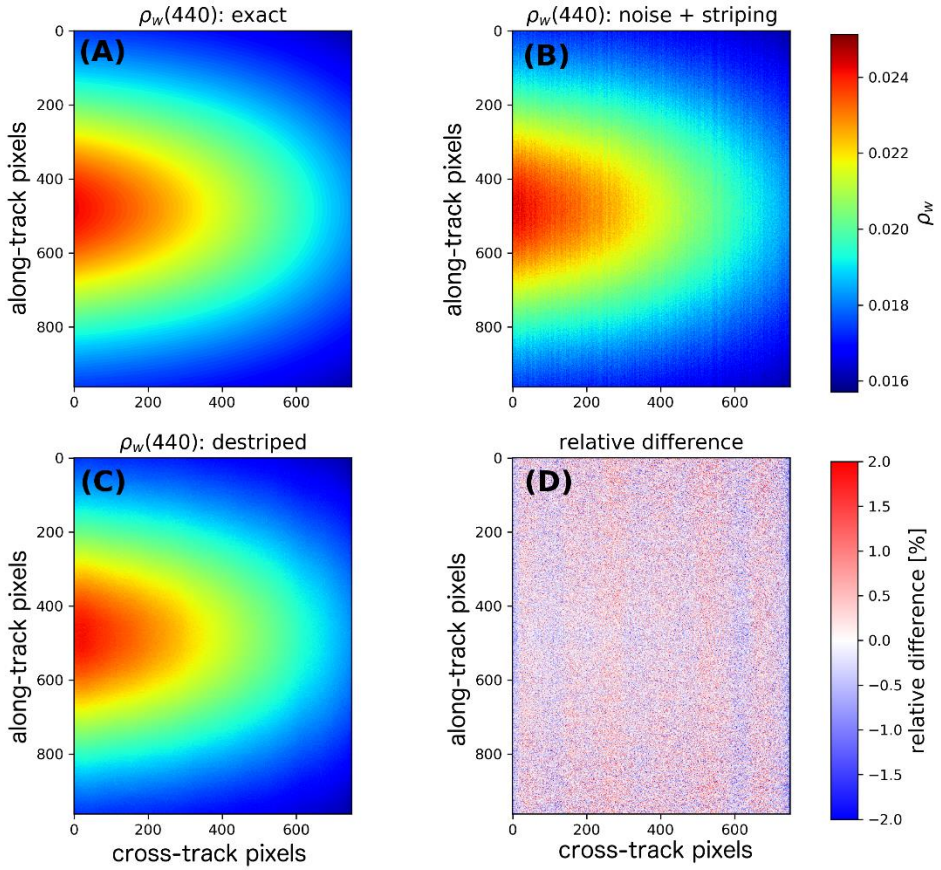

Figure 4.8: (A) Modeled $\rho_w(440)$ for a non-uniform ocean imaged by a perfectly calibrated noise free pushbroom sensor. (B) Modeled $\rho_w(440)$ for a non-uniform ocean imaged by a pushbroom sensor with 0.1% miscalibration error in the presence of sensor noise. (C) Image (B) after destriping. (C) Relative percent difference between (A) and (C) shows residual striping artifacts remain.

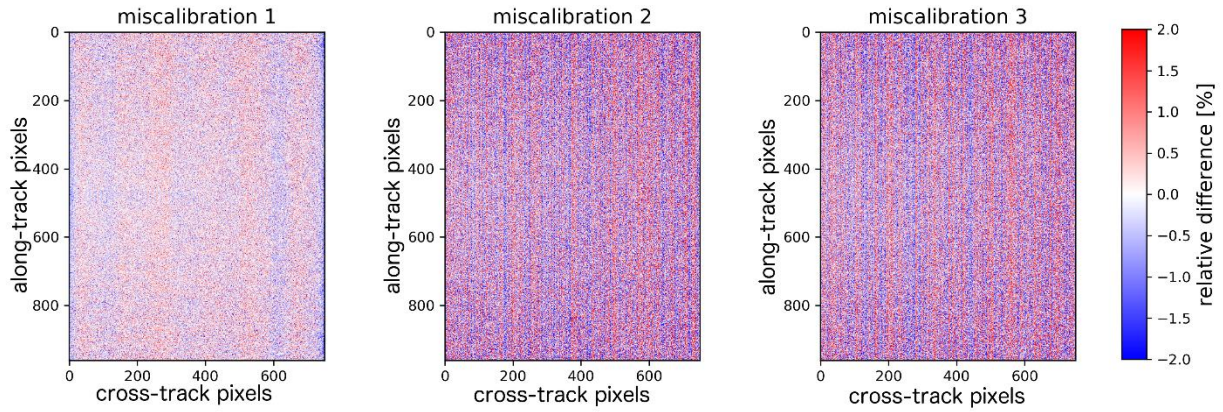

Figure 4.9: The relative percent difference between and destriped and exact values of $\rho_w(440)$. The subplots correspond to three separate detector-to-detector 0.1% miscalibration error scenarios.

4.8. Summary and Conclusion

In this study we investigated along-track striping in ocean color imagery caused by detector-to-detector miscalibration in a pushbroom imager. We found that despite much post-launch effort, along-track image striping artifacts in heritage MERIS imagery can exceed 0.5% in L_{toa}. This finding indicates that calibration and characterization of a multi-camera pushbroom imager is highly challenging.

A conceptual pushbroom model was used to simulate the impact of pushbroom striping on derived science data products. Using simulated data, we found 0.1% miscalibration error led to 1σ uncertainties in derived products in the order of ±1%. Uncertainties were also found to scale linearly with miscalibration error. These uncertainties are directly related to multi-detector miscalibration error and may be reduced by pursuing a sensor design concept with fewer detectors.

Examination of second derivative spectroscopy found the method was highly sensitive to image striping. The results showed that image striping imparted by 0.1% miscalibration error led to ±120% uncertainty in the second derivative of $\rho_w(513)$. This result suggests that a pushbroom imager concept may limit the application of novel spectroscopy-type methods.

An algorithm for removing image striping was evaluated. The approach was found to cosmetically remove along-track image stripes, however, on closer inspection the method imparted residual artifacts. It was also ascertained that the destriping method did not impart residual artifacts in a repeatable way. This study suggests that for a pushbroom imager concept, significant effort would need to be expended on developing a robust destriping methodology suitable for global ocean color processing.

Table 4.1: Relative percent difference (RPD) in top-of-atmosphere radiometric quantities between along-track MERIS stripe artifacts and the immediate neighborhood. Two stripes were considered from an image of the South Atlantic Gyre captured on 12 March 2009. Test stripes correspond to cross-track pixels 229 and 645.

Band	L_{toa} RPD at pixel 229 [%]	L_{toa} RPD at pixel 645 [%]
413	-0.33	0.21
443	-0.50	0.63
490	-0.31	0.16
510	-0.28	0.13
560	-0.51	0.26
620	-0.34	0.31
665	-0.06	0.21
681	-0.73	-0.05
709	-0.55	-0.26
754	-0.45	-0.04
762	-0.35	0.27
779	-0.27	0.17
865	-0.15	0.08
885	0.38	0.14
900	-0.03	-0.48

Table 4.2: Relative percent difference (RPD) in top-of-atmosphere radiometric quantities calculated at MERIS camera seams. RPD between cameras 4 and 3, and 5 and 4 were considered for a test image of the South Atlantic Gyre captured n the 12 March 2009.

Band	*Ltoa* Cameras 4-3 [%]	*Ltoa* Cameras 5-4 [%]
413	0.71	-0.81
443	0.23	0.18
490	-0.01	-0.26
510	0.23	-0.62
560	0.05	-0.07
620	0.28	-0.04
665	0.38	-0.37
681	0.47	-0.78
709	0.33	-0.99
754	0.20	-0.30
762	-0.84	0.59
779	0.58	-0.98
865	-0.15	-0.17
885	-0.94	-0.19
900	-0.95	0.59

Table 4.3: Spectral parameters used for image striping model

Nominal band center [nm]	Band width [nm]	SNR	E_d [mW m^{-2} um^{-1}]	L_{atm} [mW cm^{-2} um^{-1} sr^{-1}]	L_{typ} [mW cm^{-2} um^{-1} sr^{-1}]	L_{max} [mW cm^{-2} um^{-1} sr^{-1}]
350	15	300	61.05	15.81	7.46	35.5
360	15	1000	65.80	14.12	7.22	37.6
385	15	1000	63.81	10.79	6.11	38.1
412	15	1000	118.66	8.23	7.86	60.2
425	15	1000	112.63	7,27	6.95	58.5
443	15	1000	128.15	6.16	7.02	66.4
460	15	1000	136.88	5.30	6.83	72.4
475	15	1000	143.91	4.66	6.19	72.2
490	15	1000	145.69	4.11	5.31	68.6
510	15	1000	137.50	3.51	4.58	66.3
532	15	1000	137.96	2.96	3.92	65.1
555	15	1000	136.31	2.50	3.39	64.3
583	15	1000	134.71	2.05	2.81	62.4
617	15	1000	121.26	1.63	2.19	58.2
640	10	1000	120.65	1.41	1.90	56.4
655	15	1000	111.94	1.29	1.67	53.5
665	10	1000	117.47	1.21	1.60	53.6
678	10	1000	115.62	1.12	1.45	51.9
710	10	1000	104.50	0.93	1.19	48.9
748	15	600	99.47	0.76	0.93	44.7

Table 4.4: Relative error in derived bio-optical data products imparted by miscalibration error in the conceptual pushbroom imager model.

Pushbroom miscalibration error [%]	1-σ relative percent error [%]			
	δChl	$\delta a_\phi(440)$	$\delta a_{dg}(440)$	$\delta b_{bp}(440)$
0.1	1.7	1.1	1.2	0.7
0.25	4.5	2.7	3.0	1.9
0.5	8.9	5.6	6.2	3.9

Table 4.5: Selection of along-track destriping methodologies for pushbroom imagery

Technique	Evidence of use in automated operational processing	Residual striping/artifacts	Algorithm complexity	Test sensor/s	Reference
Polynomial fitting	✗	✓	Low	MOS	*Franz* [1998]
Heterogeneous single image-based band equalization	✗	✓	Low	OCM	*Lyon* [2009]
2D Wavelet Fourier-adaptive filtering	✗	✓	Moderate	Hyperion	*Pande-Chhetri and Abd-Elrahman* [2011] *Pande-Chhetri and Abd-Elrahman* [2013]
Homogenous multiple image-based band equalization	✗	✓	Moderate-to-high	MOS MERIS	*Corsini et al.* [2000] *Bouvet and Ramino* [2009]

Chapter 5

Analysis of Potential PACE Altitude Reduction

Frederick S. Patt, Science Applications International Corporation, Reston, Virginia[5]

Executive Summary

The Phytoplankton, Aerosol, Cloud, ocean Ecosystem (PACE) mission has been designed for an altitude of 676 km. During the Mission Concept Review (MCR), a recommendation was made to consider changing the altitude to between 400 and 450 km to enable constellation flying with a LIDAR mission that was being proposed for the next Decadal Survey (based on results from the CALIPSO mission in particular, [e.g. *Behrenfeld et al.*, 2013; *Behrenfeld et al.*, 2016]. This paper presents the results of analyses that were performed to determine the requirements for a PACE altitude reduction and the impacts on the mission. The conclusion was that while there could be a scientific benefit to flying PACE in constellation with a LIDAR mission, the impact to the instrument design and mission cost would be substantial. In addition, a LIDAR mission would be several years behind PACE, so a constellation would only be possible if PACE continues well beyond its design lifetime.

5.1. Introduction

The PACE mission, in particular the Ocean Color Instrument (OCI), has been planned and designed for an orbit with an altitude of 676 km. During the Mission Concept Review (MCR), a recommendation was made to consider the possibility of flying PACE in constellation with a Light Detection and Ranging (LIDAR) mission, to enable complementary science by the two missions. LIDAR missions are designed for lower altitudes, typically between 400 and 450 km. Flying PACE in constellation would require a redesign of OCI for the lower altitude, and would also entail other impacts to the mission. A study was undertaken to assess the requirements for and impacts to PACE for the lower altitude, including the following considerations: 1) mission science; 2) global coverage; 3) orbit maintenance; 4) OCI design; and 5) spacecraft impacts. Results of this study were presented to PACE Program Science in June 2016.

5.2. Considerations for Altitude Reduction

The following sections present the analysis and results for each of the major considerations for the PACE altitude reduction.

5.2.1. Mission Science

There would be no explicit impacts or gains to mission science by flying at a lower altitude, assuming that instrument performance requirements can be met. There are significant benefits to the ocean color science that would result from contemporaneous operations with a LIDAR mission. The OCI provides wide-swath views of the ocean surface, which cannot be accomplished with active sensors, while the LIDAR provides vertical views of the water column, which cannot be accomplished with passive

[5] Cite as: Patt, F. S. (2018), Analysis of potential PACE altitude reduction, in *PACE Technical Report Series, Volume 5: Mission Formulation Studies (NASA/TM-2018 – 2018-219027/ Vol. 5)*, edited by I. Cetinić, C. R. McClain and P. J. Werdell, NASA Goddard Space Flight Space Center Greenbelt, MD.

sensors. Wide-swath views of surface processes (OCI) combined with narrow views of vertical processes (LIDAR) would combine to form a three-dimensional view of the upper ocean (up to 3 optical depths).

However, there are also potential benefits to operating the two missions at the same equator crossing time but different altitudes. Flying in constellation would result in the LIDAR always sampling the center of the OCI swath. There may be advantages to having LIDAR measurements across the full range of OCI scan angles, which would result from different altitudes and orbit periods. Further study would be required to determine which configuration would provide the greatest advantages in terms of complementary science.

5.2.2. Global Coverage

PACE has a Level 1 requirement for two-day coverage [*Werdell*, 2018], within the limit of 60 degrees sensor zenith angle. Note, this limit only provides a definition for two-day coverage; the OCI will collect data at larger zenith angles. Note also that data gaps created by OCI tilt maneuvers are not considered in the definition of global coverage. The 60 degree limit primarily constrains coverage near the equator, where the one-day inter-orbit gaps are largest. The one-day equatorial coverage is equal to the ratio of the useful swath width to the orbit track spacing. At the design altitude of 676 km, this coverage is 71.9%. The coverage changes monotonically with altitude; in the study altitude range of 400 to 450 km, this figure ranges from 48.9 to 53.6%.

The two-day coverage depends on both the one-day coverage and the overlap between swaths on successive days. The latter is determined by the number of orbits per day. When this number is an exact integer, the overlap is 100%, resulting in permanent gaps at the equator, and the two-day coverage is a minimum. For example, an altitude of about 560 km results in 15 orbits per day. When the number is an odd number of half-orbits (i.e., a two-day repeat cycle) the coverage from the second day tends to fill the gaps from the first, and the overall coverage is maximized.

Because the one-day coverage within the study range is close to 50%, maximizing two-day coverage requires that the orbit be close to a two-day repeat. The orbits per day range from 15.54 at 400 km to 15.37 at 450 km, with 15.5 orbits at 412 km. This suggests that the best two-day coverage will occur close to 412 km altitude. It should be noted that the data gaps along the equator would be filled by staggering the times of tilt on successive days as was done during the SeaWiFS mission.

A simulation was performed of two-day coverage within the study altitude range. Two-line elements (TLEs) were generated for Sun-synchronous polar orbits with a 1:00 pm equator crossing time, for altitudes from 400 to 450 km at 10-km increments. Orbit ephemeris data were generated for two days (days 84 and 85 of 2020) at each altitude. OCI geolocation was simulated for the ascending (daylight) part of the orbit, including a 20-degree fore/aft tilt with a tilt change at the Equator.

Using the simulated geolocation data, the two-day coverage was analyzed for ocean color products. The useful data were identified based on the mission-specified sensor and solar zenith limits of 60 and 75 degrees, respectively. The viewed locations were then binned at SeaWiFS resolution (9.27 km bins) to determine global coverage. The two-day coverage for the range of altitudes is illustrated in Figures 5.1 through 5.5.

The simulation confirms that the two-day coverage is maximized between 410 and 420 km altitude. The global and equatorial coverage is summarized in Table 5.1. (Note that global coverage is also affected by

the tilt change data gap.) Within the 410 – 420 km altitude range, the equatorial coverage could be increased to 100% by redefining the sensor zenith angle limit from 60 to 62 degrees.

It should be noted that a repeat cycle of exactly two days is undesirable for PACE. With this orbit, a given location will always be viewed at the same scan angle. The science data quality for OCI is improved by viewing locations at a variety of atmospheric scattering phase angles, particularly when generating Level-3 temporal composites. Within the study range, an altitude chosen for PACE would represent a compromise between coverage and the repeat cycle. At the design altitude of 676 km, the orbit repeat cycle is approximately 11 days.

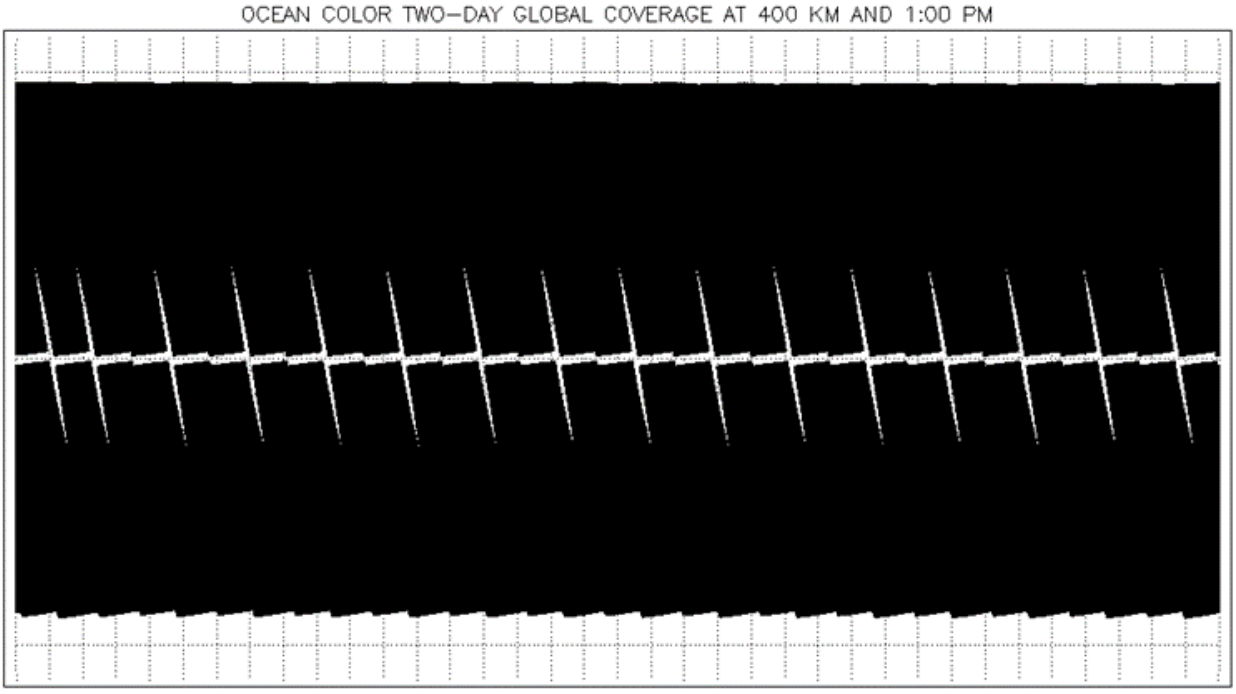

Figure 5.1. OCI two-day coverage at 400 km altitude.

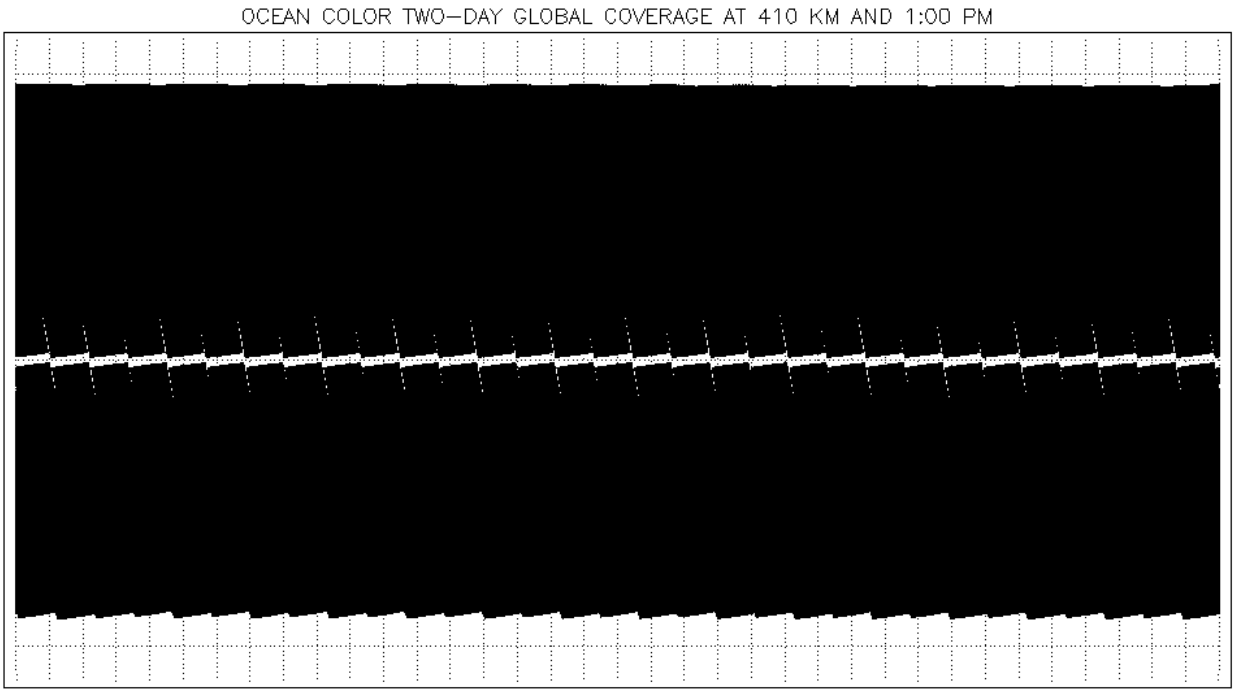

Figure 5.2. OCI two-day coverage at 410 km altitude.

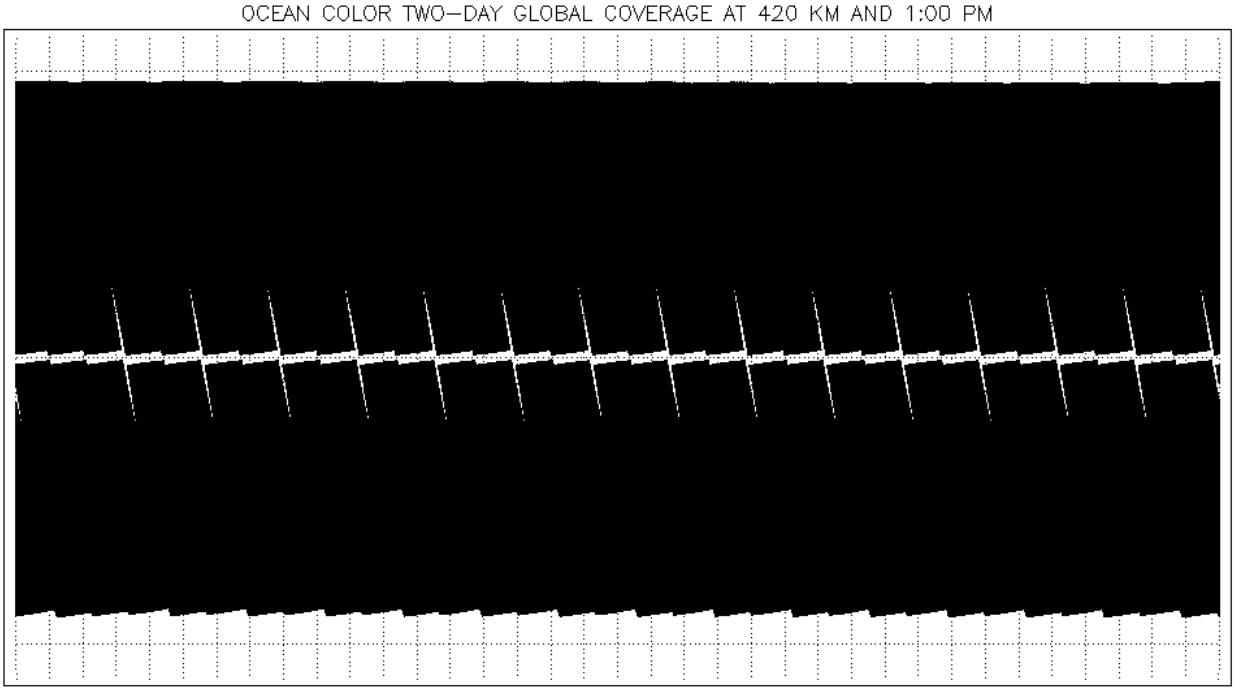

Figure 5.3. OCI two-day coverage at 420 km altitude.

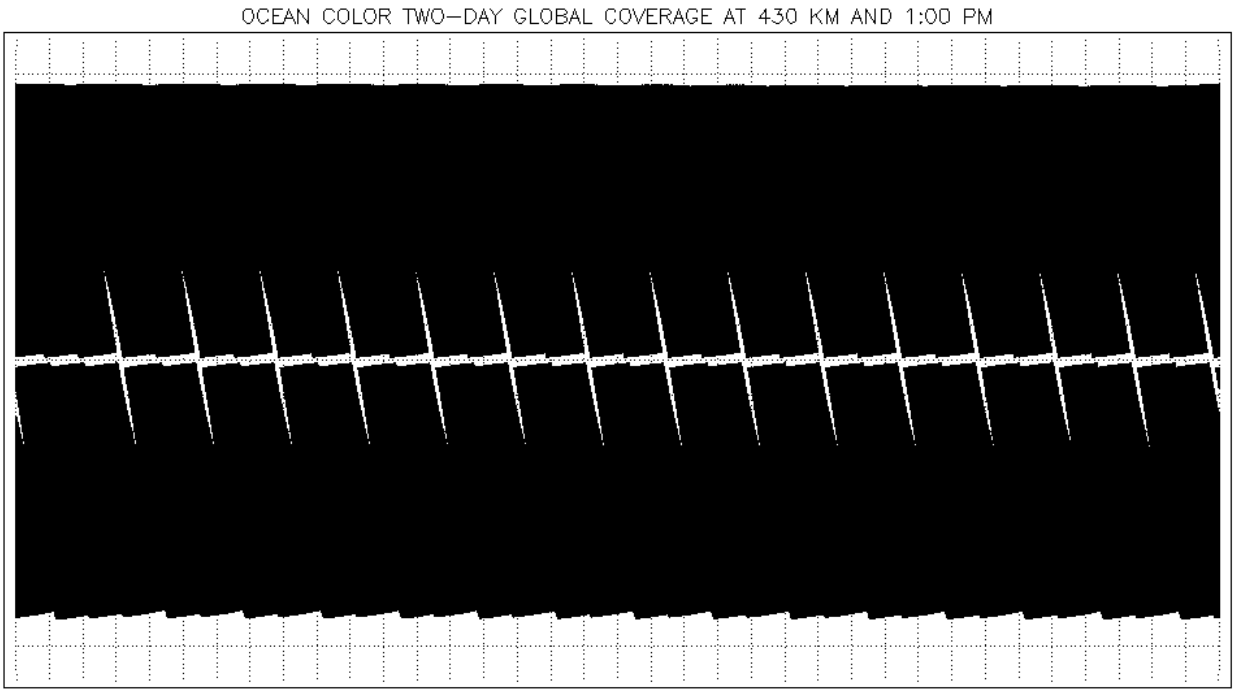

Figure 5.4. OCI two-day coverage at 430 km altitude.

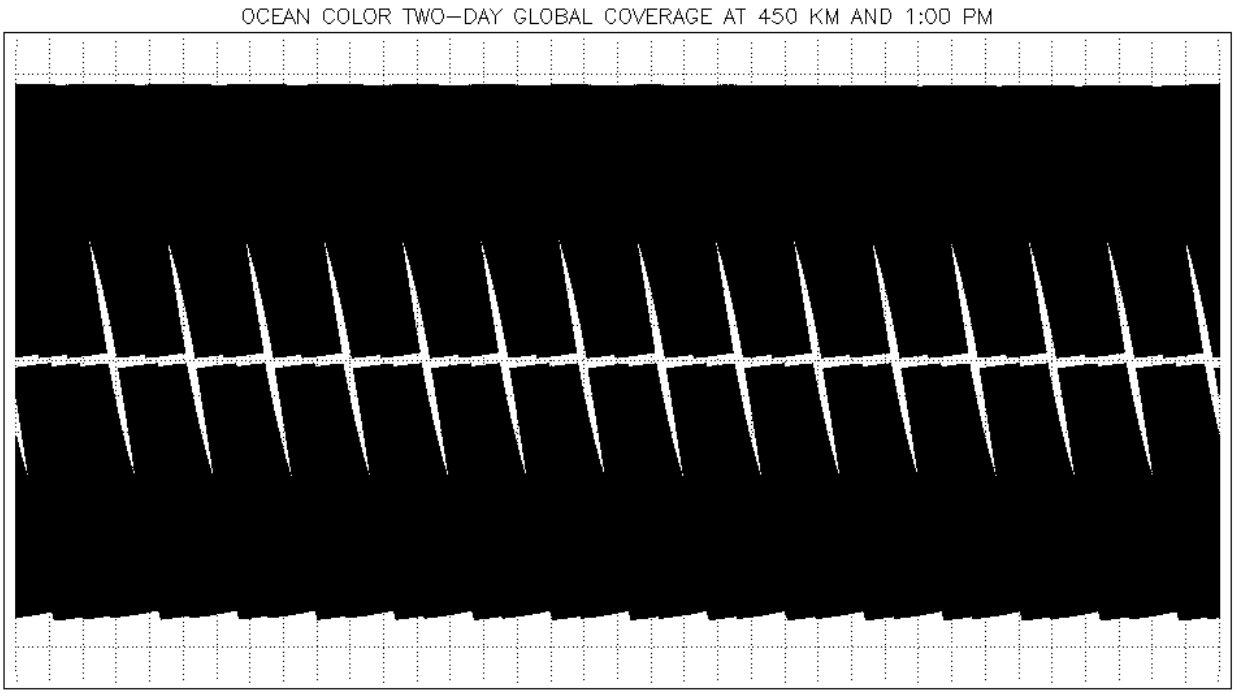

Figure 5. 5. OCI two-day coverage at 450 km altitude.

Table 5.1. Summary of Coverage Simulation Results (over a period of two days)

Altitude (km)	Global Coverage (%)	Equatorial Coverage (%)
400	95.3	93.1
410	96.6	95.5
420	96.3	95.6
430	95.3	93.2
440	92.6	88.1

5.2.3. Orbit Maintenance

The lower altitude for PACE would significantly increase the atmospheric drag on the spacecraft. A rule of thumb is that the atmospheric density doubles for every 50 km reduction in altitude; by this rule, a reduction from 676 to 415 would increase the density by a factor of 35 to 40, with a commensurate increase in drag. The density also varies significantly during the solar cycle, especially at low-Earth-orbit (LEO) spacecraft altitudes, so the timing of the mission relative to the solar maximum will have a significant effect on orbit maintenance. The next solar minimum is predicted for between 2019 and 2020; this means that the next maximum would be expected in approximately 2025, near the end of the nominal PACE mission.

PACE does not have as stringent a requirement for altitude maintenance as some LEO missions. The driving requirement is to maintain the equator crossing time within +/- 10 minutes of the nominal value. This also imposes a limit on the altitude, since the orbit plane precession rate required to maintain the equator crossing time depends on altitude. Analysis of the orbit maintenance requirements for the nominal altitude have shown that no orbit maintenance maneuvers (OMMs) may be required within the three-year mission design duration, and at most five OMMs would be required within 10 years. PACE has a Level 1 requirement [*Werdell*, 2018] to carry sufficient propellant for 10 years of orbit maintenance.

Analysis of the PACE orbit maintenance requirements at lower altitudes has not been performed. For comparison, the Tropical Rainfall Measurement Mission (TRMM) was originally operated at an altitude of 350 km, and the altitude was raised to 402.5 km in 2001 to extend the mission lifetime. The TRMM orbit maintenance requirement was +/-1 km, more stringent than for PACE. In 2008, near the solar minimum, five OMMs were required for TRMM; during a solar maximum, this number would be expected to increase by approximately an order of magnitude. Although fewer maneuvers would be required for PACE due to the less stringent requirement, the propellent usage would be similar, since the less frequent maneuvers would also be larger.

In summary, reducing the PACE altitude to within the study range would significantly increase the required orbit maintenance, which is expected to be minimal at the design altitude. A detailed study would need to be performed to quantify both the operational effort and propellant requirements for this.

5.2.4. OCI Impacts

The OCI design is closely linked to the mission altitude. At a basic level, the instrument optics are designed to produce the required ground pixel size (1 km) for a specific altitude, and the scan rate is determined by the ground track speed and the pixel size. The instrument performance is also significantly

dependent on the optics and other design parameters that would need to be changed to accommodate an altitude change.

A preliminary assessment was performed of impacts to the hyperspectral scanning OCI concept due to a change to a 415 km orbit. The goals were to explore development of a modified OCI concept to support flying at this altitude, and assess the impact on the signal-to-noise ratio (SNR), a key instrument performance parameter. These studies were incorporated into an ongoing broader trade on ground sample distance (GSD) vs SNR.

A specific OCI design, simply placed in a lower orbit without any design modifications, performs significantly worse in terms of SNR. If the IFOV is not changed, the resulting decrease in GSD results in decreased signal and decreased SNR. To maintain the baseline SNR, the instantaneous field-of-view (IFOV) would need to be increased, growing GSD somewhat. The selected GSD was 850 meters. This would require significant changes to the OCI optical design that, at a minimum, would have resulted in greater aberration, i.e., an increase in image blurriness. The lower orbit would also require a faster telescope rotation rate (order ~ 5-6%), increasing loads on the telescope and making alignment more difficult.

The assessment determined that an additional 4-6 weeks would be required to complete a detailed study of the optics, opto-mechanical, and mechanism changes required for the lower orbit. Additional technical obstacles could be uncovered, and study is needed to accurately estimate the additional time required to perform required design modifications and to understand risks. The OCI engineering team has moved forward with the baseline 676 km design since the completion of this preliminary assessment.

5.2.5. Spacecraft Impacts

A preliminary assessment was performed of the impacts to the spacecraft design of the lower altitude. In addition to the orbit maintenance impact, the following potential impacts were noted:

- Increase atomic oxygen (AO) influence: All external surfaces must be AO-resistant. This will require additional AO blanketing for the backs of solar arrays and other exposed surfaces, and the use of AO-resistant thermal blanketing, all of which will have mass and cost impacts.
- External optics (e.g, star trackers): Requires additional study to ensure there are no impacts.
- RF communications: The lower orbit will require modification to the earth coverage antenna (ECA) design and temperature requirements.
- Thermal control: The lower orbit will require an increase in the radiator sizes, which will increase the cost and mass.
- Guidance, navigation, and control: Higher aerodynamic torques could have minor impact on some components.
- Mechanical design: Some modification to structure will be required to account for additional mass.

In addition to the impacts on the spacecraft, it was noted that the reduced altitude could significantly affect the selection or design of a second instrument, specifically the Multi-Angle Polarimeter (MAP) that has been proposed for PACE. Existing polarimeter designs that the project understands best are optimized

for operation at higher orbits. A 400-450 km orbit could inject significant programmatic risk into the polarimeter selection.

5.3. Conclusion

A study was undertaken of the required changes and potential impacts to the PACE mission of reducing the mission altitude to 400 – 450 km to operate in constellation with a LIDAR mission. The study included assessments of mission science, global coverage, orbit maintenance, the OCI design and performance and the spacecraft design. The following conclusions were reached:

- The direct effect of the altitude change on mission science is neutral. There would be a significant benefit to contemporaneous operation with a LIDAR mission, but this may also be obtained by missions at different altitudes.
- Two-day global coverage is marginal at the lower altitude, and limits the altitude range to between 410 and 420 km.
- Orbit maintenance requirements would be significantly increased at the lower altitude.
- Significant redesign of OCI would be required to meet performance requirements at the lower altitude, and there are significant risks involved.
- There are multiple potential impacts to the spacecraft; these are manageable but have cost and possibly schedule impacts.
- The selection of additional instruments (e.g., MAP) will be affected.

In the absence of further direction, the mission design has continued for the 676 km orbit.

Chapter 6

PACE OCI Proxy Data Development

Bryan Franz, NASA Goddard Space Flight Center, Greenbelt, Maryland[6]

Executive Summary

Prior to the availability of real data from the Ocean Color Instrument (OCI) on PACE, it is useful to have a source of proxy data for software and algorithm development and testing, e.g., the ocean color atmospheric correction algorithm and bio-optical property retrieval capabilities. Proxy data is defined here as real data from another airborne or spaceborne instrument that approximates the OCI spectral range, such that viable OCI geophysical retrieval algorithms can be operated on the data with minimal modifications. Data from the hyperspectral AVIRIS instrument [*Vane et al.,* 1993] has been utilized for this purpose.

6.1. Introduction

This document describes the derivation and format of a dataset that may be useful as a proxy for calibrated top-of-atmosphere radiances that are expected to be provided by the PACE Ocean Color Instrument (OCI). The proxy data are derived from past airborne campaigns of the Airborne Visible / Infrared Imaging Spectrometer (AVIRIS) hyperspectral instrument [*Vane et al.,* 1993] and have been reformatted to match the expected format of a PACE OCI Level-1B file, with the primary difference being the specific band centers or spectral band sampling. A primary driving consideration in the conversion from native instrument observation to OCI-like observation is to minimize any modification of the observed radiometry that might erroneously alter the influence of higher spectral resolution features (e.g., oxygen or water-vapor absorption). As such, no resampling or interpolation has been applied to the hyperspectral observations of the source data. Only aggregation has been performed, where necessary, to better match the expected band widths of the OCI instrument. Such aggregations were performed using a weighted mean, where the weights correspond to the native band widths.

6.2. PACE OCI Assumed Spectral Channels

The OCI instrument design has not yet been finalized. It is here assumed to be a hyperspectral instrument spanning the range from 325 nm to 885 nm at 5-nm intervals, with additional spectral bands (band widths) in nm of 940 (45), 1038 (75), 1250(30), 1378 (15), 1615 (75), 2130 (50), and 2250 (75).

6.3. PACE OCI Assumed Level-1B Format

It is anticipated that OCI Level-1A and higher data products will be produced in a netCDF4 format with CF and ISO-compliant meta-data similar to that currently produced by the Ocean Biology Processing Group (OBPG) for all standard Level-2 ocean color products. The proxy Level-1B files produced here thus follow that general structure. The data fields in the Level-1B file include per-pixel longitude and

[6] Cite as: Franz, B. (2018), PACE OCI Proxy Data Development, in *PACE Technical Report Series, Volume 5: Mission Formulation Studies (NASA/TM-2018 – 2018-219027/ Vol. 5)*, edited by I. Cetinić, C. R. McClain and P. J. Werdell, NASA Goddard Space Flight Space Center Greenbelt, MD.

latitude, solar and view zenith and azimuth angles, and the observed radiances pixel, line, and band in the form of a data cube. Examples of the full data structure are provided for each proxy data source in the sections that follow.

6.4. PACE OCI Proxy Data Derived from AVIRIS Classic (OCIA)

AVIRIS Classic is an airborne hyperspectral instrument with 224 bands spanning the 360nm to 2500nm spectral range at 10-nm spectral sampling. AVIRIS has been flown on the ER-2 high altitude aircraft during a multitude of field campaigns spanning several decades. As such, there are many existing datasets readily available that may be useful for PACE algorithm development and testing. Table 6.1 shows the spectral band centers and band widths of AVIRIS Classic, and the corresponding 62 spectral band centers and band widths of the OCI proxy data derived from AVIRIS (OCIA). Note that the mapping is one for one over the 360 to 890nm spectral range, with the wider AVIRIS band widths maintained. At the longer wavelengths, the 10-nm AVIRIS bands are aggregated to match the wider spectral bands of OCI.

Unfortunately, AVIRIS does not cover the shortest (ultraviolet, UV) wavelength range of OCI, and there is no existing imaging spectrometer that spans the full spectral range expected from OCI. Also, AVIRIS radiometric performance below 400-nm is poor (Vane et al. 1993). Thus, testing of advanced algorithms that utilize the UV spectral range will not be possible with this proxy dataset. Such testing will require simulated data, or additional efforts to connect UV imaging instruments with AVIRIS or another visible-to-SWIR spectrometer.

Table 6.1: AVIRIS Classic Band Centers and Widths and Mapping to OCIA Bands

AVIRIS Band	Wavelength	Width		OCI Band	Wavelength	Width
1	365.92981	9.852108		1	365.92981	9.852108
2	375.59399	9.796976		2	375.59399	9.796976
3	385.26254	9.744104		3	385.26254	9.744104
4	394.93552	9.693492		4	394.93552	9.693492
5	404.61288	9.64514		5	404.61288	9.64514
6	414.29462	9.599048		6	414.29462	9.599048
7	423.98077	9.555216		7	423.98077	9.555216
8	433.6713	9.513644		8	433.6713	9.513644
9	443.36621	9.474332		9	443.36621	9.474332
10	453.06552	9.43728		10	453.06552	9.43728
11	462.7692	9.402488		11	462.7692	9.402488
12	472.47729	9.369956		12	472.47729	9.369956
13	482.18976	9.339684		13	482.18976	9.339684
14	491.90665	9.311672		14	491.90665	9.311672
15	501.6279	9.28592		15	501.6279	9.28592
16	511.35355	9.262428		16	511.35355	9.262428
17	521.08356	9.241196		17	521.08356	9.241196
18	530.81799	9.222224		18	530.81799	9.222224
19	540.55682	9.205512		19	540.55682	9.205512
20	550.30005	9.19106		20	550.30005	9.19106
21	560.04767	9.178868		21	560.04767	9.178868
22	569.79962	9.168936		22	569.79962	9.168936
23	579.55603	9.161264		23	579.55603	9.161264
24	589.31677	9.155852		24	589.31677	9.155852
25	599.08191	9.1527		25	599.08191	9.1527
26	608.8515	9.151808		26	608.8515	9.151808
27	618.62543	9.153176		27	618.62543	9.153176
28	628.40375	9.156804		28	628.40375	9.156804
29	638.18646	9.162692		29	638.18646	9.162692
30	647.97357	9.17084		30	647.97357	9.17084
31	657.76508	9.181248		31	657.76508	9.181248
34	664.59937	9.8487076		32	664.59937	9.8487076

35	674.40125	9.7987116		33	674.40125	9.7987116
36	684.19794	9.7584824		34	684.19794	9.7584824
37	693.98938	9.72802		35	693.98938	9.72802
38	703.77563	9.7073244		36	703.77563	9.7073244
39	713.55664	9.6963956		37	713.55664	9.6963956
40	723.33252	9.6952336		38	723.33252	9.6952336
41	733.10309	9.7038384		39	733.10309	9.7038384
42	742.86853	9.72221		40	742.86853	9.72221
43	752.62872	9.7503484		41	752.62872	9.7503484
44	762.38373	9.7882536		42	762.38373	9.7882536
45	772.13348	9.8359256		43	772.13348	9.8359256
46	781.87805	9.8933644		44	781.87805	9.8933644
47	791.61743	9.96057		45	791.61743	9.96057
48	801.35156	10.0375424		46	801.35156	10.0375424
49	811.08051	10.1242816		47	811.08051	10.1242816
50	820.80426	10.2207876		48	820.80426	10.2207876
51	830.52277	10.3270604		49	830.52277	10.3270604
52	840.23608	10.4431		50	840.23608	10.4431
53	849.94415	10.5689064		51	849.94415	10.5689064
54	859.64709	10.7044796		52	859.64709	10.7044796
55	869.34479	10.8498196		53	869.34479	10.8498196
56	879.03723	11.0049264		54	879.03723	11.0049264
57	888.72449	11.1698		55	888.72449	11.1698
61	927.42145	11.9269624		56	936.436901	32.47029665
62	937.0827	10.78153				
63	946.73871	9.76180425				
69	1004.56531	9.76637025		57	1038.234675	78.306347
70	1014.18488	9.770633				
71	1023.79919	9.77589625				
72	1033.40833	9.78216				
73	1043.01221	9.78942425				
74	1052.61096	9.797689				
75	1062.20447	9.80695425				
76	1071.79272	9.81722				
94	1243.49097	10.173089		58	1252.996974	30.60809325
95	1252.98022	10.20236425				
96	1262.46436	10.23264				
110	1382.39978	10.77621301		59	1382.39978	10.77621301
131	1591.71082	10.7250623		60	1616.619561	64.33927434
132	1601.67529	10.72413901				
133	1611.63965	10.72335321				
134	1621.60364	10.72270491				
135	1631.5675	10.72219411				
136	1641.53101	10.7218208				
186	2236.70459	10.63353648		61	2246.639718	53.06395905
187	2246.68066	10.61310867				
188	2256.65454	10.592364				
189	2266.62622	10.57130247				
198	2236.70459	10.63353648		62	2261.579439	63.48846453
199	2246.68066	10.61310867				
200	2256.65454	10.592364				
201	2266.62622	10.57130247				
202	2276.59546	10.54992408				
203	2286.5625	10.52822883				

The full structure of PACE OCI proxy netCDF4 data file produced from AVIRIS is shown for one sample scene (OA2011281160543.L1B_LAC) in Table 6.2.

Table 6.2: Level-1B data file structure

```
netcdf OA2011281160543.L1B_LAC {
dimensions:
        number_of_lines = 1502 ;
        pixels_per_line = 837 ;
        number_of_bands = 62 ;
```

```
// global attributes:
                :title = "OCIA Level-1B Data" ;
                :sensor = "OCIA" ;
                :product_name = "OA2011281160543.L1B_LAC.nc" ;
                :processing_version = "V1.0" ;
                :Conventions = "CF-1.6" ;
                :institution = "NASA Goddard Space Flight Center" ;
                :license = "http://science.nasa.gov/earth-science/earth-science-data/data-information-policy/";
                :naming_authority = "gov.nasa.gsfc.sci.oceandata" ;
                :date_created = "2016266163258000" ;
                :keywords_vocabulary = "NASA Global Change Master Directory (GCMD) Science Keywords" ;
                :stdname_vocabulary = "NetCDF Climate and Forecast (CF) Metadata Convention" ;
                :creator_name = "NASA/GSFC" ;
                :creator_email = "data@oceancolor.gsfc.nasa.gov" ;
                :creator_url = "http://oceancolor.gsfc.nasa.gov" ;
                :project = "PACE Project" ;
                :publisher_name = "NASA/GSFC" ;
                :publisher_url = "http://oceancolor.gsfc.nasa.gov" ;
                :publisher_email = "data@oceancolor.gsfc.nasa.gov" ;
                :processing_level = "L1B" ;
                :cdm_data_type = "swath" ;
                :orbit_number = 0 ;
                :history = "Generated by avirisbil2oci; cdlfile=OCI_Level-1B_Data_Structure.cdl";
                :startDirection = "Descending" ;
                :endDirection = "Descending" ;
                :day_night_flag = "Day" ;
                :time_coverage_start = "2011-10-08T16:05:43.418Z" ;
                :time_coverage_end = "2011-10-08T16:07:57.108Z" ;
```

```
group: sensor_band_parameters {
 variables:
        float wavelength(number_of_bands) ;
                wavelength:_FillValue = -32767.f ;
                wavelength:long_name = "wavelengths" ;
                wavelength:valid_min = 350.f ;
                wavelength:valid_max = 2250.f ;
                wavelength:units = "nm" ;
        float fwhm(number_of_bands) ;
                fwhm:_FillValue = -32767.f ;
                fwhm:long_name = "fwhm" ;
                fwhm:valid_min = 0.f ;
                fwhm:valid_max = 100.f ;
                fwhm:units = "nm" ;
 } // group sensor_band_parameters
```

```
group: observation_data {
 variables:
        float Lt(number_of_bands, number_of_lines,
pixels_per_line) ;
                Lt:_FillValue = -999.f ;
                Lt:long_name = "Top of Atmosphere
Radiance" ;
                Lt:valid_min = 0.f ;
                Lt:valid_max = 500.f ;
                Lt:units = "W m-2 sr-1" ;
        short altitude(number_of_lines) ;
                altitude:_FillValue = -32767s ;
                altitude:long_name = "altitude" ;
                altitude:valid_range = 0s ;
                altitude:valid_max = 25000s ;
                altitude:units = "meters" ;
 } // group observation_data
}
```

```
group: navigation_data {
 variables:
        float lon(number_of_lines, pixels_per_line) ;
                lon:_FillValue = -999.f ;
                lon:long_name = "Longitude" ;
                lon:valid_min = -180.f ;
                lon:valid_max = 180.f ;
                lon:units = "degrees_east" ;
        float lat(number_of_lines, pixels_per_line) ;
                lat:_FillValue = -999.f ;
                lat:long_name = "Latitude" ;
                lat:valid_min = -0.f ;
                lat:valid_max = 90.f ;
                lat:units = "degrees_north" ;
```

```
group: scan_line_attributes {
 variables:
        double scan_start_time(number_of_lines) ;
                scan_start_time:_FillValue = -999. ;
                scan_start_time:long_name = "Scan start
time (UTC)" ;
                scan_start_time:valid_min = 0. ;
                scan_start_time:valid_max = 2000000000.
;
                scan_start_time:units = "seconds" ;
        double scan_end_time(number_of_lines) ;
                scan_end_time:_FillValue = -999. ;
                scan_end_time:long_name = "Scan end
time (UTC)" ;
```

```
        short range(number_of_lines, pixels_per_line) ;
                range:_FillValue = -32767s ;
                range:long_name = "Aircraft-to-surface
distance (range)" ;
                range:valid_range = 0s ;
                range:valid_max = 25000s ;
                range:units = "meters" ;
        float senz(number_of_lines, pixels_per_line) ;
                senz:_FillValue = -999.f ;
                senz:long_name = "Solar zenith angle" ;
                senz:valid_min = 0.f ;
                senz:valid_max = 90.f ;
                senz:units = "degrees" ;
        float sena(number_of_lines, pixels_per_line) ;
                sena:_FillValue = -999.f ;
                sena:long_name = "Solar azimuth angle" ;
                sena:valid_min = 0.f ;
                sena:valid_max = 90.f ;
                sena:units = "degrees" ;
        float solz(number_of_lines, pixels_per_line) ;
                solz:_FillValue = -999.f ;
                solz:long_name = "Solar zenith angle" ;
                solz:valid_min = 0.f ;
                solz:valid_max = 90.f ;
                solz:units = "degrees" ;
        float sola(number_of_lines, pixels_per_line) ;
                sola:_FillValue = -999.f ;
                sola:long_name = "Solar azimuth angle" ;
                sola:valid_min = 0.f ;
                sola:valid_max = 90.f ;
                sola:units = "degrees" ;
 } // group navigation_data
```

```
                scan_end_time:valid_min = 0. ;
                scan_end_time:valid_max = 2000000000.
;
                scan_end_time:units = "seconds" ;
        short altitude(number_of_lines) ;
                altitude:_FillValue = -32767s ;
                altitude:long_name = "altitude" ;
                altitude:valid_range = 0s ;
                altitude:valid_max = 25000s ;
                altitude:units = "meters" ;
 } // group scan_line_attributes
```

Chapter 7

PACE Instrument Design Lab Studies – Summary and Overview on Meeting Science Requirements

Antonio Mannino, NASA Goddard Space Flight Center, Greenbelt, Maryland

Brian Cairns, NASA Goddard Institute for Space Studies, New York, New York

7.1. Introduction

The PACE Project conducted a series of Instrument Design Lab (IDL) studies at GSFC, as part of the pre-Phase A trade studies, to evaluate various instrument concepts to accomplish the mission science objectives and to meet science requirements while optimizing the PACE instrument capabilities under the design-to-cost constraints. These IDL studies also addressed many of the science requirement trade studies that NASA PACE Program Science directed the project to conduct during pre-Phase A (summarized in Tables 7.1-7.2; see section 7.5 Appendix A for the complete Program Science Trades and Feasibility Study document). The vast majority of the IDL studies focused on the Ocean Color Instrument (OCI), since this instrument would be designed to meet and exceed all of the PACE threshold science requirements. In addition, the project conducted an IDL study for a Multi-Angle Polarimeter (MAP) to address the Program Scientists' trade and feasibility recommendations (Table 7.2) and to inform the project on what could be expected in terms of resources required and performance achieved for an instrument similar to the MAP described in the PACE SDT report (i.e., CNES-developed Multi-viewing, Multi-channel, Multi-polarisation Imager or 3MI sensor) in preparation for a formal request for information (RFI) and a request for proposal (RFP) from industry and other institutions. In addition, the PACE Program Scientists requested the PACE project to conduct a trade and feasibility study on a high spatial resolution coastal ocean color sensor (Table 7.3). Therefore, the project conducted a dedicated coastal camera IDL study and issued an RFI seeking input from industry on potential performance, cost and size of a coastal camera. The PACE project coordinator for the OCI and coastal camera IDL studies was Eric Gorman (currently OCI instrument systems engineer). Because the PACE OCI management and systems engineering team anticipated challenges in meeting the OCI threshold requirements in conjunction with achieving the goal requirements of 500 m to 250 m or better spatial resolution from a single instrument, the project decided to separate the higher spatial resolution goal requirements into a second instrument called the Coastal Camera (CC), which was consistent with the Program Science Trades and Feasibility Study.

Table 7.1: Summary of the Ocean Color Instrument (OCI) trades and feasibility study requested by NASA Program Science.

Global Ocean Color Sensor (OCI)	
Design Drivers	
Global Coverage	2-day
Lunar Calibration	through Earth viewing port that illuminates all detectors at the same time
Spectral range & resolution	hyperspectral (5 nm) UV-VIS-NIR
Signal-to-Noise ratio (SNR)	consistent with PACE SDT document
Spectral subsampling	~1-2 nm resolution from 655 to 710 nm
Spectral artifacts	spectral degradation tracking involving the minimum number of detector elements possible to minimize striping, cross-talk, and other artifacts in instrument level data
Driver Consequences	
Fore-optics	Meeting all design drivers requires a Sea-WiFS-like fore-optics system such that all ground pixels are observed with the same set of detector elements, which represents the minimum number of detectors that must be calibrated and tracked for degradation.
Drawbacks	Fast telescope spin rates to enable all science pixels with the same minimum GSD result in short dwell times on detectors, so increasing spin rate can translate to decreasing signal or lower SNR
Trade Recommendations	
Ground Sample Distance Baseline 1 km at nadir	(1) evaluate what the highest achievable resolution is that still meets SNR and other requirements, (2) evaluate what design options/approaches are available to achieve this resolution at all scan angles
Spectral Range Baseline resolution of 5 nm from 350 – 800 nm	evaluate design modifications, risks, and costs for (1) expanding the spectral range (a) below 350 nm or (b) up to 900 nm, (2) improving resolution to < 5 nm at either all wavelengths or for specific spectral regions.
SWIR bands	Evaluate low-risk instrument modifications required to add the mission threshold and baseline SWIR measurement requirements onto OCI and determine the changes in mission risk and changes in total cost to the mission.

Table 7.2: PACE Multi-Angle Polarimeter (MAP) sensor trade and feasibility studies requested by NASA Program Science.

Atmosphere/Ocean Polarimeter (MAP)	
Trade Recommendations	
SWIR Bands	940, 1378, 2250 nm for cloud property measurements
Uncertainty in DOLP[1]	<0.5%
Swath width	±30° and ±45°
Angular range	±70°
GSD	Study reduction to (1) 1 km and (2) 500 m
Radiometric accuracy	<3%
SWIR bands	Evaluate low-risk instrument modifications required to add the mission threshold and baseline SWIR measurement requirements onto MAP and determine the changes in mission risk and changes in total cost to the mission.

[1] *Degree of Linear Polarization*

Table 7.3: PACE trade studies requested by NASA Program Science for the Coastal Camera (CC).

Coastal Ocean Color Sensor (CC)	
Design Drivers	
GSD	50-100 m
Sensor degradation tracking	Comparable to MODIS-Aqua
Visible and near-IR bands	Consistent with SeaWiFS visible and NIR bands
UV bands	Centered at 360 and 380 nm with bandwidth ≤20 nm
SNR	Comparable to OLI[1] on Landsat-8 or HICO[2]
Spatial coverage	Comparable to OLI[1] on Landsat-8 or HICO[2]
Spectral resolution and sampling	e.g., similar to HICO with 5.7 nm resolution with sampling at 1.9 nm intervals enabling 10 nm bands from 400-745 nm and 20 nm bands for NIR (746-900 nm)
Driver Consequences	
50-100 m GSD	Requires instrument architecture similar to MODIS or MERIS with 2D array to provide required SNR
Drawbacks	Instrument artifacts will exist; SNR will be lower than OCI
Trade Recommendations	
Heritage sensor designs	Evaluate (a) existing space and airborne sensors that can achieve threshold requirements, (b) changes in mission risk with addition of coastal camera, and (c) changes in cost to the mission
Alternate sensor designs	Evaluate (a) other design concepts that can achieve requirements and science, (b) changes in mission risk and TRL[3], and (c) changes in cost to the mission
SWIR bands	Evaluate low-risk instrument modifications required to add the mission threshold and baseline SWIR measurement requirements onto CC and determine the changes in mission risk and changes in total cost to the mission.

[1] *OLI refers to the Operational Land Imager, which has an SNR of 144 to 478 in visible bands for typical ocean top-of-atmosphere radiance (Ltyp) at 30 m GSD [Franz et al., 2015] and 185 km swath providing 16-day global coverage.*

[2] *HICO refers to the Hyperspectral Imager for the Coastal Ocean, which has an SNR of ~100-400 in visible bands at Ltyp for ~92m GSD [Hu et al., 2012]and scenes of 50 km cross-track x 200 km along-track.*

[3] *TRL refers Technology Readiness Level, i.e., technical maturity*

7.2. OCI Study Parameters and Requirements

The project conducted a detailed architecture study on what instrument concepts would be capable of achieving and exceeding the threshold science requirements attributed to OCI. The team concluded that three instrument concepts would be worth pursuing in more detail within the GSFC Instrument Design Lab: HyperSpectral Scanner (HSS), HyperSpectral Pushbroom (HSP), and multi-band scanner (MBS) (Fig. 7.1).

Figure 7.1. Schematic of the Ocean Color Instrument concepts considered as part of the architecture design study. Diagram courtesy of Ulrik Gliese, Eric Gorman and Bryan Monosmith.

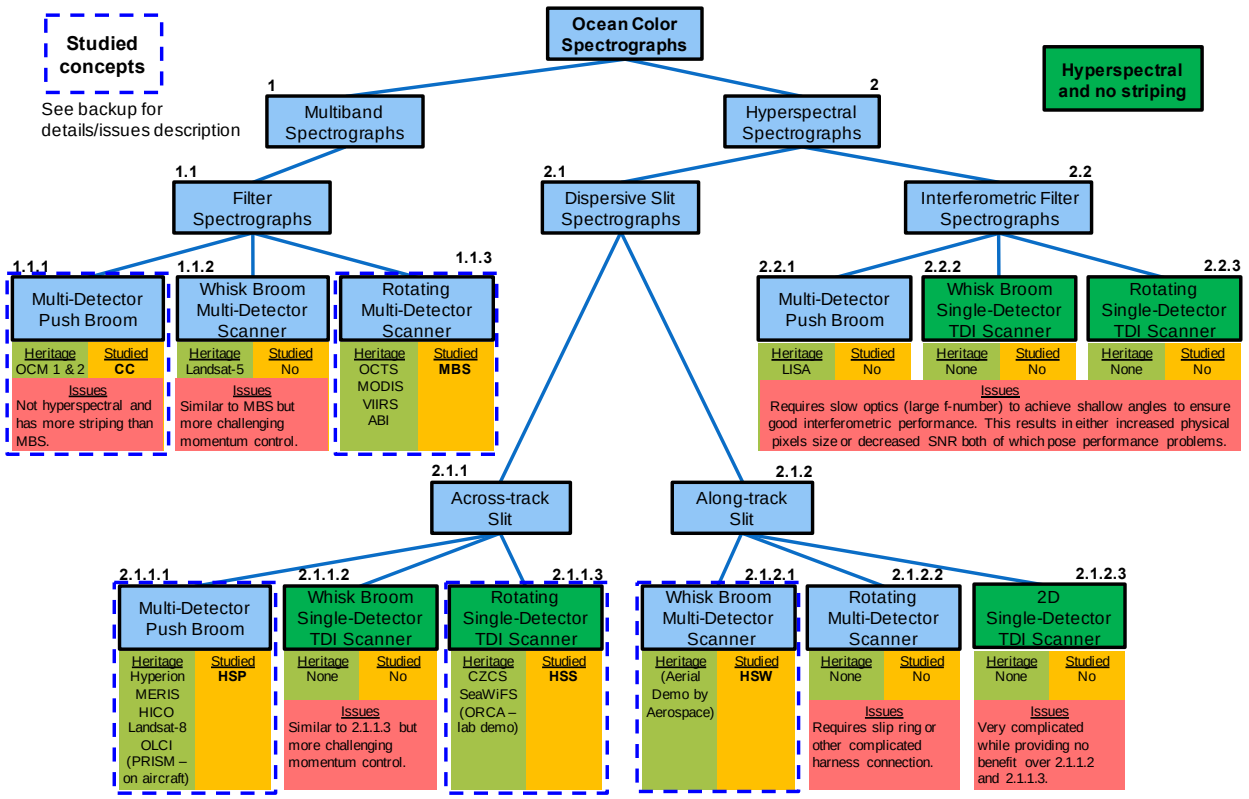

Over the course of several weeks to several months, a subset of the IDL team worked with the project to develop a first order optical-mechanical design for each of the three instrument concepts. The maturity of this preliminary design concept largely determines the level of detail that the IDL team can provide in their one-week focused study that involves all relevant engineering disciplines (systems, mechanical, optical, electrical, thermal, radiometry [signal-to-noise determination], detectors, contamination, reliability, flight software, and cost modeling). The project and OCI systems engineering and instrument science teams provided the IDL optical and mechanical engineering designers with the starting parameters for the optical-mechanical design such as platform altitude, instrument ground sample distance (GSD, spatial resolution), aperture diameter, spectral range, spectral sampling and resolution, swath width, and field-of-view (FOV). The OCI instrument architecture and science team computed the aperture diameter based on the PACE OCI signal-to-noise ratio (SNR) science requirements recommended in the PACE Science Definition Team report [2018]. The GSD for each instrument concept was based on science requirements and presumed technical feasibility. The IDL pre-work team developed the following optical-mechanical designs: HSP at 260 m GSD, HSS at 500 m GSD, and MBS at 500 m GSD. It was well understood that an HSP would be the most capable concept (presumed lowest technical

risk) to achieve the GSD goal requirement while meeting and exceeding the SNR requirements but could yield image artifacts that would exceed OCI threshold requirements. OCI systems engineering and management took the lead for the IDL studies from the PACE project perspective. Project science and OCI instrument science personnel actively participated in each of the IDL studies along with project management. OCI engineering staff worked closely with the IDL team and in several instances the IDL team was staffed or otherwise supported by OCI engineers.

For each instrument concept, the IDL team provided to the project the technical resource requirements (mass, power, data rate, volume, master equipment list (MEL)), parametric instrument cost, and assessments on performance (SNR, image quality, polarization sensitivity, etc.), technical feasibility, and risk. Starting from the optical-mechanical design pre-work, the full IDL engineering team developed a complete first-order design for each of the three OCI concepts over the course of a 5-day study week. Next, the IDL team and OCI engineers conducted subsequent instrument scaling studies to determine the technical resource requirements, feasibility, risk, cost, and estimated performance for alternate OCI GSD. The IDL team studied multiple spatial resolution cases for each concept ranging in GSD from ~250 m to 500 m. Table 7.4 lists the science requirements for each possible sensor concept and GSD case. The color code in the table denotes whether an instrument concept would be capable of meeting each science requirement. Technical resource requirements determined from the IDL studies were utilized by the project to obtain independent cost estimates (Table 7.6) for the various instrument concepts. It should be noted that GSFC had been studying the HSS concept since 2001 under the name Ocean Radiometer for Carbon Assessment (ORCA) including two Instrument Incubator Program-funded projects and several IDL studies over the course of about 10 years [*McClain et al.*, 2012]. Thus, this concept was by far the best understood.

The HSS concept draws its heritage from the earliest ocean color satellite sensors, the Coastal Zone Color Scanner (CZCS) and the Sea-Viewing Wide Field-of-View Sensor (SeaWiFS). The front-end optics of the HSS concept is composed of a rotating telescope similar to SeaWiFS. This rotating telescope sweeps the slit across the flight track onto effectively a single detector time-delay integration (TDI) system. This is the concept that the project ultimately selected as the most capable for meeting the mission science requirements.

The MBS concept possesses similarities in design to VIIRS, SeaWiFS, and MODIS. Like VIIRS and SeaWiFS, the front-end optics of the MBS concept is composed of a rotating telescope assembly. Multiple detectors are employed to accomplish measurements for 39 spectral bands between 350 nm to 2250 nm band centers. This approach is similar to MODIS and VIIRS, which enables the heritage sensors to collect observations at 250 m and 375 m GSD, respectively.

The HSP concept is a pushbroom sensor composed of multiple cameras to achieve the desired cross-track field-of-view. Heritage pushbroom instruments include MERIS, Hyperion, OLI, HICO, and OLCI. The 260 m GSD concept was comprised of 6 cameras each with a 28 mm pupil diameter, which was oversized due to an erroneous calculation by an OCI team member during the optical design development. This resulted in too much light entering the focal planes of each camera requiring the incoming signal to be attenuated by a factor of 2 with neutral density filters (implemented in the design to prevent saturation of the detectors). A more appropriate pupil diameter would have yielded a smaller instrument concept. The HSP 500 m version was a 5-camera system with a properly sized 12 mm pupil diameter.

The technical resource requirements and SNR performance results from the IDL study illustrate significant differences among the three sensor concepts. MBS concepts are by far the largest in mass and volume and HSS was generally smaller and lighter than the other two concepts except for the HSP 500 m

and 1 km versions (Table 7.5). The different GSD concepts within each sensor type yielded small differences except in data rates and in the size (mass and volume) for the two higher resolution HSP concepts, some of which can be attributed to the improperly sized pupil diameter of the 260 m version. All concepts either exceed or are close to meeting the SNR performance requirements with HSS yielding the highest SNR at most of the bands. It should be noted here that the mass for the current OCI design (HSS at 1 km) that the project is implementing is estimated at ~260 kg (current best estimate as of August 2018) excluding the tilt mechanism that has been shifted to the spacecraft. We point this out to express the rudimentary level of design coming out of a single IDL study. Many design iterations are required to attain a high-fidelity design concept for estimating technical resources and cost at a high confidence level. Therefore, an IDL study represents a starting point for an instrument design.

Table 7.4: Assessment of requirements compliance by the various OCI concepts studied in the IDL. Courtesy of the PACE OCI team. The green, yellow, and red color scheme represents whether the sensor concept meets, could potentially meet or does not meet the mission requirement.

Heading	HSP 260M Compliance	HSP 500M Compliance	MBS 250m Compliance	MBS 500m Compliance	HSS 350m Compliance	HSS 500m Compliance	HSS 1Km Compliance
Wavelength Range and Resolution 350 - 800nm with 5nm resolution	5nm	5nm	10nm	10nm	5nm	5nm	5nm
Image Striping Artifacts <0.5%	6 cameras with 1k x 1k pixel detectors will have significant striping	5 cameras with 640 x 1k pixel detectors will have significant striping	Some striping over custom array	Some striping over custom array	No striping due to virtual single pixel	No striping due to virtual single pixel	No striping due to virtual single pixel
Monthly Lunar Calibration	Raster Pattern	Raster Pattern	Lunar Scan	Lunar Scan	Lunar Scan	Lunar Scan	Lunar Scan
Spatial Resolution ≤1km	250m x 250m	500m x 500m	250m x 250m	500m x 500m	350m x 350m	500m x 500m	1Km x 1Km
2 Day Global Coverage Zenith sensor view angles ≤ 60°	104° @ 820Km with 5 cameras	104° @ 820Km with 5 cameras	120° @ 650Km	120° @ 650Km	120° @ 650Km	120° @ 650Km	120° @ 650Km
Sun Glint	±20° tilt mechanism for glint						
Measurement Accuracies 20% @ 0.004 350 - 395nm 5% @ 0.001 400 - 600nm 10% @ 0.002 600 - 900nm	SNR not met for all bands during study, but are achievable in the design space when aggregated to 1Km	SNR not met for all bands during study, but are achievable in the design space when aggregated to 1Km	Meets SNR requirements with custom dual gain detectors when aggregated to 1Km	Meets SNR requirements with custom dual gain detectors when aggregated to 1Km	Meets SNR across all bands when aggregated to 1Km Requires detector arrays for all SWIR bands	Meets SNR across all bands when aggregated to 1Km Requires detector arrays for all SWIR bands	Meets SNR across all bands Requires detector arrays for 2 SWIR bands
Atmospheric Correction Bands 350nm, 748nm, 865nm, 940nm plus at least 4 SWIR bands	Hyperspectral 342nm - 955nm 5 SWIR bands at 1240, 1378, 1640, 2130 and 2250	Hyperspectral 342nm - 955nm 5 SWIR bands at 1240, 1378, 1640, 2130 and 2250	Bands at 350nm, 748nm, 865nm, 940nm 5 SWIR bands at 1240, 1378, 1640, 2130 and 2250	Bands at 350nm, 748nm, 865nm, 940nm 5 SWIR bands at 1240, 1378, 1640, 2130 and 2250	Hyperspectral 340nm - 940nm 5 SWIR bands at 1240, 1378, 1640, 2130 and 2250	Hyperspectral 340nm - 940nm 5 SWIR bands at 1240, 1378, 1640, 2130 and 2250	Hyperspectral 340nm - 940nm 5 SWIR bands at 1240, 1378, 1640, 2130 and 2250
Resolution of data product 5km	5km	5km	10nm	10nm	5km	5km	5km
Mission Duration 18 months	All trades were performed with a minimum mission of 3 years						
Atmospheric Aerosol Measurements Aerosol Optical Depth Fraction of Total Visible Optical Depth	Meets SNR requirements and calibration requirements for UV through SWIR bands The requirements for cloud and aerosol data products can be met when the OCI SNR and calibration requirements are met for aggregation of 1km						
Cloud Measurements Cloud Layer Detection Cloud Top Pressure Cloud Water Path Optical Thickness Effective Radius Shortwave Radiative Effect	Meets SNR requirements and calibration requirements for UV through SWIR bands The requirements for cloud and aerosol data products can be met when the OCI SNR and calibration requirements are met for aggregation of 1km						

Table 7.5. Resource and performance metric results from the Ocean Color Instrument IDL studies.

	MBS	MBS	HSP	HSP	HSS	HSS
GSD (m)	250 m	500 m	260 m	500 m	350 m	500 m
Mass (kg)	284.6	279	203	120.5	134.1	131
Volume (m)	2.56 x 1.6 x 1.63	2.56 x 1.6 x 1.4	1.83 x 1.22 x 1.23	1.3 X 0.76 x 0.99	1.2 x 1.2 x 1.16 x	1.2 x 1.2 x 1.16 x
Power (W)	88.9	82.9	126.8	121.7	225.2	200.1
Data Rate (Mbps)	22.8	5.8	62.8	16.64	36.4	17.8
SNR @						
443 nm	2372	2360	2676	2312	1663	2140
678 nm	996	1002	1012	872	929	1236
865 nm	892	904	558	478	884	1306
1640 nm	332	346	177	140	289	338
@ Ltyp for 1 x 1 km pixel						

Table 7.6. Criteria applied by the PACE project to select the OCI design concept to pursue in Phase A. Courtesy of the PACE OCI Team. Costs shown were obtained from independent cost model analyses and are based on point design attributes (mass, volume, power, etc.) and estimated at the 65% confidence levels (C.L.) of the modeled "S" cost curves. RAO – NASA GSFC Resource Analysis Office; Aerospace – commercial company offering independent cost modeling analysis.

Instrument Concept	GSD/Pixel Size	Cost (RY$)		Science Assessment			Technical Risk Assessment		Path Forward
		RAO (65% C.L.)	Aerospace (65% C.L.)	Striping	Hyper-spectral	Lunar Calibration	Instrument Implementation	Calibration	
HSP	250m	N/A	$268M	High	Yes	Challenge	Low*	Medium	Eliminated by Cost
	500m	$186M	$207M	High	Yes	Challenge	Low*	Medium	Eliminated by Science (L1 Image Striping and Lunar Calibration capability not met)
	1000m	$168M	$191M	High	Yes	Challenge	Low*	Medium	
MBS	250m	N/A	$274M	Some	No	Yes	High	Low	Eliminated by Science (L1 Hyperspectral capability not met)
	500m	N/A	$262M	Some	No	Yes	High	Low	Technically Eliminated (custom detector development, rotation rate and electronics)
	1000m	$359M	$252M	Some	No	Yes	High	Low	
HSS	350m	N/A	N/A	No	Yes	Yes	High	Low	Technically Eliminated (rotation rate and electronics)
	500m	$241M	$221M	No	Yes	Yes	Medium	Low	Complete GSD capability trade in Phase A
	1000m	$226M	$213M	No	Yes	Yes	Low	Low	

The project concluded that only the HSS concepts are capable of meeting the PACE OCI Level-1 requirements. The spectral capabilities of MBS are clearly inferior to the other concepts, which provide hyperspectral data from the UV to the NIR at 5 nm resolution or 110 unique spectral bands compared to the 39 bands at 10 nm or coarser bandwidth for MBS (Table 7.4). The HSP concepts would suffer from significant striping artifacts and deemed incapable of achieving that Level 1 requirement (Table 5). For further details on image striping analysis see *McKinna et al.* [2018] . The lunar calibration by HSP would require a more complicated raster imaging pattern that would not accomplish the same level of end-to-end instrument long-term trend calibration as the lunar scan by HSS see *Patt* [2018]. These disadvantages of the HSP concepts led the project science team to recommend HSS as the concept most capable of accomplishing Level 1 requirements and continuing the ocean color climate quality data records begun with SeaWiFS in 1997. The project decided to proceed with the 1 km GSD HSS concept due to the technical risks associated with the 350 m and 500 m GSD instrument concepts (Table 7.6). The finer GSD concepts require spinning of the rotating telescope assembly at much higher frequency resulting in

significant stress on the instrument structure as well as requiring faster electronics and greater digitization rates that were unachievable at the time with flight qualified components.

7.3. Multi-Angle Polarimeter

The PACE Project conducted a single Instrument Design Lab (IDL) study at GSFC on a polarimeter instrument, as part of the pre-Phase A trade studies. In this case the purpose was not to evaluate a full range of design concepts, but rather to: i) Provide a resource footprint for this instrument so that the mission-level resources can be appropriately allocated; ii) Provide an instrument and operational summary so that the PACE mission would be well prepared to write an RFI (Request For Information) and evaluate vendor responses if that path were to be followed. To that end, a point design with the same functional architecture and polarization analysis method as used by the European Space Agency (ESA) 3MI and the French Centre National d'Etudes Spatiales (CNES) Polarization and Directionality of the Earth Radiation (POLDER) instruments was used to provide a baseline cost and resource estimate. This design uses a wide field camera to obtain overlapping images with each ground pixel being observed at multiple (12-15) different viewing angles and a continuously rotating filter wheel to provide spectral selection and polarization analysis.

The baseline requirement for the IDL point design was to have 4km pixels at nadir and a view angle range of ±50° from nadir, which provides two-day global coverage. The polarization analysis technique is a continuously rotating filter wheel with the polarization state being determined using polarizers with three polarization azimuths (0°, 60° and 120°) that are used to capture sequential images.

Table 7.7. IDL polarimeter instrument resources, with summary of items included in the Master Equipment List (MEL).

PACE IDL Polarimeter	Total Mass [kg]	Total Operating Power [W] (Effective Average)	Data Rate [Mbps]	Volume [mm^3]
VIS Telescope with Baffle, IR Telescope with Baffle, Filter Wheel Assembly Front End Electronics Main Electronics Box Harness Thermal Subsystem 5% Misc Hardware	25.9	73.9	1.1	1000x432x375

The cost estimate for the IDL point design is $45M with an assumption of 30% reserves. This cost also has a "wrap" that includes FPGA (Field Programmable Gate Array) development, Ground Support Equipment, Environmental Testing, Flight Spares and an Engineering Test Unit.

The required radiometric performance was for an uncertainty of less than 5% and the required polarimetric performance was for an uncertainty of less than 1%. The spectral locations and band widths of the spectral bands and the required SNR for each measurement are given in Table 7.8. It should be noted that while these SNRs are much lower than those required for the ocean color instrument (OCI), the data acquisition approach for the polarimeter is such that observations at a minimum of 12 view angles are obtained for each ground pixel and provide a net SNR for each pixel that is comparable with the OCI.

The point design selected uses a conceptually simple polarimetric analysis technique (rotating filter wheel) that facilitated a comprehensive optical, mechanical and thermal design within the week available

for the study. The wide field of view camera implementation with two-day global coverage is a good match to the required global coverage for the OCI sensor.

*Table 7.8. Specification of spectral bands and signal to noise ratio (SNR) for the IDL polarimeter design. Bands with a * include polarization measurements.*

Center Wavelength (nm)	Band Width (nm)	SNR
412*	20	100
443*	20	100
490*	20	100
555*	20	100
670*	20	100
763	10	100
765	40	100
865*	39	100
910	20	70
1378*	35	50
1610*	60	100
2130*	75	100

The sequential polarization analysis technique provides **no** guaranteed polarimetric accuracy over heterogeneous scenes, since changes in total radiance between sequential measurements can be aliased into apparent changes in polarization. While this would not be an issue for clear scenes over ocean, it would present challenges in analyzing the data over land.

The point design based on a 3MI/POLDER type sensor that the IDL analyzed provided useful information on likely resource requirements. It also allowed the feasibility of meeting performance requirements with a simple, compact sensor to be assessed and helped to define the scope of the information that would be required in an RFI/RFP if the project were to procure a polarimeter.

7.4. Coastal Camera

The PACE SDT Report identified a scientific goal for multi- to hyperspectral ocean color observations at a ground sample distance (GSD) of 250 m or better and identified advantages of similar GSD capability for cloud and aerosol studies. PACE Program Scientists recommended the project study the feasibility of a 50-100 m spatial resolution Coastal Camera for ocean color observations at the land-water interface and for detection of events such as oil spills and harmful algal blooms (see section 7.5 Appendix A). In coastal ecosystems, physical processes regulate the spatial-temporal dynamics of biological and biogeochemical processes and constituent distributions. High spatial resolution capability is necessary to resolve the spatial variability of these processes and constituents. A sensor on the order of 100 m GSD on PACE would spatially resolve the biogeochemical properties and their responses to physical processes within coastal ocean, estuarine and inland waters including phytoplankton blooms, water quality, and gradients of materials across coastal plumes, and further our understanding of the role of continental margins in carbon export. Hence as part of the pre-phase A trade studies, the project explored concepts

for a high spatial resolution coastal camera through an RFI (see section 7.6 Appendix B) and an IDL study. The information obtained from the RFI is proprietary and thus not included in this document. The aim for the CC IDL study was to determine whether a low-cost (~$10M) do-no-harm instrument would be feasible for accomplishing PACE science goals. The IDL Coastal Camera uses a simple refractive optical design (a single pushbroom camera) and a butcher-block filter assembly to image 12 bands onto a single off the shelf detector. An additional two spectral bands could be added with little to no impact on the design and cost. Several innovative design ideas allowed for incorporation of advanced features such as the cross-track rotation mechanism (leadscrew stepper motor) and the solar calibration capability at the 0° tilt position using a stationary Spectralon reflective diffuser; science observations would be conducted at the ±20° tilt positions. In addition, the estimated SNR performance for the specified OCI Ltyp values and bandwidths are in-line with OCI requirements (Table 7.9). In summary, the IDL study produced a complete and technically viable coastal camera concept that could provide scientific value to PACE. However, the in-house and independent cost estimates exceeded the available project resources. Thus, the project decided that it could not pursue either an in-house or procured coastal camera.

Table 7.9. Specifications, resource and performance metric results from the Coastal Camera IDL studies.

	Coastal Camera	
GSD (m)	100 m	
Spectral Band Centers and Bandwidth (nm)	Band	Bandwidth
	360	15
	412	10
	443	10
	490	10
	510	10
	555	10
	617	10
	665	10
	678	10
	710	10
	748	10
	865	15
FOV cross-track	12.7° ±15° with rotation mechanism	
Swath	160 km	
Sun glint	±20° tilt with mechanism	
Solar Cal	Daily stationary Spectralon diffuser	
Lunar Cal	Monthly	
Mass (kg)	23.7	
Volume (m)	0.763 m x 0.61 m diameter MEB: 0.018 x 0.024 x 0.015m	
Power (W)	42.9	
Data Rate (Mbps)	15.2	
SNR @ **443 nm** **555 nm** **678 nm** **865 nm** **@ Ltyp for 100 x 100 m pixel**	 1667 1237 798 533	

7.5. Appendix A: PACE Program Science Trades and Feasibility Study Document (Version 5 – May 8, 2015)

7.5.1. Trade Studies on PACE.

The PACE mission is intended to serve multiple science disciplines, including supporting observations for ocean, aerosol, and cloud investigations. A variety of configurations can be envisioned for the mission payload, but the funding framework is 'design to cost'. To optimize science returns from the mission, it is desired that focused studies be conducted regarding potential measurement trades/feasibility. This document outlines three sets of specific desired trade/feasibility studies, with a requirement that due diligence is documented regarding the evaluation of each. The framework assumed here is that of a 'modular' instrument configuration for the mission sensors (in the sense that a combination of more than two separate instruments could be considered), with the desired studies organized with respect to a module. It is recommended that these studies follow a series of milestones, in the order: (1) evaluate the technical feasibility of the various options (and if it is not technically feasible, document why), (2) report out, (3) provide a cost estimate on the technically feasible options, and (4) conduct the cost delta evaluation relative to the baseline configuration.

Module 1: Global Ocean Color Sensor (GOCS)

Design drivers – (1) Lunar calibration through Earth viewing port that illuminates all detectors at the same time, (2) Spectral system degradation tracking involving the minimum number of 'detector elements' possible to minimize striping, cross-talk, and other artifacts in instrument level data, (2) hyperspectral (5 nm) UV-VIS-NIR resolution, (4) SNR's consistent with SDT document, (5) 2-day global coverage, (6) pectral subsampling at ~1-2 nm resolution from 655 to 710 nm (to enable refined characterization of the chlorophyll fluorescence spectrum).

Driver consequences – Meeting the above design drivers (particularly 1 & 2) with a demonstrated approach requires that the GOCS falls into the SeaWiFS-like category of sensor types, in the sense of fore-optics. In other words, all ground pixels are observed with the same set of detector elements, which represents the minimum number of detectors that must be calibrated and tracked for degradation. Drawbacks of this approach are that telescope spin rates are fast and all science pixels have the same minimum ground dimension. Rapid spin rates equate to short dwell times on detectors, so increasing spin rate can translate to decreasing signal or lower SNR, which can jeopardize key science aspects of the mission, including continuity of fluorescence retrievals.

Trade/feasibility Recommendations –

(1) If the baseline ground resolution for GOCS is 1 km at nadir, evaluate what the highest achievable resolution is that still meets SNR (and other) requirements. This evaluation needs to consider (a) modifications to the baseline design, such as increasing detector-detector integration to increase SNR, (b) changes in mission risk due to higher resolution (e.g., sensor lifetime, increased complexity/optical or electrical components), and (c) changes in cost due to increased data download/handling, design and construction, mass, etc.

(2) For a given design for the spatial resolution identified in (1) above, evaluate what design options/approaches are available to achieve this resolution at all scan angles. This evaluation needs to consider changes in design, risk, and cost (as above),

(3) If the baseline UV-VIS-NIR resolution for GOCS is 5 nm from 350 – 800 nm, evaluate design modifications, risks, and costs for (a) expanding this range below 350 nm or to 900 nm and (b) improving resolution to < 5 nm at either all wavelengths or for specific spectral regions.

Module 2: Coastal Ocean Color Sensor (COCS)

Design drivers – (1) Ocean color measurements near land-ocean interfaces and for specific events (e.g., oil spills, cruise support) at 50 – 100 meter resolution, (2) Sensor degradation tracking comparable to MODIS Aqua, (3) ≤20 nm bandwidth spectral measurement bands with center wavelengths at 360 and 380 nm and additional bands consistent with the SeaWiFS at visible and NIR wavelengths, (4) SNR's and spatial coverage comparable to OLI on Landsat-8 or HICO. With respect to spectral resolution, one example of an overall approach that might be considered is something similar to HICO (As an example, HICO provided data at 5.7 nm spectral resolution, with spectral data collected at 1.9 nm resolution. To increase the signal to noise ratio, three bands were combined on the detector to produce wavelength centers 5.7 nm apart. A smoothing filter (Gaussian) was then applied to the uncalibrated spectral data to fix etaloning at the longer wavelengths. The size of the filter is 1Hi0 nm for the shorter wavelengths (400 - 745 nm) and 20 nm for the longer wavelengths (746 - 900 nm). Thus the data are 10 (or 20) nm width data centered on 5.7 nm wavelength centers.)

Driver consequences – Meeting the above design drivers (particularly 1) with a demonstrated approach requires that the COCS falls into the MODIS-like or MERIS-like category of sensor types, in the sense that (a) 2-dimensional detector array(s) is (are) required for sufficient dwell time to achieve appropriate SNR's. Drawbacks of these approaches are that instrument artifacts are likely to exist in, even up to Level 3, retrieved products and SNR's will be lower than for the GOCS. A SeaWiFS-type sensor will not work for this module.

Trade/feasibility Recommendations –

(1) Evaluate existing sensor designs (space or aircraft heritage) that can achieve instrument/science requirements for COCS. This evaluation needs to consider (a) simplifications to heritage designs that reduce cost or complexity while achieving threshold requirements, (b) changes in mission risk associated with Module 2 and its addition to the mission payload, and (c) changes in cost due to increased data download/handling, design & construction, mass, etc.

(2) Evaluate alternative sensor designs (i.e., different than heritage sensors) that can achieve instrument/science requirements for COCS. This evaluation needs to consider (a) minimum sensor design requirements to achieve science threshold requirements, (b) changes in mission risk due to addition of the instrument to the mission payload and TRL, and (c) changes in cost due to increased data download/handling, design & construction, mass, etc.

Module 3: Atmosphere/Ocean Polarimeter (AOP)

Design drivers –

Driver consequences –

Trade/feasibility Recommendations –

Recommended Cost Trade Studies

(1) Inclusion / Addition of bands at 940, 1378, 2250 for cloud property measurements
(2) Reduction of the uncertainty in DOLP to 0.5%
(3) Increase swath width to ±30° and ±45°
(4) Increase the number of measurement angles to 50 and 100
(5) Increase in angular range to ±70°
(6) Reduce pixel size to 1 km and 500 m
(7) Improve radiometric accuracy to 3%

Additional Trade/Feasibility Studies

Mission observations at specific short-wave infrared bands (SWIR) are desirable for multiple coastal and atmospheric science applications. However, the platform instrument module used to achieve these measurements is flexible. The ocean science application for the SWIR data is for improved atmospheric corrections in highly turbid (e.g., coastal, estuarine) waters, where water leaving radiances in the NIR are non-negligible. Accordingly, inclusion of the SWIR bands on the COCS, rather than GOCS, may be preferable. A disadvantage of integrating the SWIR bands into the COCS instrument is its likely narrower swath width and the GOCS instrument, which may diminish atmospheric science returns. Alternatively, it may be advantageous to make the SWIR measurements from the AOP. Given the 'design to cost' framework for the PACE mission, it is desired that trade/feasibility studies be conducted to evaluate these three SWIR integration options (i.e., as part of the GOCS, COCS, and AOP modules). These evaluations allow informed decisions regarding the SWIR measurements for various mission scenarios involving one, two, or three modules.

Design drivers – Threshold and baseline SWIR measurements with bandwidths, band centers, and SNR requirements as defined by the mission SDT.

Trade/feasibility Recommendations –

(1) Evaluate instrument designs modifications necessary to include the threshold and baseline SWIR measurement requirements into the COCS module. This evaluation needs to consider (a) low-risk instrument design options to achieve requirements, (b) changes in mission risk due to addition of the SWIR measurement capability, and (c) changes in cost due to increased data download/handling, design & construction, mass, etc.

(2) Evaluate instrument designs modifications necessary to include the threshold and baseline SWIR measurement requirements into the GOCS module. This evaluation needs to consider (a) low-risk instrument design options to achieve requirements, (b) changes in mission risk due to addition of the SWIR measurement capability, and (c) changes in cost due to increased data download/handling, design & construction, mass, etc.

(3) Evaluate instrument designs modifications necessary to include the threshold and baseline SWIR measurement requirements into the AOP module. This evaluation needs to consider (a) low-risk instrument design options to achieve requirements, (b) changes in mission risk due to addition of the SWIR measurement capability, and (c) changes in cost due to increased data download/handling, design & construction, mass, etc.

7.6. Appendix B: Coastal Camera Request for Information (RFI)

REQUEST FOR INFORMATION (RFI)

Pre-Aerosol, Clouds and Oceans Ecosystem (PACE) mission

THIS IS *NOT* A REQUEST FOR PROPOSAL OR INVITATION TO BID NOTICE.

The Pre-Aerosol, Clouds and Oceans Ecosystem (PACE) Project is considering the purchase of multi-band high spatial resolution camera to complement its primary ocean color instrument. The PACE mission is primarily being conducted to collect global measurements of ocean color. These measurements will extend contemporary data records of ocean ecological and marine biogeochemical parameters. The multi-band high spatial resolution camera will collect additional data at high spatial resolution when the PACE observatory is in sight of coastal regions. This data will be combined with hyperspectral data from the primary ocean color instrument with lower spatial resolution.

PACE will enable advanced research on:

- Plankton Stocks – Distinguish living phytoplankton from other optically-active water column constituents, such as re-suspended sediments and dissolved carbon;
- Plankton Diversity – Identify phytoplankton community structure;
- Ocean Carbon – Assess changes in carbon stocks, primary production, net community production, and carbon export to the deep sea;
- Human Impacts – Evaluate changes in land-ocean interactions and water quality;
- Forecasting Futures – Resolve mechanistic linkages between biology and environmental physical forcings to support of process-based predictive modeling.

The purpose of this RFI is to identify potential interest in providing a multi-band high spatial resolution camera for the PACE Project. This is for information and planning purposes and to allow industry the opportunity to verify reasonableness and feasibility of the requirements and to promote competition.

While our intent may be to team with industrial partner(s), we are not bound by this RFI to do so. This is not a Request for Proposal, nor a Request for Quotation, nor an Invitation to Bid. Therefore, this RFI is not to be construed as a commitment by the Government to enter into a contract nor will the Government pay for information provided in response to this RFI.

The desired characteristics for the multi-band high spatial resolution camera are the following:

Orbit: 650 km, ~98 degree inclination polar, sun synchronous orbit with a local equator crossing time close to noon. (Note, the sun will always stay on the same side of the spacecraft. Additionally, the beta angle is nearly always close to zero)

Mission Life: 3 years

Spatial resolution: in the range of 50 to 150 m

Spectral Range: The camera should cover the VIS-NIR range and include two NIR bands for atmospheric correction, for example 748 nm and 865 nm. Coverage of the VIS-NIR range can be accomplished with either a spectrograph design or with the selection of 8 to 12 spectral bands as preferred by the vendor. Coverage in the UV range is desirable, but optional to help keep cost down.

To aid in the design of the camera the following information is provided in the table below.

1) Ltyp, the expected open ocean cloud free radiance per spectral band

2) Lmax, the maximum expected radiance – typically for cloud cover. Note, the camera should not saturate at Lmax

The swath width should be on the order of 400 to 600 km.

	Band Width (nm)	L_{typ} * mW/(cm^2 μm sr)	L_{max} ** mW/(cm^2 μm sr)	Purpose
350 (optional)	15	7.46	35.6	Atmospheric Correction, Ocean color science
360 (optional)	15	7.22	37.6	Ocean color science
385 (optional)	15	6.11	38.1	Ocean color science
412	15	7.86	60.2	Ocean color science
425	15	6.95	58.2	Ocean color science
443	15	7.02	66.4	Ocean color science
460	15	6.83	72.4	Ocean color science
475	15	6.19	72.2	Ocean color science
490	15	5.31	68.6	Ocean color science
510	15	4.58	66.3	Ocean color science
532	15	3.92	65.1	Ocean color science
555	15	3.39	64.3	Ocean color science
583	15	2.81	62.4	Ocean color science
617	15	2.19	58.2	Ocean color science
640	10	1.90	56.4	Ocean color science
655	15	1.67	53.5	Ocean color science
665	10	1.60	53.6	Ocean color science
678	10	1.45	51.9	Ocean color science
710	15	1.19	48.9	Ocean color science
748	10	0.93	44.7	Ocean color science
820	15	0.59	39.3	Ocan color science
865	40	0.45	33.3	Ocean color atmosheric correction
940	30	0.78	21	Cloud and aerosol science

This RFI is to solicit specific capability information from industry and promote competition. For planning purposes, we are requesting that the responses to this RFI include the following information:

1) A brief description of the technical capabilities, key interfaces, and heritage of the camera.
2) Provide the expected Signal to Noise Ratios that can be achieved with the camera.
3) The approximate mass, power and volume requirements for a single camera. How do these requirements change with the addition of a second and/or third camera?
4) A brief description of company capabilities, applicable facilities, and experience designing and building cameras.
5) Notional schedule for instrument implementation through delivery to the project. The vendor should assume an authority to proceed data of April 2017.
6) The approximate cost of a single camera design and the cost of adding a second and/or possibly a third camera. Costs should be in real year dollars.
7) Description of key technical, schedule, and price drivers and options to mitigate risks and/or reduce schedule.

To consolidate our planning, responses from industry are requested by Friday, August 14, 2015, in the form of written and illustrated concepts, estimates for development costs and schedule, assumptions used for cost and schedule estimates including interface and design assumptions, and descriptions of capabilities. Responses can be submitted via email. The subject line of the submission should be "RFI for Multi-band Camera," and attachments should be in Microsoft WORD, POWERPOINT, or PDF format. The email text must give a point-of-contact and provide his/her name, address, telephone/fax numbers, and email address. The information is requested for planning purposes only, subject to FAR Clause 52.215-3, entitled "Solicitation for Information for Planning Purposes."

It is not NASA's intent to publicly disclose vendor proprietary information obtained during this solicitation. To the full extent that it is protected pursuant to the Freedom of Information Act and other laws and regulations, information identified by a respondent as "Proprietary or Confidential" will be kept confidential.

It is emphasized that this RFI is for planning and information purposes only and is NOT to be construed as a commitment by the Government to enter into a contractual agreement, nor will the Government pay for information solicited.

No solicitation exists; therefore, do not request a copy of the solicitation. If a solicitation is released, it will be synopsized in FedBizOpps and on the NASA Acquisition Internet Service. It is the potential offeror's responsibility to monitor these sites for the release of any solicitation or synopsis.

Technical questions should be directed to: Leslie Hartz at Leslie.S.Hartz@nasa.gov or Eric Gorman at Eric.T.Gorman@nasa.gov. Procurement related questions should be directed to: Ayana Briscoe at Ayana.A.Briscoe@nasa.gov

Interested offerors shall address the requirements of this RFI in written format as described in the previous paragraphs by electronic mail to: Leslie Hartz at Leslie.S.Hartz@nasa.gov, no later than 5:00 PM EST on Friday, August 14, 2015.

An ombudsman has been appointed -- See NASA Specific Note "B".

The solicitation and any documents related to this procurement will be available over the Internet. These documents will be in Microsoft Office 97 format and will reside on a World Wide Web (WWW) server, which may be accessed using a WWW browser application. The Internet site, or URL, for the NASA/GSFC Business Opportunities home page is http://prod.nais.nasa.gov/cgi-bin/eps/bizops.cgi?gr=C&pin=51. It is the offeror's responsibility to monitor the Internet site for the release of the solicitation and amendments (if any). Potential offerors will be responsible for downloading their own copy of the solicitation and amendments, if any. Any referenced notes may be viewed at the following URLs linked below.

Chapter 8

Case for the Addition of a Coastal Ocean Color Imager (COCI) to PACE

Antonio Mannino, NASA Goddard Space Flight Center, Greenbelt, Maryland[7]

Susanne E. Craig, GESTAR/Universities Space Research Association, Columbia, Maryland

Nima Pahlevan, Science Systems and Applications Inc, Lanham, MD

Executive Summary

This chapter describes the scientific justifications for the addition of a hyperspectral coastal ocean color imager (COCI) to the PACE mission. COCI was specifically designed to image small-scale to mesoscale processes in the coastal ocean, estuarine, and inland waters. This pushbroom sensor has a nominal ground sample distance of 100 m, and spectral characteristics equivalent to the PACE Ocean Color Instrument (OCI). The information acquired from such a sensor is highly complementary to ocean color and atmospheric measurements from OCI and polarimeters. Principally, COCI would substantially enhance the capabilities of PACE to reveal ecological and biogeochemical processes in these important, but vulnerable, waters. Many individuals contributed to defining the PACE-relevant science and requirements associated with COCI (see Tables 8.2 and 8.3 for a complete list).

8.1. Introduction

The NASA Climate-Centric Architecture document included an objective for the PACE ocean color instrument to quantify water quality in coastal regions with "new, high quality information on the biogeochemical properties of coastal waters and their implications for ecosystem and human health" [*NASA*, 2010, p. 20]. The PACE Science Definition Team (SDT) Report [PACE Science Definition *Team*, 2018] identified a scientific goal for multi- to hyperspectral ocean color observations at a ground sample distance (GSD) of 250 m and identified advantages of similar GSD capability for cloud and aerosol studies. The Report described several benefits that would result if PACE met these goal requirements [*NASA*, 2010, p. xvii]:

- "Increase the area of inland waters that can be studied using remote sensing, including increased coverage of the Great Lakes and a large number of smaller water bodies
- Increase temporal resolution by reducing interference from clouds
- Improve satellite product validation in coastal areas where large spatial gradients in observable variables are expected

[7] Cite as: Mannino, A., S. E. Craig, and N. Pahlevan (2018), Case for the Addition of a Coastal Ocean Color Imager (COCI) to PACE, in *PACE Technical Report Series, Volume 5: Mission Formulation Studies (NASA/TM-2018 – 2018-219027/ Vol. 5)*, edited by I. Cetinić, C. R. McClain and P. J. Werdell, NASA Goddard Space Flight Space Center Greenbelt, MD.

- Increase the use of satellite ocean color observations in coastal research and management applications globally
- Develop and implement applications to advance assessments of critical ocean ecosystem services [that] affect human health and welfare"

Under Design-to-Cost (DTC) constraints, the PACE Project determined that it could not achieve both the threshold requirements and the high spatial resolution goal recommended by the PACE SDT with a single sensor. The Program Scientists requested the Project explore the feasibility of including a high spatial resolution instrument for coastal environments (i.e., coastal camera) as a tertiary instrument on the PACE mission. The Project released a Request for Information (RFI) in July 2015 and conducted an Instrument Design Lab (IDL) study in October 2015 to define the range of capabilities and associated costs for implementing a low-cost coastal camera on PACE. Coastal camera sensors with two levels of capabilities and implementation costs were identified ranging from class D to C instruments. The Project determined that a coastal camera could not be accommodated within the DTC constraints and could only be implemented with additional funds from NASA [see Mannino and Cairns, 2018 – Ch. 7].

The Canadian Space Agency (CSA) and the U.S. Naval Research Lab (NRL) proposed to contribute a class C hyperspectral coastal camera designated the Coastal Ocean Color Imager (COCI) to NASA's PACE mission. An *ad hoc* NASA PACE COCI science team (Table 8.2) was assembled to provide input on the recommended instrument capabilities and high priority science questions that COCI would aim to resolve. A joint NASA-CSA-NRL COCI user and science team meeting was convened at GSFC on June 1-2, 2016 to discuss the science and application priorities, sensor capabilities, and a range of implementation topics.

In July 2016, the Canadian government designated COCI for implementation on PACE as its highest priority mission with final approval planned by April 2017. CSA and Fisheries and Oceans Canada (DFO) convened a 2nd COCI user and science team meeting in Ottawa on July 21-22, 2016, which focused on the science and application priorities of Canadian government and academic stakeholders. Representatives from U.S. EPA, U.S. Fish and Wildlife Service and the PACE project participated in this meeting.

CSA, in collaboration with the NRL team that built HICO, and PACE Project personnel have defined a design and concept of operations that will meet the desired PACE COCI capabilities (Table 8.1) and high priority science questions and application objectives defined by the *ad hoc* NASA PACE COCI science team (see below).

8.2. Science Justification

With the inclusion of COCI, the PACE mission would be able to spatially resolve, in the most dynamic regions of the Earth, the cycling of elements critical to life and climate, the effects of fluxes of terrigenous materials and pollutants into vital aquatic ecosystems, and the development of harmful algal blooms (HABs) and other threats to human health and security, and the health of our coastal ecosystems and the economies that depend on them. Specifically, COCI would significantly augment PACE's capability to spatially resolve the biogeochemical properties and their responses to physical processes within open ocean, coastal ocean, nearshore waters, estuaries, rivers, lakes and reservoirs. These include phytoplankton dynamics, sub-mesoscale processes, water quality and clarity, and gradients of materials across riverine and coastal plumes, thus furthering our understanding of the role of continental margins in carbon export and sequestration (Figure 8.1). COCI can also address PACE aerosol and cloud science

objectives, which include the characterization of aerosol gradients in the coastal zone for both urban and rural regions, investigation of aerosol-cloud interactions including the transition region between aerosols and clouds, the determination of air quality, and examination of aerosol-ocean interactions at the land-water interface. It is proposed that COCI would collect ocean and atmospheric information coincident with that collected by PACE OCI, but at a spatial resolution of ~0.01 km^2 that is two orders of magnitude finer than the planned PACE OCI (~1 km^2). The resulting data would greatly add to our knowledge of OCI sub-pixel variability as a function of physical province and biogeochemical process. Convolving datasets from the narrow-swath COCI with the wide-swath OCI and polarimeter would greatly enhance the breadth of science that can be accomplished with PACE. OCI and polarimeters provide the greater temporal frequency and spatial coverage context to COCI observations while COCI would contribute the fine spatial and spectral resolution for synergistic use with OCI and polarimeter data.

8.2.1. Ocean Color Measurements

Fine scale ocean color satellite observations are required to observe and quantify impacts of natural and human induced hazards on ocean biology, biodiversity and ecosystem functioning [*IOCCG*, 1999]. For example, spatial resolution of 50-150 m is recommended for oil-spill detection by satellite remote sensing [*Brekke and Solberg*, 2005]. High-spatial resolution is key for observing and studying coastal shallow habitats [*Lee et al.*, 2010] due to strong patchiness and spatial gradients.

Analyses of extensive datasets acquired from *in situ* measurements and air- and space-borne hyperspectral imagers (e.g. AVIRIS, PHILLS, PRISM, Hyperion, HICO) have demonstrated the utility of and need for ~100 m to 200 m GSD hyperspectral ocean color observations to adequately resolve the dynamics and scope of events in coastal and open ocean, estuaries, rivers, and lakes that would otherwise be masked by OCI. *Dierssen et al.* [2015] captured the spatial distribution and unique spectral signature of a *Mesodinium rubrum* bloom with HICO's 100 m hyperspectral data, which could not be captured in the 1 km MODIS imagery (Figure 8.2). Numerous other HICO images illustrate the diversity of blooms, sediment plumes, and coastal and lake features that require ~100 m hyperspectral data for visualization (http://hico.coas.oregonstate.edu).

Factors such as the small size of many water bodies (e.g., reservoirs and water supplies), land-adjacency, and ice-adjacency effects significantly constrain the utilization of moderate resolution ocean color sensors to characterize water quality, ecosystem function, and biogeochemical gradients and rate processes [*Hestir et al.*, 2015; *Mouw et al.*, 2015]. Approximately 20 million water bodies fall within the COCI to OCI pixel size range of 0.01 to 1 km^2 [*Verpoorter et al.*, 2014]. Ocean color observations from OCI will be limited in nearshore coastal and inland waters due to land adjacency effects [*Bulgarelli et al.*, 2014]. Adjacency effects are also present in biologically active marginal ice zone where OCI measurements will mostly be invalid in commonly cloudy polar regions [*Bélanger et al.*, 2007]. Ocean color data from OCI will be limited to science-quality data no closer than ~3 km from shore or ice margin due to bright target adjacency effects. This results in significant gaps in data along the shores throughout the globe and waters surrounding sea ice in polar regions. The maturity and level of preparedness of the scientific community will ensure full exploitation of COCI data. While COCI will provide valid observations in such dynamic coastal regions, coincident COCI-OCI-polarimetry data will enable better understanding of the complexity of radiometric measurements at the land-water-air interface.

Field observations in estuarine and coastal environments have demonstrated that satellite sensors with finer spatial sampling (i.e. generally finer than 200 m GSD) are needed to resolve the steep gradients of carbon pools, phytoplankton communities, suspended sediments and nutrients observed at the land-ocean and sea-ice margins such as within 1 km of tidal wetlands [e.g. *Tzortziou et al.*, 2011] and waters adjacent

to and within sea ice [*Arrigo et al.*, 2014; *IOCCG*, 2015]. An analysis by *Moses et al.* [2016] of *in situ* optical measurements and airborne ocean color and lidar observations from diverse turbidity and phytoplankton population regimes, concluded that a spatial resolution of <200 m is required to capture the fine-scale features that are common in the coastal ocean. An independent study found similar results using Landsat 8 OLI images [*Pahlevan et al.*, 2018]. Furthermore, coarser (≥1 km) observations can lead to misinterpretations of satellite biogeochemical products from coastal and inland waters [*Kutser*, 2004; *Lee et al.*, 2012]. COCI data can be applied to correct for sub-pixel spatial heterogeneity in OCI ocean color properties [*Pahlevan et al.*, 2016] and consequently biogeochemical data products.

Recent studies have strongly suggested the importance of meso- and sub-mesoscale events to the annual carbon cycle and phytoplankton populations [*Claustre et al.*, 1994; *Lévy et al.*, 2012; *Mahadevan et al.*, 2012; *Omand et al.*, 2015]. Spatial resolutions finer than 200 m are needed to verify and quantify the biogeochemical importance of such events in a variety of systems.

8.2.2. Atmospheric Measurements

Analyses of data from high-spatial resolution imagers, both airborne (AVIRIS, MAS, eMAS) and satellite (e.g. Landsat, ASTER, etc.), have led to advances in monitoring aerosols and quantifying the continuum between aerosols and clouds. *Koren et al.* [2008] used Landsat to show that clouds exist at all scales. Subpixel clouds will adversely affect retrievals of aerosols or ocean surface properties [*Martins et al.*, 2002]. However, a moderate resolution sensor (~500 m) has subpixel clouds that cannot be discerned by any reasonable cloud mask scheme. At the same time, there is a continuum between aerosols and clouds [e.g. *Charlson et al.*, 2007]. Fine resolution imagers (like COCI) with corresponding in situ measurements help to characterize the nature of this continuum [*Twohy et al.*, 2009], but further work is required [*Brock et al.*, 2016].

The aerosols within a cloud field may be significantly different than aerosols far from the cloud field in terms of their physical and optical properties, and in their climate effects [*Koren et al.*, 2009]. Moderate-resolution sensors (e.g. MODIS) cannot observe these gradients (Figure 8.3). Additionally, smoke plumes from fires, gradients of urban pollution, and other fine-scale phenomena are often missed by moderate resolution remote sensing [*Chudnovsky et al.*, 2013; *Livingston et al.*, 2014; *Raffuse et al.*, 2013]. Targeting coastal regions with high spatial resolution remote sensing enhances monitoring of aerosols that are detrimental to human health and visibility, particularly in highly populated coastal areas.

Liquid water cloud horizontal heterogeneity on 1 km scales can result in biases in imager cloud detection, cloud optical thickness, cloud effective particle size, and/or inferred water path. Both theoretical [*Zhang et al.*, 2016; *Zinner et al.*, 2010] and empirical studies [*Alexandrov et al.*, 2016; *Coakley et al.*, 2005] support the need for spatial resolution better than the threshold OCI GSD, especially for broken maritime cloud regimes. Retrieval biases caused by horizontal heterogeneity in ice clouds have also started to be investigated [*Fauchez et al.*, 2018] and are anticipated to be reduced with smaller GSD.

8.3. Science Questions Addressed by COCI

Top priority science questions that can be addressed with COCI data

- What are the spatial scales, composition, magnitudes and successional patterns of phytoplankton populations, including blooms, in inland waters, estuaries, coastal ocean and open ocean, and how are these phytoplankton populations driven by natural and human-induced change?
- How do the fine-scale (100-200 m) features of oceanic and coastal and inland water interfaces (oceanic fronts, land-ocean, sea-ice margins, wetlands-estuary, river plumes, land-freshwater,) contribute to regional and synoptic scale biogeochemical processes and associated distributions of carbon, nutrients and sediments?
- How are water quality, water clarity, ecological integrity and trophic status being altered in response to natural and human-induced change within inland waters, estuaries, nearshore and coastal ocean waters both in managed and unmanaged systems?
- What are the spatial scales of variability of aerosols in the coastal zone and adjoining urban centers and what are the implications for improving atmospheric correction in these zones and understanding the impact on air quality and human health?

Other priority PACE-relevant science questions that can be addressed with COCI:

- How can data assimilation of high spatial resolution ocean color observations into models improve model predictions of ocean physical and biogeochemical processes?
- Does the high productivity often observed in coastal, inland and estuarine waters alter aerosol assemblages? If so, how significant are contributions from these waters to global inventories of climate-relevant trace reactive gases and their radiative forcing?
- What are the characteristics of aerosols within a cloud field? Can we identify and then quantify the radiative impacts of hydrated aerosols, cloud fragments versus adjacency effects? Can we observe new particle generation in cloud fields? How do we quantify the continuum region, and its associated effect on the radiative budget of Earth's climate?
- How do fine-scale features of aerosol affect air quality in coastal urban environments, and how does this play out in terms of public health and social justice?
- What fine-scale features of aerosol plumes can be linked to their sources, injection height and transport predictability?
- What are the global areal extent, distribution, composition, status, and change in marshes, mangrove forests, coral reefs and sea grass meadows? Climate change and intensifying pressures of a growing human population are strongly impacting these ecosystems. Given large uncertainties for the areal extent, distribution and loss rates of these vital habitats, it is critical and urgent to establish an accurate baseline and to quantify change of coastal and inland aquatic communities (emergent and benthic).
- What are the structural and biochemical characteristics of plant canopies? How are these characteristics related to carbon, water, and energy fluxes? Can these characteristics describe plant species and plant functional type diversity?

8.4. COCI Applied Science Objectives:

While the goal of COCI is to address these fundamental science questions the data will also be valuable for NASA, NOAA, EPA, USGS, USFWS, BOEM, the U.S. Navy, numerous state and local agencies, as well as Canadian and other international stakeholders to address key coastal and water resource management objectives including:

- Identification of quantification of harmful algal blooms (HABs) and nuisance algal blooms
- Quantification and monitoring of water quality and clarity
- Enhanced precision/accuracy in water-quality products (e.g., phytoplankton abundance) in lakes/reservoirs compared to that those from existing multispectral missions (e.g., Landsat)
- Determination of variability in phytoplankton biomass and community structure that are key to developing improved ecosystem-based water quality and resource management strategies
- Understand spatio-temporal dynamics of lakes/reservoirs and plans for minimizing the occurrences of major ecosystem disasters like fish-kill events
- Investigation of the link between terrestrial exports to eutrophication, HABs and hypoxia in coastal zones
- Detection of changes in ice coverage, phytoplankton populations and associated biogeochemical properties within coastal polynyas
- Detection and tracking of oil spills and seeps
- Development of indicators of water-borne pathogens
- Detection and quantification of event-scale features (responses to storms, upwelling, volcanic eruptions, etc.) that impact annual primary productivity and biogeochemical cycles
- Mapping of marine protected areas and ecologically and biologically significant areas
- Mapping of preferred habitat for invasive species
- Characterization of fine-scale aerosol variability in urban and coastal zones that affect air quality and impact human health
- Characterization of point source aerosol plumes (e.g., smoke)
- Characterization of terrestrial ecosystem diversity, biochemistry, and function

8.5. Summary

While PACE will continue our monitoring of the global ocean and atmosphere for the impacts of climate change, COCI, with similar spectral capabilities and a spatial resolution that is 100 times finer (~0.01 km^2) than OCI, takes us further into the near-shore ocean, estuaries, rivers and large lakes and reservoirs where we are already seeing the impacts of human populations on a large scale on the water supply, fisheries, air quality, recreational activities and human health for the majority of the world's population that lives near the coast.

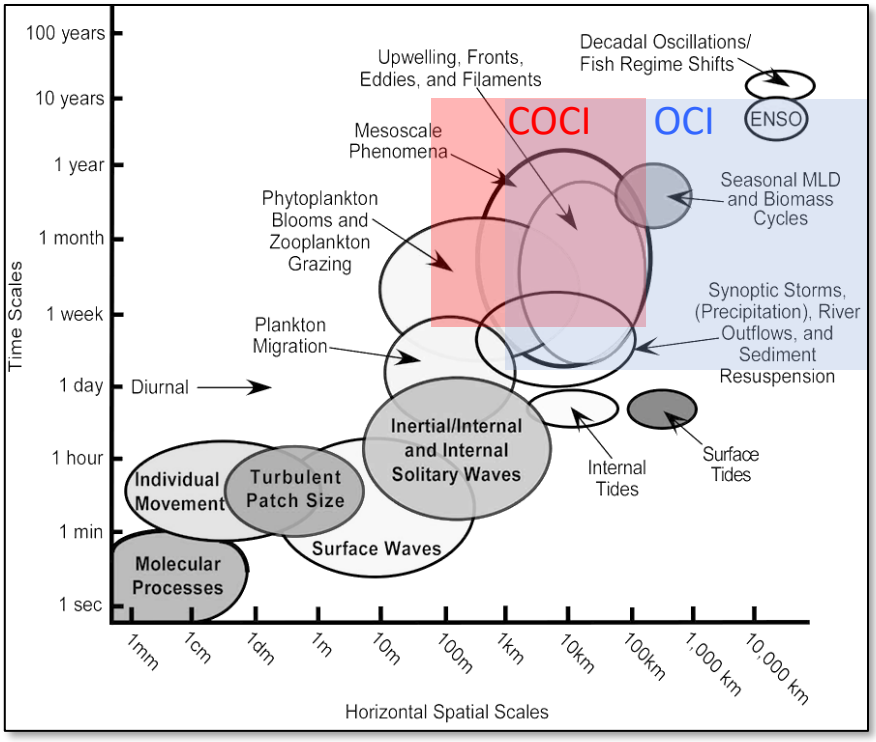

Figure 8.1. Plot of the ocean-relevant time and horizontal space scales illustrating physical and biological processes overlain with the presumed scales resolved by COCI (red) and OCI (blue) (assumes mission extension beyond planned 3 years on-orbit). (Figure modified from Dickey [2003]).

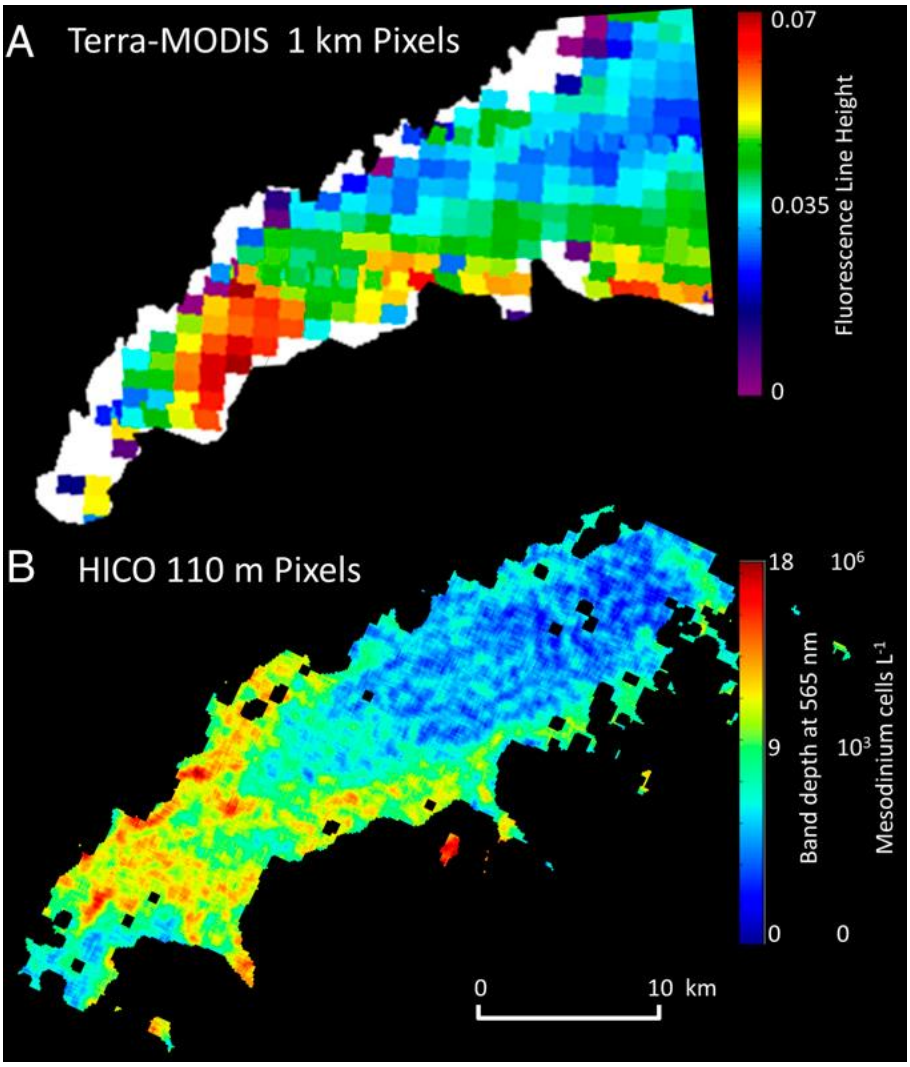

Figure 8.2. (A) Image of West Long Island Sound at a resolution of 1 km from the MODIS Terra sensor shows an elevated chlorophyll-a fluorescence patch on September 23, 2012, but the type of bloom cannot be distinguished from the limited spectral bands. (B) In contrast, hyperspectral HICO imagery reveals characteristic yellow fluorescence due to phycoerythrin pigment within the enslaved chloroplasts of the ciliate M. rubrum. Dense and patchy near-surface blooms of this motile and actively photosynthesizing mixotrophic marine protist periodically dominates primary productivity in the region. (from Dierssen et al. [2015])

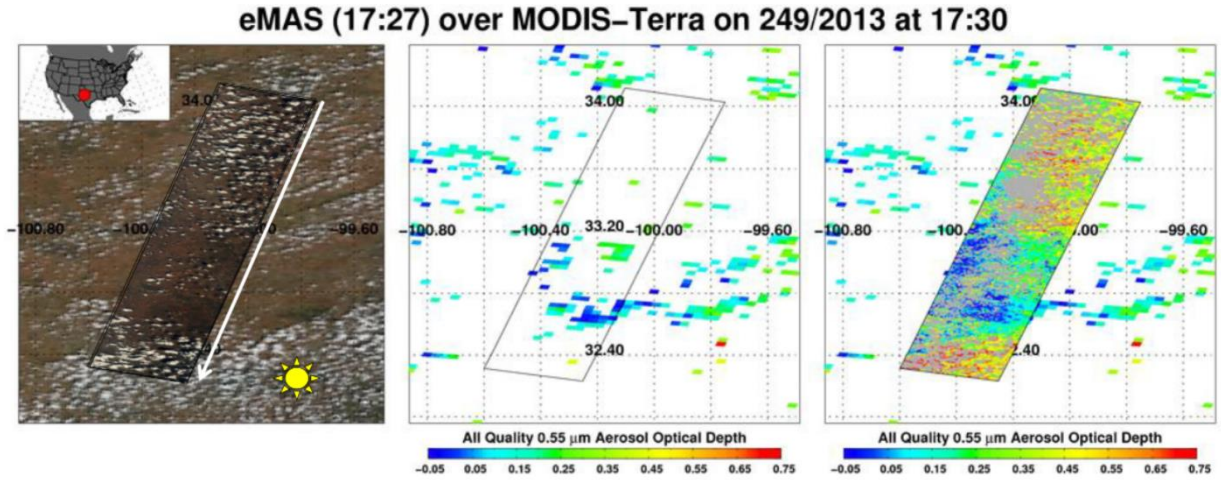

Figure 8.3. Scene from SEAC4RS on day 249 of 2013 with images from MODIS-Terra at 17:30 UTC with the strip from the high resolution eMAS imager aboard the NASA ER-2 taken at 17:27 UTC. Left: RGB image showing eMAS superimposed on MODIS, along with direction of ER-2 flight and location of the sun. Middle: Aerosol optical depth (AOD) retrieved from MODIS image with outline of eMAS strip. Right: AOD retrieval from eMAS superimposed on operational MODIS retrievals. Spatial resolution of MODIS RGB is 500 m and aerosol product is 10 km. Spatial resolution of eMAS RGB is 50 m and aerosol product is 1 km. Note that because of the many small cumulus clouds, the cloud mask applied to the moderate-resolution MODIS image prevents retrieval of the local aerosol gradients as well as aerosols within the cloud field. Although the AOD retrieved in the cloudy sections of the strip are much higher than the AOD retrieved in the relatively cloud-free portions, analysis shows that classical "cloud contamination" is not the reason for the enhanced AOD. Instead, it is a combination of adjacency effects and differences in aerosol properties near clouds. Figure courtesy of R. Levy and L. Munchak.

Table 8.1. Planned COCI specifications compared with desired PACE coastal camera capabilities.

Parameter	PACE 2015 Coastal Camera Trade Studies	*ad hoc* NASA PACE COCI Science Team		COCI [a] *current best estimates*
	Minimum / Preferred	Threshold	Baseline	
APPROACH Ocean Color		Measure weekly dynamics of coastal and estuarine waters, large lakes and rivers with more frequent sampling for US and Canada and target events.	Measure weekly dynamics of coastal and estuarine waters, coastal polynyas, large lakes and rivers globally with more frequent sampling for target sites and events. Monitor ocean event-scale features	**Exceeds threshold**
APPROACH Aerosol and Clouds		Quantify fine-scale aerosol properties for selected ocean, land and coastal scenes.	Time series of fine-scale aerosol properties and cloud properties for selected ocean, land and coastal scenes.	**Exceeds threshold**
Ground Sample Distance (GSD)	150 m / ≤100 m	≤125 m	≤100 m	100 m
# Spectral Bands	8 / 12 or more	Hyperspectral (50)	Hyperspectral (110 + SWIR)	Hyperspectral (110 + 3 SWIR)
Spectral Range	400-900 nm / 360-900 nm	400-900 nm	350-900 nm	360-910 nm SWIR <2.2 um
Bandwidth (FWHM)	20 nm / 10 nm	10 nm	≤5 nm	5 nm notional 1.25 nm capable
Signal-to-Noise Ratio (SNR)	600 / >1000 Vis 300 / >600 NIR	>600 for 400-600 nm >500 for 600-700 nm >300 for NIR	>1000 for 400-600nm >700 for 600-700 nm >500 for NIR	700-940 for 400-600 nm[b] 540-700 for 600-700 nm[b] 200-500 for NIR[b]
SWIR	None / none	None	Critical: 2.1 um Secondary: 1.24 and 1.64 um	TBD - 3 or 4 bands (including 1.245, 1.64 and 2.135 um)
Revisit frequency	15 day / <8 day	3 to 5 day for target sites <16 day global inland/coastal	2 to 4 day for target sites <12 day global inland/coastal	2 to 3 day for target sites Global (nadir view): ≤11 day at 45° N; ≤14 day at EQ
Glint avoidance	None / ±20° tilt	+20° tilt	±20° tilt	±20° tilt
Cross-track pointing	None / >±15°	>±15°	±45°	±45° [c]
Swath	100 km / >300 km	240 km	>300 km	240 km

[a] *Nominal values provided by CSA and NRL in August 2016*

[b] *for a 5% Albedo normalized to a 100 m GSD and 10 nm bandwidth for beginning of life.*

[c] *Gimbal motion is ±35° and COCI's 19.4° field of regard enables ±44.7° pointing capability.*

8.6. Appendix A

Table 8.2. Ad hoc NASA PACE COCI Science Team members.

NASA PACE COCI Science Team Members	Affiliation	Participated in 1st COCI User and Science Team (June 1-2, 2016)
Brian Cairns	NASA GSFC/GISS	Yes
Curt Davis	Oregon State University	Yes (remotely)
Liane Guild	NASA Ames	No
Steven Lohrenz	University of Massachusetts Dartmouth	Yes
Antonio Mannino	NASA GSFC	Yes
Matthew Oliver	University of Delaware	Yes
Hans Paerl	University of North Carolina	Yes
Lorraine Remer	University of Maryland Baltimore County	Yes
Blake Schaeffer	U.S. EPA	Yes
Walker Smith	Virginia Institute of Marine Science	No
Rick Stumpf	NOAA	No
Maria Tzortziou	City College of New York	Yes
Jeremy Werdell	NASA GSFC	Yes
Richard Zimmerman	Old Dominion University	No

Table 8.3. Other contributors to science talking points white paper

Contributors	Affiliation	Member of PACE Science Team
Steven Ackleson	Narval Research Lab D.C.	Yes
Martin Bergeron	Canadian Space Agency	No
Emmanuel Boss	University of Maine	Yes
Susanne Craig	Dalhousie University	Yes
Emmanuel Devred	Fisheries and Oceans Canada	No
Robert Frouin	Scripps Institution of Oceanography	Yes
Fred Huemmrich	UMBC/NASA GSFC	No
Zhongping Lee	University of Massachusetts	Yes
Rob Levy	NASA GSFC	Yes
Charles McClain	Oregon State University	No
Steve Platnick	NASA GSFC	Yes
Christopher Sioris	Environment and Climate Change Canada	No
Kevin Turpie	UMBC/NASA GSFC	No

8.7. Appendix B. PACE Mission Applications White Papers pertaining to COCI

Harmful Algal Blooms (**https://pace.oceansciences.org/docs/pace_oceans_white_paper_habs.pdf**)

Air Quality (**https://pace.oceansciences.org/docs/pace_atmos_white_paper_air_quality.pdf**)

Marine ecosystem resources: Fisheries (**https://pace.oceansciences.org/docs/pace_oceans_white_paper_fisheries.pdf**)

Chapter 9

Analysis of a Pushbroom Ocean Color Instrument Lunar Calibration

Frederick S. Patt, Science Applications International Corporation, Reston, Virginia[8]

Executive Summary

During the PACE Pre-Phase A period, a study was performed of various instrument concepts for the Ocean Color Instrument (OCI). One of the concepts studied was a pushbroom radiometer. PACE has a Level 1 requirement to perform at least monthly lunar calibrations to track the temporal response of the OCI. This paper presents an analysis of the requirements for performing a lunar calibration for the pushbroom instrument concept for the OCI.

9.1. Introduction

The lunar calibration has been an integral element of the radiometric calibration methodology for every NASA ocean color sensor since it was first used for the Sea-viewing Wide Field-of-view Sensor (SeaWiFS) in 1997 [*Eplee et al.*, 2012; *Woodward et al.*, 1993]. Based on this highly successful track record, PACE has a Level-1 requirement to perform OCI lunar calibrations. The threshold requirement is:

PACE shall provide:

g) Monthly characterizations of OCI instrument detector and optical component temporal stability. This will include lunar observations through the earth viewing port that illuminate all detector elements

The baseline requirement is for two lunar calibrations per month, and is otherwise identical.

A pushbroom sensor has a linear array of detectors that view in the cross-track direction, imaging a swath as the sensor (mounted on a spacecraft) moves in orbit. The OCI pushbroom concept instrument had several thousand detectors in the array. This creates difficulties in performing a lunar calibration operation to "illuminate all detector elements."

The model of the lunar irradiance is provided by the Robotic Lunar Observatory (ROLO) model developed by the U. S. Geological Survey [*Kieffer and Stone*, 2005]. The ROLO model provides the disk-integrated irradiance (DII) to compare with the instrument observations of the Moon; this requires that the instrument observations also be used to generate a DII. To satisfy the Level 1 requirement, a separate DII would need to be generated for each detector in the pushbroom array, a very challenging requirement to meet.

While pushbroom instruments have been used successfully for other disciplines (Land and Atmosphere), they have not had the same calibration requirements as Ocean Color, and in general on-

[8] Cite as: Patt, F. S. (2018), Analysis of a Pushbroom Ocean Color Instrument Lunar Calibration, in *PACE Technical Report Series, Volume 5: Mission Formulation Studies (NASA/TM-2018 – 2018-219027/ Vol. 5)*, edited by I. Cetinić, C. R. McClain and P. J. Werdell, NASA Goddard Space Flight Space Center Greenbelt, MD.

orbit calibration approaches for existing pushbroom sensors do not address the requirements for Ocean Color.

The following sections present the inputs that were used in this analysis; describe a maneuver sequence that would meet the Level 1 requirement for all of the pushbroom detectors; discuss the analysis that was performed to determine the requirements for the maneuvers; present the impacts to the mission; and summarize the key requirements.

9.1.1. Inputs

The objective of the maneuver sequence is to collect a full-disk lunar image for every cross-track IFOV (i.e., detector) of the instrument, with an accuracy and consistency that meets the overall requirements for temporal calibration response (0.1%).

The diameter of the Moon is 3475 km, and the Earth-Moon distance ranges from about 356,000 to 414,000 km. Since the lunar measurements will be performed during the orbit nighttime, the spacecraft-Moon distance will be less than this by up to the orbit radius, 7193 km.

The total cross-track FOV of the instrument is 104 degrees.

The IFOV is 297.48 μradian (0.017044 degree, about 1 arcminute). The sample interval is 0.039 seconds. The same sampling will be used for the lunar measurements as for the Earth data collection.

The orbit altitude is 815 km, corresponding to an orbit period of 6072 seconds.

The Earth data collection will be performed to cover the solar zenith angle range to 75 degrees, corresponding to 2530 seconds of the orbit. This leaves 3542 seconds, or about 59 minutes, for the lunar calibration operations during each orbit. If the maneuvers are timed to the terminator crossings, then 50.5 minutes is available.

The spacecraft is capable of inertial slew rates of up to 2 degree/sec. It takes 180 seconds to achieve that rate starting from 0, corresponding to an angular acceleration of 2/180 (~0.01111111) degree/sec^2. The acceleration is assumed to be linear. Note that while accelerating from 0 to 2 degree/sec, the spacecraft would rotate by 180 degrees, so for smaller maneuvers the maximum rate would not be achieved; the ADCS would accelerate at the maximum rate up to the midpoint of the maneuver and decelerate to the end.

The estimated control accuracy is about 1.2 arcminutes (1 sigma), approximately equivalent to 1 IFOV.

9.1.2. Maneuver Sequence

The proposed maneuver sequence is as follows:

1. After the end of Earth data collection, the spacecraft is pitched to position the pushbroom FOV just above the Moon, and rolled to position it to one side of the Moon.

2. The spacecraft begins a roll/pitch raster maneuver sequence, to cause the entire pushbroom array to view successive "slices" of the Moon. For each slice, the spacecraft is held at a constant inertial pitch and maneuvered in roll to cause the entire array to view the Moon. The roll maneuver is then stopped, the pitch is incremented by one IFOV, and the roll maneuver is repeated in the opposite direction. This sequence is illustrated in Figure 9.1.

3. As the spacecraft approaches the start of Earth data collection, it is pitched to nadir, with time for settling before the start of collection.

4. This sequence is repeated for successive orbits to view the entire Moon. At the start of each orbit's raster sequence, the pushbroom FOV is positioned to perform the raster for the next slice after the last one from the previous orbit.

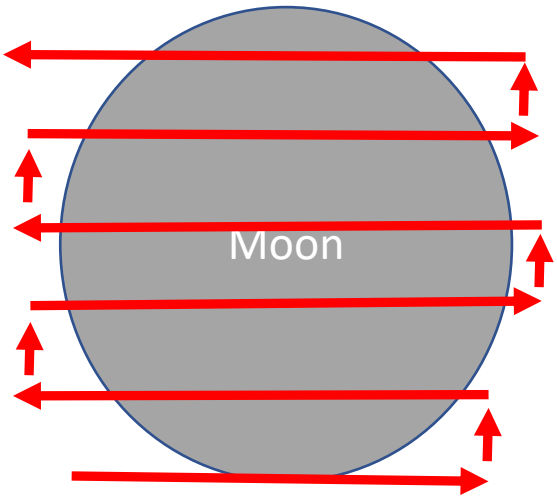

Figure 9.1. Sequence of Raster Maneuvers

9.2. Analysis

The key elements of the proposed lunar calibration maneuver sequence are: the time required; the maneuver accuracy and stability; geometry and viewing conditions that can affect the observations; and the non-uniformity of the lunar disk. Each of these is discussed below.

9.2.1. Timing

If the pitch maneuver is started immediately after the end of Earth data collection (15 degrees before the terminator crossing), the average pitch maneuver will be 75 degrees. Based on the angular acceleration rate, this would take 165 seconds. This maneuver would also be performed before the start of the next Earth data collection, for a total of 330 seconds. This allows 53.5 minutes between the maneuvers.

If the maneuver is delayed to the terminator crossing, the average pitch would be 90 degrees, which would take 180 seconds. This allows 47.5 minutes between pitch maneuvers.

The required roll rate during the raster maneuver is one IFOV per sample period, which corresponds to 0.437 degree/sec. To view the lunar disk using the 104-deg FOV at that rate will require 4 minutes. The time required to reverse the roll rate will be 79 seconds, so the total time for each raster is about 5 minutes 20 seconds.

The time available to perform the rasters depends on the timing of the pitch maneuvers, and also whether there is a requirement to perform the lunar observations in eclipse. The eclipse period is 35 minutes per orbit. The number of rasters per orbit for each case is as follows:

53.5 minutes	10 rasters
47.5 minutes	9 rasters
35 minutes	6 rasters

The maximum size of the lunar disk is 0.00993 radian (0.569 degree). This means that it will require up to 34 rasters to view the entire disk. At 9 rasters/orbit, four orbits will be required; this will also allow one raster above and below the disk to ensure that a full-disk image is collected. At 6 rasters per orbit, six orbits will be required.

9.2.2. Maneuver Accuracy and Stability

The requirement is to collect full-disk images for every detector with high consistency places stringent requirements on the raster maneuver accuracy and stability. The Moon is a significantly non-uniform source, which is why the approach using full-disk images has been used for heritage missions.

Given the duration of each raster, the roll rate will need to be either maintained or measured to the required consistency (0.1%). At the roll rate of 0.437 degree/sec, or 1573 arcsecond/sec, the required stability or knowledge is 1.6 arcsecond/sec. While it is probably difficult to maintain the roll rate at that accuracy, it should be possible to measure it using gyro data, and correct the lunar disk images for each detector using the gyro data.

Pointing control during the maneuvers is more problematic. The lunar disk is not a uniform source, and therefore variations in the pointing control during the maneuvers will cause variations in the radiometric measurements among the detectors. Potential error sources are:

1. Pitch and yaw deviations. To collect uniform slices of the Moon, the pitch angle increments between rasters need to be equally uniform, and the yaw angle needs to be controlled as well. Deviations in the pitch angle increments will cause nonuniform sampling of the disk across all of the rasters, and deviations in yaw will cause variations among detectors during a raster. The specific control requirements will more stringent than the requirements for Earth data collection, which allow control errors of about 2 IFOV. The effects of these deviations on lunar disk sampling are illustrated in Figure 9.2.

2. Pitch and yaw stability. Variations in the pitch or yaw angles during a raster would also result in nonuniform sampling of the disk among the detectors.

3. Maneuver axis variations. Deviations of the raster maneuver axis from the spacecraft roll axis would cause variations in the effective pitch and/or yaw angles during the raster.

Note that for any of these, pointing knowledge cannot be used to rectify the lunar disk images to account for pointing control errors.

9.2.3. Geometry and Viewing

There are three issues that arise in the geometry of the lunar view during the maneuvers, due to the time required.

1. The lunar phase will change significantly over the course of the maneuvers. The phase changes by up to 1 degree per orbit, or up to 5 degrees between the first and last set of observations. This means that the lunar irradiance changes with phase will need to be corrected for in order to combine the observations from all of the rasters to generate a full-disk measurement.

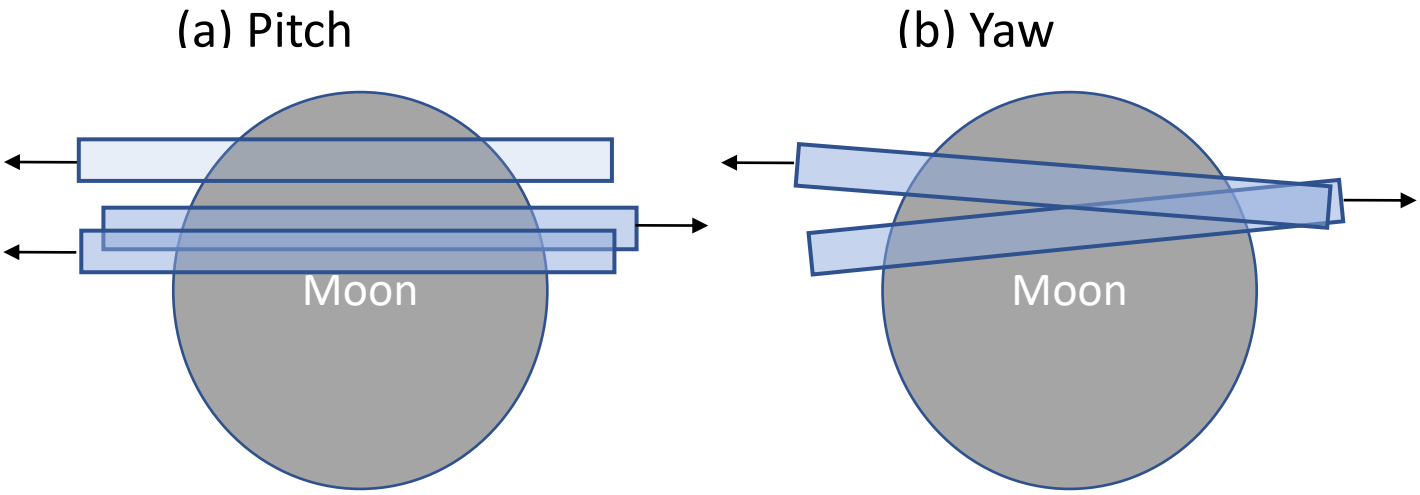

Figure 9.2. Effects of pointing control errors on lunar disk sampling; (a) pitch; (b) yaw

2. The spacecraft motion during each set of rasters will be significant, and will need to be accounted for in the pitch and yaw angles during the rasters. The spacecraft velocity is 7.5 km/sec. This would cause an apparent motion of the Moon in the opposite direction, at an angular rate of up to 20 μradians/sec. The effect of this motion on the viewing geometry will vary over the orbit nighttime as the direction of the velocity changes. Accounting for this would require adjustments to the pitch increments and yaw angles that would vary for each raster.

3. The average motion of the Moon is 0.5 degree/hour, or about 2 IFOV during one raster. Depending on the season, up to 50% of this motion will be in the pitch direction. The motion would be essentially constant during the full set of maneuvers. Accounting for this would also require adjustments to the pitch increments and yaw angles; these would be constant for one set of maneuvers, but would vary from one month to the next.

The effect of the first issue would be to increase the uncertainly in the full-disk image radiances, while the second and third issue would significantly complicate the planning of the maneuvers.

9.2.4. Lunar Disk Sampling Analysis

To estimate the effects of the pointing control variations on the full-disk lunar radiance, an analysis was performed using MODIS lunar images. The analysis used the MODIS 250m bands, which have similar spatial resolution to the proposed pushbroom instrument.

The analysis was performed by skipping some rows of the lunar image and replacing them by double-sampling adjacent rows. This simulates the effect of pitch and/or yaw control errors equivalent to 1 IFOV.

The results of the analysis showed variations in the disk-integrated radiances of up to 1%. If the average value was about 0.5%, this analysis indicates that in order to reduce the variations to 0.1%, the control accuracy would need to be equivalent to 0.2 IFOV, or about 0.2 arcminute (12 arcseconds).

9.3. Mission Impacts

The performance of the pushbroom lunar calibration would result in both technical and cost impacts to the mission.

There were two proposals for performing the raster maneuvers:

- The spacecraft ADCS performs all pitch and roll maneuvers required. This would require significant augmentation of the ADCS to achieve the required accuracy.
- The instrument could be mounted on a two-axis gimbal, which would perform the pitch and roll rasters. The spacecraft would perform pitch maneuver to point nadir axis at Moon. This would require real-time feedback of pointing errors to gimbal controls to maintain pointing accuracy, and might also require a dedicated star tracker to maintain pointing knowledge during rasters.

Both of these would have cost impacts, which were not estimated as part of this study.

The maneuvers would also require significant operational efforts, resulting in further cost impact. Each calibration requires a complicated sequence of pitch and raster maneuvers and up to six orbits per monthly calibration event. This would require a significant planning and operations effort each month to carry out the required set of maneuvers. It was estimated that at least one additional FTE per year would be required to plan and execute the monthly calibration maneuvers, compared to the effort required for a scanning instrument. In addition, at least two additional FTEs per year would be required to perform additional data analyses (~6000 detectors).

9.4. Summary of Key Requirements

The proposed lunar calibration activity for the ocean color pushbroom instrument is designed to obtain full-disk images for every detector in the pushbroom array. The combination of pitch and raster maneuvers that are required to accomplish this are complicated, and would take four to six orbits per monthly calibration event.

The requirement for 0.1% consistency across all of the detectors places very stringent requirements on the pointing control accuracy during the raster maneuvers. An analysis based on MODIS lunar calibration images indicates that control accuracy of 0.2 arcminute would be required to meet the radiometric requirement.

In addition, the geometric viewing conditions will change significantly during each orbit (due to the spacecraft velocity) and for each calibration event (due to the Moon's motion). This will require extensive planning of the raster maneuvers for each calibration event in order to achieve the required consistency of the lunar images.

References

Alexandrov, M. D., B. Cairns, B. van Diedenhoven, A. S. Ackerman, A. P. Wasilewski, M. J. McGill, J. E. Yorks, D. L. Hlavka, S. E. Platnick, and G. T. Arnold (2016), Polarized view of supercooled liquid water clouds, *Remote Sens. Environ.*, *181*, 96-110, doi:https://doi.org/10.1016/j.rse.2016.04.002.

Archer, C. L., and M. Z. Jacobson (2005), Evaluation of global wind power, *Journal of Geophysical Research: Atmospheres*, *110*(D12), doi:doi:10.1029/2004JD005462.

Arrigo, K. R., et al. (2014), Phytoplankton blooms beneath the sea ice in the Chukchi Sea, *Deep Sea Research Part II: Topical Studies in Oceanography*, *105*(0), 1-16, doi:http://dx.doi.org/10.1016/j.dsr2.2014.03.018.

Behrenfeld, M. J., Y. Hu, C. A. Hostetler, G. Dall'Olmo, S. D. Rodier, J. W. Hair, and C. R. Trepte (2013), Space-based lidar measurements of global ocean carbon stocks, *Geophys. Res. Lett.*, *40*(16), 4355-4360.

Behrenfeld, M. J., et al. (2016), Annual boom–bust cycles of polar phytoplankton biomass revealed by space-based lidar, *Nature Geoscience*, *10*, 118, doi:10.1038/ngeo2861.

Bélanger, S., J. K. Ehn, and M. Babin (2007), Impact of sea ice on the retrieval of water-leaving reflectance, chlorophyll a concentration and inherent optical properties from satellite ocean color data, *Remote Sensing of Environment*, *111*(1), 51-68, doi:http://dx.doi.org/10.1016/j.rse.2007.03.013.

Bézy, J.-L., S. Delwart, and M. Rast (2000), MERIS – A New Generation of Ocean Colour Sensor onboard Envisat, *ESA Bulletin*(103), 48-56.

Bouvet, M., and F. Ramino (2009), Equalization of MERIS L1b products from the 2nd reprocessing*Rep.*, ESA.

Brekke, C., and A. H. S. Solberg (2005), Oil spill detection by satellite remote sensing, *Remote Sens. Environ.*, *95*(1), 1-13, doi:https://doi.org/10.1016/j.rse.2004.11.015.

Bricaud, A., A. Morel, M. Babin, K. Allali, and H. Claustre (1998), Variations of light absorption by suspended particles with the chlorophyll a concentration in oceanic (Case 1) waters : analysis and implications for bio-optical models, *J. Geophys. Res. Oceans*, *103*, 31033-31044.

Brock, C. A., N. L. Wagner, B. E. Anderson, A. R. Attwood, A. Beyersdorf, P. Campuzano-Jost, A. G. Carlton, D. A. Day, G. S. Diskin, and T. D. Gordon (2016), Aerosol optical properties in the southeastern United States in summer–Part 1: Hygroscopic growth, *Atmospheric Chemistry and Physics*, *16*(8), 4987-5007.

Bulgarelli, B., V. Kiselev, and G. Zibordi (2014), Simulation and analysis of adjacency effects in coastal waters: a case study, *Appl. Optics*, *53*(8), 1523-1545.

Charlson, R. J., A. S. Ackerman, F. A.-M. Bender, T. L. Anderson, and Z. Liu (2007), On the climate forcing consequences of the albedo continuum between cloudy and clear air, *Tellus B: Chemical and Physical Meteorology*, *59*(4), 715-727.

Chudnovsky, A. A., A. Kostinski, A. Lyapustin, and P. Koutrakis (2013), Spatial scales of pollution from variable resolution satellite imaging, *Environ Pollut*, *172*, 131-138, doi:10.1016/j.envpol.2012.08.016.

Claustre, H., P. Kerherve, J. C. Marty, and L.Prieur (1994), Phytoplankton adaptation related to some frontal physical processes, *J. Mar. Syst.*, *5*, 251-265.

Coakley, J. A., M. A. Friedman, and W. R. Tahnk (2005), Retrieval of Cloud Properties for Partly Cloudy Imager Pixels, *Journal of Atmospheric and Oceanic Technology*, *22*(1), 3-17, doi:10.1175/jtech-1681.1.

Corsini, G., M. Diani, and T. Walzel (2000), Striping removal in MOS-B data, *IEEE Transactions on Geoscience and Remote Sensing*, *38*(3), 1439-1446, doi:10.1109/36.843038.

Cox, C., and W. Munk (1954), Measurement of the Roughness of the Sea Surface from Photographs of the Sun's Glitter, *J. Opt. Soc. Am.*, *44*(11), 838-850, doi:10.1364/JOSA.44.000838.

Craig, S. E., S. E. Lohrenz, Z. Lee, K. L. Mahoney, G. J. Kirkpatrick, O. M. Schofield, and R. G. Steward (2006), Use of hyperspectral remote sensing reflectance for detection and assessment of the harmful alga, Karenia brevis, *Appl. Opt.*, *45*(21), 5414-5425, doi:10.1364/AO.45.005414.

Dickey, T. D. (2003), Emerging ocean observations for interdisciplinary data assimilation systems, *J. Mar. Syst.*, *40*, 5-48.

Dierssen, H., G. B. McManus, A. Chlus, D. Qiu, B.-C. Gao, and S. Lin (2015), Space station image captures a red tide ciliate bloom at high spectral and spatial resolution, *Proceedings of the National Academy of Sciences*, *112*(48), 14783-14787, doi:10.1073/pnas.1512538112.

Eplee, R. E., G. Meister, F. S. Patt, R. A. Barnes, S. W. Bailey, B. A. Franz, and C. R. McClain (2012), On-orbit calibration of SeaWiFS, *Appl. Opt.*, *51*(36), 8702-8730, doi:10.1364/AO.51.008702.

Fauchez, T., S. Platnick, O. Sourdeval, C. Wang, K. Meyer, C. Cornet, and F. Szczap (2018), Cirrus Horizontal Heterogeneity and 3-D Radiative Effects on Cloud Optical Property Retrievals From MODIS Near to Thermal Infrared Channels as a Function of Spatial Resolution, *Journal of Geophysical Research: Atmospheres*, *123*(19), 11,141-111,153, doi:doi:10.1029/2018JD028726.

Franz, B. A. (1998), A Simple Destriping Algorithm for MOS Images*Rep.*, NASA/SIMBIOS Project https://oceancolor.gsfc.nasa.gov/staff/franz/papers/franz_1998_mosberlin.pdf.

Franz, B. A., S. W. Bailey, N. Kuring, and P. J. Werdell (2015), Ocean color measurements with the Operational Land Imager on Landsat-8: implementation and evaluation in SeaDAS, *Journal of Applied Remote Sensing*, *9*(1), 096070-096070.

Gordon, H. R., O. B. Brown, R. H. Evans, J. W. Brown, R. C. Smith, K. S. Baker, and D. K. Clark (1988), A Semianalytic Radiance Model of Ocean Color, *Journal of Geophysical Research*, *93*(D9), 10909-10924.

Gregg, W. W., and F. S. Patt (1994), Assessment of tilt capability for spaceborne global ocean color sensors, *IEEE Transactions on Geoscience and Remote Sensing*, *32*(4), 866-877, doi:10.1109/36.298014.

Group, A. O. W. (2018), ACE Ocean Working Group recommendations and instrument requirements for an advanced ocean ecology mission*Rep.*, NASA Goddard Space Flight Center, Greenbelt, MD.

Hestir, E. L., V. E. Brando, M. Bresciani, C. Giardino, E. Matta, P. Villa, and A. G. Dekker (2015), Measuring freshwater aquatic ecosystems: The need for a hyperspectral global mapping satellite mission, *Remote Sens. Environ.*, *167*, 181-195, doi:http://dx.doi.org/10.1016/j.rse.2015.05.023.

Hu, C., L. Feng, Z. Lee, C. O. Davis, A. Mannino, C. R. McClain, and B. A. Franz (2012), Dynamic range and sensitivity requirements of satellite ocean color sensors: learning from the past, *Appl. Opt.*, *51*(25), 6045-6062, doi:10.1364/AO.51.006045.

IOCCG (1999), *Status and Plans for Satellite Ocean-Colour Missions: Considerations for Complementary Missions*, IOCCG Dartmouth,, Canada.

IOCCG (2006), *Remote Sensing of Inherent Optical Properties: Fundamentals, Tests of Algorithms, and Applications*, IOCCG, Dartmouth, Canada.

IOCCG (2015), *Ocean Colour Remote Sensing in Polar Seas*, IOCCG Dartmouth,, Canada.

Kieffer, H. H., and T. C. Stone (2005), The Spectral Irradiance of the Moon, *The Astronomical Journal*, *129*(6), 2887.

Koren, I., G. Feingold, H. Jiang, and O. Altaratz (2009), Aerosol effects on the inter-cloud region of a small cumulus cloud field, *Geophys. Res. Lett.*, *36*(14).

Koren, I., L. Oreopoulos, G. Feingold, L. Remer, and O. Altaratz (2008), How small is a small cloud?, *Atmospheric Chemistry and Physics*, *8*(14), 3855-3864.

Kutser, T. (2004), Quantitative detection of chlorophyll in cyanobacterial blooms by satellite remote sensing, *Limnol. Oceanogr.*, *49*(6), 2179-2189.

Lee, Z., C. Hu, R. Arnone, and Z. Liu (2012), Impact of sub-pixel variations on ocean color remote sensing products, *Opt. Express*, *20*(19), 20844-20854, doi:10.1364/OE.20.020844.

Lee, Z., C. Hu, B. Casey, S. Shang, H. Dierssen, and R. Arnone (2010), Global Shallow—Water Bathymetry From Satellite Ocean Color Data, *Eos, Transactions American Geophysical Union*, *91*(46), 429-430.

Lee, Z. P., K. L. Carder, and R. A. Arnone (2002), Deriving inherent optical properties from water color: a multiband quasi-analytical algorithm for optically deep waters, *Appl. Opt.*, *41*, 5755-5772.

Lévy, M., R. Ferrari, P. J. S. Franks, A. P. Martin, and P. Rivière (2012), Bringing physics to life at the submesoscale, *Geophys. Res. Lett.*, *39*(14), L14602, doi:10.1029/2012GL052756.

Livingston, J., J. Redemann, Y. Shinozuka, R. Johnson, P. Russell, Q. Zhang, S. Mattoo, L. Remer, R. Levy, and L. Munchak (2014), Comparison of MODIS 3 km and 10 km resolution aerosol optical depth retrievals over land with airborne sunphotometer measurements during ARCTAS summer 2008, *Atmospheric Chemistry and Physics*, *14*(4), 2015-2038.

Lubac, B., H. Loisel, N. Guiselin, R. Astoreca, L. Felipe Artigas, and X. Mériaux (2008), Hyperspectral and multispectral ocean color inversions to detect Phaeocystis globosa blooms in coastal waters, *Journal of Geophysical Research: Oceans*, *113*(C6), doi:10.1029/2007JC004451.

Lyon, P. E. (2009), An automated de-striping algorithm for Ocean Colour Monitor imagery, *International Journal of Remote Sensing*, *30*(6), 1493-1502, doi:10.1080/01431160802468263.

Mahadevan, A., E. D'Asaro, C. Lee, and M. J. Perry (2012), Eddy-Driven Stratification Initiates North Atlantic Spring Phytoplankton Blooms, *Science*, *337*(6090), 54-58, doi:10.1126/science.1218740.

Martins, J. V., D. Tanré, L. Remer, Y. Kaufman, S. Mattoo, and R. Levy (2002), MODIS cloud screening for remote sensing of aerosols over oceans using spatial variability, *Geophysical Research Letters*, *29*(12), MOD4-1-MOD4-4.

McClain, C., et al. (2012), The Ocean Radiometer for Carbon Assessment (ORCA): Development History within and Advanced Ocean Mission Concept, Science Objectives, Design Rationale, and Sensort Prototype Description, NASA/TM-2012-215894*Rep.*, NASA Goddard Space Flight Center, Greenbelt, MD.

McClain, C. R., G. Meister, and B. Monosmith (2014), Chapter 2.1 - Satellite Ocean Color Sensor Design Concepts and Performance Requirements, in *Experimental Methods in the Physical Sciences*, edited by G.

Zibordi, C. J. Donlon and A. C. Parr, pp. 73-119, Academic Press, doi:https://doi.org/10.1016/B978-0-12-417011-7.00005-2.

McKinna, L. I. W., R. Lossing, and J. Werdell (2018), Assessment of hyperspectral pushbroom image striping artifacts in ocean color products, in *PACE Technical Report Series, Volume 5: Mission Formulation Studies (NASA/TM-2018 – 2018-219027/ Vol. 5)*, edited by I. Cetinić, C. R. McClain and P. J. Werdell, NASA Goddard Space Flight Space Center Greenbelt, MD.

Moses, W. J., S. G. Ackleson, J. W. Hair, C. A. Hostetler, and W. D. Miller (2016), Spatial scales of optical variability in the coastal ocean: Implications for remote sensing and in situ sampling, *Journal of Geophysical Research: Oceans*, n/a-n/a, doi:10.1002/2016JC011767.

Mouw, C. B., et al. (2015), Aquatic color radiometry remote sensing of coastal and inland waters: Challenges and recommendations for future satellite missions, *Remote Sens. Environ., 160*(0), 15-30, doi:10.1016/j.rse.2015.02.001.

NASA (2010), Responding to the Challenge of Climate and Environmental Change: NASA's Plan for a Climate-Centric Architecture for Earth Observations and Applications from Space, edited, p. 48.

O'Reilly, J., E., S. Maritorena, B. G. Mitchell, D. Siegel, A., K. Carder, L., S. Garver, A., M. Kahru, and C. McClain (1998), Ocean color chlorophyll algorithms for SeaWiFS, *Journal of Geophysical Research: Oceans, 103*(C11), 24937-24953, doi:10.1029/98JC02160.

Omand, M. M., E. A. D'Asaro, C. M. Lee, M. J. Perry, N. Briggs, I. Cetinić, and A. Mahadevan (2015), Eddy-driven subduction exports particulate organic carbon from the spring bloom, *Science, 348*(6231), 222-225, doi:10.1126/science.1260062.

Pahlevan, N., S. Sarkar, and B. A. Franz (2016), Uncertainties in coastal ocean color products: Impacts of spatial sampling, *Remote Sens. Environ., 181*, 14-26.

Pahlevan, N., S. R. Signorini, and I. Cetinić (2018), Estimating coastal ocean feature sizes for optimal remote sensing of coastal waters, in *PACE Technical Report Series, Volume 7: Ocean Color Instrument (OCI) Concept Design Studies (NASA/TM-2018 – 2018-219027/ Vol. 7)*, edited by I. Cetinić, C. R. McClain and P. J. Werdell, NASA Goddard Space Flight Space Center Greenbelt, MD.

Pande-Chhetri, R., and A. Abd-Elrahman (2011), De-striping hyperspectral imagery using wavelet transform and adaptive frequency domain filtering, *ISPRS Journal of Photogrammetry and Remote Sensing, 66*(5), 620-636, doi:https://doi.org/10.1016/j.isprsjprs.2011.04.003.

Pande-Chhetri, R., and A. Abd-Elrahman (2013), Filtering high-resolution hyperspectral imagery in a maximum noise fraction transform domain using wavelet-based de-striping, *International Journal of Remote Sensing, 34*(6), 2216-2235, doi:10.1080/01431161.2012.742592.

Patt, F. (2002), Navigation algorithms for the SeaWiFS mission*Rep.*, NASA GSFC, Greenbelt, USA.

Patt, F. S. (2018), Analysis of a Pushbroom Ocean Color Instrument Lunar Calibration, in *PACE Technical Report Series, Volume 5: Mission Formulation Studies (NASA/TM-2018 – 2018-219027/ Vol. 5)*, edited by I. Cetinić, C. R. McClain and P. J. Werdell, NASA Goddard Space Flight Space Center Greenbelt, MD.

Patt, F. S., and W. W. Gregg (1994), Exact closed-form geolocation algorithm for Earth survey sensors, *Int. J. Remote Sens., 15*(18), 3719-3734, doi:10.1080/01431169408954354.

Raffuse, S. M., M. C. McCarthy, K. J. Craig, J. L. DeWinter, L. K. Jumbam, S. Fruin, W. James Gauderman, and F. W. Lurmann (2013), High-resolution MODIS aerosol retrieval during wildfire events in California for use in exposure assessment, *Journal of Geophysical Research: Atmospheres*, *118*(19), 11,242-211,255.

PACE Science Definition Team (2018), Pre-Aerosol, Clouds, and ocean Ecosystem (PACE) Mission Science Definition Team Report*Rep.*, NASA Goddard Space Flight Center, Greenbelt, MD.

Twohy, C. H., J. A. Coakley Jr, and W. R. Tahnk (2009), Effect of changes in relative humidity on aerosol scattering near clouds, *Journal of Geophysical Research: Atmospheres*, *114*(D5).

Tzortziou, M., P. J. Neale, J. P. Megonigal, C. L. Pow, and M. Butterworth (2011), Spatial gradients in dissolved carbon due to tidal marsh outwelling into a Chesapeake Bay estuary, *Mar. Ecol. Prog. Ser.*, *426*, 41-56.

Vane, G., R. O. Green, T. G. Chrien, H. T. Enmark, E. G. Hansen, and W. M. Porter (1993), The airborne visible/infrared imaging spectrometer (AVIRIS), *Remote Sens. Environ.*, *44*(2-3), 127-143.

Verpoorter, C., T. Kutser, D. A. Seekell, and L. J. Tranvik (2014), A global inventory of lakes based on high-resolution satellite imagery, *Geophys. Res. Lett.*, *41*(18), 6396-6402.

Wang, M., and S. W. Bailey (2001), Correction of sun glint contamination on the SeaWiFS ocean and atmosphere products, *Appl. Opt.*, *40*(27), 4790-4798, doi:10.1364/AO.40.004790.

Werdell, P. J. (2018), PACE Ocean Color Science Data Product Requirements, in *PACE Technical Report Series, Volume 6: Data Product Requirements and Error Budgets (NASA/TM-2018 – 2018-219027/ Vol. 6)*, edited by I. Cetinić, C. R. McClain and P. J. Werdell, NASA Goddard Space Flight Space Center Greenbelt, MD.

Werdell, P. J., et al. (2013), Generalized ocean color inversion model for retrieving marine inherent optical properties, *Appl. Opt.*, *52*(10), 2019-2037, doi:10.1364/AO.52.002019.

Woodward, R. H., R. A. Barnes, C. R. McClain, W. E. Esaias, W. L. Barnes, and A. Mecherikunnel (1993), SeaWiFS Technical Report Series: Modeling of the SeaWiFS Solar and Lunar Observations*Rep.*, 26 pp, NASA Goddard Space Flight Center, Greenbelt, Maryland.

Xi, H., M. Hieronymi, R. Röttgers, H. Krasemann, and Z. Qiu (2015), Hyperspectral Differentiation of Phytoplankton Taxonomic Groups: A Comparison between Using Remote Sensing Reflectance and Absorption Spectra, *Remote Sensing*, *7*(11), doi:10.3390/rs71114781.

Zhang, Z., F. Werner, H.-M. Cho, G. Wind, S. Platnick, A. S. Ackerman, L. Di Girolamo, A. Marshak, and K. Meyer (2016), A framework based on 2-D Taylor expansion for quantifying the impacts of subpixel reflectance variance and covariance on cloud optical thickness and effective radius retrievals based on the bispectral method, *Journal of Geophysical Research: Atmospheres*, *121*(12), 7007-7025, doi:doi:10.1002/2016JD024837.

Zinner, T., G. Wind, S. Platnick, and A. Ackerman (2010), Testing remote sensing on artificial observations: impact of drizzle and 3-D cloud structure on effective radius retrievals, *Atmospheric Chemistry and Physics*, *10*(19), 9535-9549.

Previous Volumes in This Series

Volume 1 *April 2018*	ACE Ocean Working Group recommendations and instrument requirements for an advanced ocean ecology mission
Volume 2 *May 2018*	Pre-Aerosol, Clouds, and ocean Ecosystem (PACE) Mission Science Definition Team Report
Volume 3 *October 2018*	Polarimetry in the PACE mission: Science Team consensus document
Volume 4 *October 2018*	Cloud retrievals in the PACE mission: Science Team consensus document